LA-11591-MS

History and Geophysical Description of Hazardous Waste Disposal Area A Technical Area 21

Los Alamos

Los Alamos National Laboratory is operated by the University of California for the United States Department of Energy under contract W-7405-ENG-36.

An Affirmative Action/Equal Opportunity Employer

LA-11591-MS

UC-721
Issued: October 1989

History and Geophysical Description of Hazardous Waste Disposal Area A Technical Area 21

Michael Gerety
John Nyhan
Ronald Oliver

Los Alamos National Laboratory
Los Alamos, New Mexico 87545

CONTENTS

LIST OF FIGURES

HISTORY AND GEOPHYSICAL DESCRIPTION OF HAZARDOUS WASTE DISPOSAL AREA A TECHNICAL AREA 21

by

Michael Gerety, John Nyhan, and Ronald Oliver

ABSTRACT

Los Alamos National Laboratory has been disposing of a variety of radioactive and hazardous wastes in pits and trenches around Los Alamos since 1944. The Area A site history and engineering drawings presented in this report, along with the geophysical results, demonstrate that much of the historical information merely indicates what was originally planned for the site and does not represent the final distribution of material.

This report demonstrates that geophysical remote sensing can determine pit and trench geometry, accurately locate material, and determine the physical properties of sites and buried material. The geophysical techniques illustrated in this report are magnetics, electromagnetics, resistivity, radar, and self-potential. Each of the techniques has its own merit; combining the techniques is the only way to obtain an accurate image of the site and its properties.

At Area A, geophysical measurements were definitive in locating and characterizing all known targets as well as discovering several undocumented ones. With these data, we can safely perform necessary remedial activities such as monitoring, drilling, and relocating material without the fear of breaching an unknown or misplaced storage facility. Furthermore, these data are obtained remotely and without disrupting the ground surface.

1. INTRODUCTION

During the period from 1944 to the present, a large volume of radioactive and hazardous wastes was buried in shallow trenches and pits at the Los Alamos National Laboratory (LANL) in Los Alamos, New Mexico. As part of the DOE Environmental Restoration Program, personnel from the Laboratory are examining several possible methods for managing this waste material. One of the methods under consideration involves retrieval, treatment, and transport of the materials to another waste repository. However, to implement this approach or others (e.g., monitoring the environment), it is necessary to locate buried waste material and to accurately determine the boundaries of existing pits and trenches. Geophysical exploration techniques are used for this purpose because of the noninvasive nature of the surveys and because past experience has demonstrated that pre-1950 burial site location records can be misleading.

This report summarizes the history of Area A, located at Technical Area 21, in Los Alamos, New Mexico, and presents the results of the geophysical investigation performed at the site. The purpose of the geophysical investigation was to characterize the physical properties of the site, to confirm the historical records of the past 45 years, and to confirm the locations of covered excavations and objects for future considerations of site closure. Part of this investigation is also to help determine the relative merits of different geophysical techniques for waste disposal site evaluation at Los Alamos.

1.1 Site Description and Waste Use History

Material disposal Area A is located on a narrow eastward-trending mesa that is part of the Pajarito Plateau in northern New Mexico. The land surface slopes north about 100 m and then drops steeply into DP canyon (approximately 30 m below the mesa top).

Area A (SE 1/4 section 14, T.19N, R.6E) is located in Technical Area 21 (TA-21), approximately 0.25 mile east of the intersection of DP Road and the northern perimeter road of TA-21. The total area of the site is 1.52 acres. Figure 1 is a map of Area A and its immediate vicinity, taken from Rogers (1977).

Area A was first used for the burial of solid wastes containing polonium, plutonium, uranium, thorium, and other unidentified chemicals. These wastes were placed in a series of trenches in the eastern end of Area A between 1945 and July 1946. According to one reference (Rogers 1977), four trenches 38.1 x 5.5 x 2.8 m (125 x 8 x 12 ft) were originally shown at this location on engineering drawing ENG-1266. A more accurate depiction (ENG-C2076) shows only two rectangular trenches (Fig. 2). The trenches were excavated into Unit 3 of the Tshirege Member of the Bandelier Tuff. Later,

in 1946, crushed Bandelier Tuff was used to backfill and cover the trenches (Figs. 3-5). Figure 3 shows two trenches on the eastern side of the site.

Two large storage tanks (known locally as the "General's Tanks" after Major General Leslie Groves, head of the Manhattan Engineering District during World War II) were buried at the west end of Area A in 1945. Figures 4 and 5 show the building located immediately to the south of the tanks as indicated in Fig. 1. There are no photographs available that show the tanks. Plutonium and americium waste solutions were stored in these tanks through 1946, with the hope that chemical recovery processes would improve so that the plutonium in them could be recovered. These two 50 000-gal. (189-m^3) cylindrical steel storage tanks are shown on engineering drawing ENG-C2076 as being 3.66 m in diameter and 19.2 m long (12 x 63 ft); details relative to their exact emplacement in the ground are also given.

During the 1950s, the surface of Area A was used to store hundreds of drums of wastes containing radioactive iodide (Figs. 6-8). Many of the 55-gal. mild steel drums, stored on the eastern end of Area A, corroded before they were removed to TA-21-35 and TA-45 in 1960.

Area A was reactivated in April 1969 with the construction of a large pit (45.7 x 12.2 x 6.7 m or 150 x 40 x 22 ft) in the center of the disposal area (Figs. 9-15). Between June 1969 and December 1971, the pit received waste materials from TA-21.

In 1972, the pit was enlarged (52.4 x 40.8 x 6.7 m or 172 x 134 x 22 ft). Between February and July 1973 it received plutonium contaminated building debris (Figs. 12-15) from the demolition of building TA-21-12 (Christensen et al. 1975). Figures 16 and 17 show backfill being stockpiled in Area A. The pit continued to receive waste from TA-21 through September 1977 (Fig. 18) and was finally backfilled with crushed tuff in May 1978, thus retiring Area A as an active materials disposal area (Figs. 19-22). The total buried waste volume is about 14 159 m^3 (500 000 ft^3).

The original structure of TA-21-12 consisted of a two-story frame and masonry building with about 900 m^2 of floor area, metal ducting, transitional plenums and filter housings, four blowers, and four 15.2-m stacks. Almost all of the materials listed were constructed of galvanized steel sheet metal, similar to the materials found in building TA-21-153 (Harper and Garde 1981), which was demolished about 5 yr later and sent to materials disposal Area G. The demolition of TA-21-12 (Christensen et al. 1975) resulted in

1. 1320 plastic-lined cardboard boxes (0.56 m^3) containing small and/or highly contaminated materials;

2. 69 plastic-lined plywood crates (1.2 x 1.2 x 2.4 m);

3. 1200 m^3 of transit, doors, lumber, pipes, roofing materials, and metals (unboxed, uncrated);

4. 400 m^3 of concrete, contaminated soil, and large metal items (steel columns used for primary structural support for the facility).

The waste management records (Christensen et al. 1975) indicate that these waste materials were buried at Area G (TA-54) and at Area A. The wastes listed in items 1 and 2 probably went to TA-54, but some of the wastes listed in item 3 and all of the waste materials listed in item 4 went to Area A (Figs. 12-15).

In 1983, the liquid wastes in the General's Tanks were removed for processing, leaving a small, semisolid precipitate layer in the tanks. In FY 1985, several small openings in the tanks were sealed and covered. Final site stabilization activities such as removing surface contamination, adding cover material, recontouring, and reseeding were also performed at this time.

1.2 Methodology

Almost the full spectrum of geophysical techniques pertinent to the physical characterization of the very near surface (<10 m) was performed. Standard seismic work was not performed because it cannot resolve objects as small and as near to the surface as in Area A. Gravity measurements were not made because density contrasts and mass excesses were not considered large enough to give reliable gravity signatures using standard gravity procedures.

An electromagnetic induction (EMI) survey was performed to locate metallic objects such as steel drums, ductwork, aluminum, and stainless steel. Both the in-phase and quadrature components of the signal were measured. EMI techniques are among the most widely used in geophysical investigations; consequently, the variety of techniques available is large, and they are routinely applied to waste management and remedial investigation problems. McNeil (1982) outlines the basic approach to mapping contaminant plumes; Tyagi et. al. (1983) outline the basic theory for the technique used at Area A and illustrate its use for detecting buried drums. Greenhouse and Harris (1983) and Greenhouse and Slaine (1986) use EMI to map contaminated groundwater. Saunders and Germeroth (1985) apply EMI to mapping subsurface hydrocarbons leaking from underground pipes. Lord et. al. (1982) and Lord and Koerner (1986) apply EMI techniques to locating buried containers. Koerner and Lord (1984) investigate the use of EMI for the detection of containers buried in saline soils.

A resistivity survey was performed to locate low-conductivity contrasts such as changes in permeability, moisture content, and, for example, areas where hard rock such as the Bandelier Tuff has been removed and replaced with other materials. Though both resistivity and EMI techniques investigate conductivity, they are sensitive to different regimes. For example, resistivity techniques do not locate small but highly conductive material such as sheets of aluminum. Both techniques are necessary to characterize the conductivity structure of the ground in some waste disposal environments.

Greenhouse and Harris (1983) present an excellent case history of a variety of techniques, including resistivity, to assist in the mapping of contaminant migration over an abandoned landfill. Walther et al. (1983) test different methods (including resistivity) for geophysical monitoring of contaminants. Both Greenhouse and Slaine (1986) and Walther et al. (1983) conclude that resistivity is much more expensive and does not give as good results as do the EMI techniques. This result is true for the relatively conductive environments in which they worked. At Los Alamos, the waste sites are carved out of highly resistive volcanic tuff and are often filled with concrete mixtures that are quite resistive. Resistivity is the only technique that does a good job separating resistive targets from one another.

Magnetic methods are very good for locating buried magnetic objects such as steel drums. The magnetic response of a metallic object can be used to determine if it is a magnetic alloy, or not. This makes the combination with EMI good for discriminating between aluminum and steel, for instance. A total-field magnetic survey was performed to look for changes in magnetic susceptibility created by the placement of magnetic material or the disturbance of natural magnetic minerals by heat or excavation. Magnetic methods are mainstream geophysical techniques and enjoy a wide range of applications including waste management and remedial investigation problems. Tyagi et al. (1983), Lord et al. (1982, 1986), and Koerner and Lord (1984) all used magnetometry to locate buried drums.

A self-potential (SP) study was performed at Area A to investigate electrochemical potentials related to variations in soil chemistry due to leaking containers, the oxidation of metallic material, or changes in the type of soil used to cover the site. Electrokinetic potential resulting from the movement of fluid through porous media is another source of SP voltage but is not considered an important mechanism at Area A.

SP has been used extensively by the mining industry for detecting massive sulfide (metallic) deposits (Telford et al. 1976), the leakage of fluids through dams and near drainage structures (Bogoslovsky and Ogilvy 1973), and it has also been used extensively for geothermal exploration and reservoir development (Corwin and Hoover 1979).

Radar has the potential for much higher resolution and depth discrimination than any other technique. It has been used almost as a matter of course for investigating waste disposal and spill problems. It is sensitive to changes in the dielectric constant (clay and water primarily) and can be used to find metallic conductors. Olhoeft (1986) illustrates the use of radar over a petroleum pipeline spill near Bemidji, Minnesota, where oil is floating on the water table. He also shows its use with a creosote plume in Pensacola, Florida. Stanfill and McMillan (1985) show its use for detecting buried drums, chemical plumes, faults, and fractures. Tsuneo et al. (1987) show how radar can be used in archaeological investigations to locate burial mounds, trenches, and floors of ancient dwellings. Several authors have conducted experiments on depth discrimination and location of various conductive drums (Koerner et al. 1982, Koerner and Lord 1984, Lord et al. 1982). Lord and Koerner (1986) conducted an experiment for locating plastic containers with radar.

1.3 Geophysical-Sampling Interval and Grid System

The data-sampling interval chosen for Area A was based on the expected size and depth of known targets. The following lists events relevant to expected targets and their dimensions:

1945 Construction of four trenches on the eastern end of Area A (38.1 x 5.5 x 2.8 m or 125 x 18 x 12 ft deep) and placement of two storage tanks 3.66 m in diameter and 19.2 m long (12 x 62 ft)

1969 Large pit constructed in the center of Area A (45.7 x 12.2 x 6.7 m or 150 x 40 x 22 ft deep)

1972 Large pit in center of Area A enlarged to bury building materials from the demolition of building TA-21-12 (52.4 x 40.8 x 6.7 m or 172 x 134 x 22 ft deep).

It was decided that a 2-m sampling interval would yield unambiguous results for the targets under consideration. To accomplish this result, 21 parallel east/west lines oriented 101.5 deg east of true north and separated by 2 m were marked on the ground. These lines, labeled A-V, are parallel to the northern boundary fence. Figure 23 shows Area A and every other line of the geophysical grid system. Point A2 (2S,2E) is a point located 2 m south and 2 m east of the northwest fence corner. Point C12 (6S,12E) is a point located 6 m south and 12 m east of the northwest fence corner. There are four brass caps cemented in place at the corners of Area A. These caps can be used to reestablish the grid when the wooden stakes have deteriorated. The coordinates of the brass caps are 1.65S,1.55E; -2.7S,141.6E; 43.4S,154.8E; and 30.1S,1.07E.

The placement of targets from Fig. 1 with respect to the geophysical coordinate system (Fig. 24) requires two assumptions: the northern fence line has not changed from what is indicated on Fig. 2, and the northwestern fence corner remains today as it was presented on Fig. 2. With these two criteria, most of the fence line features of Fig. 1 fit well with the fence line as it exists today. The location of the large central pit was taken from Fig. 1. Note the ambiguity between the description of the two trenches depicted on Figs. 1 and 2 and the description of the four trenches constructed on the eastern end of the Area A in 1945.

The Area A interpretation map, Fig. 25, is presented here as a convenience. Each of the following sections makes reference to this map. The map was compiled using data gathered from all the individual techniques, then determining the combination of regions that yielded the simplest, physically plausible interpretation. This map is a two-dimensional "image" of identifiable objects within Area A. The placement of the General's Tanks, pit, and trenches is based on an integrated interpretation of all the geophysical data. A complete list of the coordinates of these objects is found in Sec. 7.

2. RESISTIVITY

A direct current (DC) resistivity survey was performed at Area A to locate low-conductivity contrasts such as changes in permeability, moisture content, and areas where hard rock such as the Bandelier Tuff has been removed and replaced with other types of filler.

DC techniques are most effective in mapping changes in resistivity when the resistivities of both target and host are greater than 500 ohm-m. In addition, DC methods are size-dependent in that small high-contrast objects may not be detected and large low-contrast objects will be detected. Resistivity methods will generally not be able to distinguish between nonmetallic and metallic conductors. For these reasons, it takes both DC and EMI techniques to delineate the electrical structure of the ground in many environments.

The Schlumberger electrode configuration (Fig. 26) was chosen for Area A because it has the deepest penetration for the smallest electrode configuration. Figure 26 is a schematic representation of the Schlumberger array, which uses two electrodes for injecting current into the ground (A and B) and two for measuring the induced voltage (M and N). The distance between the MN electrodes must be less than one-fifth the distance between the AB electrodes.

For Area A, AB = 8.0 m, and MN = 1.0 m. These values were based on Schlumberger soundings (Figs. 27 and 28) performed at 26S,64E in July and August

1987. The July data show approximately 75 ohm-m material for AB/2 < 3.1 m, whereas the August data indicate approximately 60 ohm-m. The differences in apparent resistivity could be caused by changes in moisture from rain or differences in the field procedure used to obtain the data.

The outside electrode distance (AB = 8 m) was chosen because that spacing is sensitive to both very conductive (metallic) material and to very resistive (unaltered Bandelier Tuff) material beneath a 3-m-thick, 60-ohm-m cap. The 8-m spacing effectively scans to a depth of 3 m.

The apparent resistivity of the ground in the vicinity of the array is computed from the current, voltage, and array geometry and then plotted at the center point (P_1, Fig. 26). The array was consistently oriented parallel to the grid lines (A-V). Measurements were made at 2-m intervals. Figures 29 and 30 are the resulting apparent resistivity maps.

2.1 Equipment and Calibration

The equipment used for this survey is manufactured by Bison Instruments, Inc., 5708 West 36th St, Minneapolis, MN 55416. The system comes in three pieces: transmitter (model 2390-T50), receiver (model 2390-R), and calibration box (model 2227).

To ensure instrument reliability, calibration was checked using the manufacturer's calibration box and then checked with an oscilloscope. Calibration was generally performed at the beginning and end of each day. The calibration box contains two sets of resistors. One set is designed to load the transmitter and check its ability to supply constant current. The second set creates a known voltage drop to be measured by the receiver unit, thereby checking the receiver's ability to measure voltage accurately.

Figure 31 is a graph of the system error as measured on a regular basis during the survey. The measurements made with the 0.11-ohm resistor at the 10-mV range (squares) result in approximately 2 mV with -3.5% to 8% error. The measurements made with the 1-ohm resistor at the 100-mV range (triangles) result in approximately 20 mV with 2.5% to 4% error. The measurements made with the 10-ohm resistor at the 1000-mV range (diamonds) result in approximately 200 mV with 2.5% to 4% error.

For the geometry used at Area A, these data imply that 5-ohm-m measurements will contain errors between -3.5% and 8%, 50-ohm-m measurements will contain errors between 2.5% and 4%, and 500-ohm-m measurements will contain errors between 2.5% and 4%.

At Area A two different measurement frequencies were used: 1 Hz and 2 Hz. Before beginning the survey, we measured using a variety of frequencies to determine which frequencies result in valid DC requirements. For the resistivities and electrode

separations being used at Area A, both the 1-Hz and 2-Hz frequencies were found to be adequate.

2.2 Results

Figure 29 presents unfiltered apparent resistivity data contoured at 10-ohm-m intervals. Figure 30 presents the same data filtered to remove some of the "jitter" observed in the raw data. The contour interval of Fig. 30 is 4-ohm-m. The filter used to smooth the data is a five-point mask that averages a data point with its closest four neighbors. The central value is weighted twice the surrounding values. All the features observed in the filtered data can be observed in the unfiltered data as well, but they are more clearly presented.

Figure 30 shows that Area A can be divided into distinctive resistivity environments; Fig. 25 shows how these zones have been interpreted. The western zone is the relatively conductive area (<60 ohm-m) that contains the General's Tanks, which are described in the Introduction.

Adjacent to the highly conductive zone on the west end of the area is a resistive zone (>75 ohm-m) that forms a north/south-oriented ridge. This region results from a section of Bandelier Tuff that has not been excavated and serves to separate the General's Tanks (A1 and A2) from the central pit (C0).

The rest of the area shows a diverse and complex resistivity structure. Within this complexity, two resistive regions stand out (B1 and B2). These >80-ohm-m zones trend east/west and result from the two trenches shown on Figs. 1-3.

Soil cap. The only data collected that relate directly to the properties of the soil cap are the two Schlumberger soundings performed at 26S,64E (Figs. 27 and 28). These soundings show the cap to be 60-70 ohm-m and overlying more conductive material. The soundings are located directly over the central pit (C0) and are affected by the large amount of metal in the pit as well as the fill material and moisture content.

General's Tanks (A1 and A2). The location of the storage tanks is reasonably well constrained by the resistivity data. Examination of data profiles indicates two resistivity lows separated by slightly higher values, indicating two objects rather than one single, low-resistivity zone. This interpretation is only possible with prior knowledge of two tanks, rather than one tank. The data are very consistent from line to line, but the effect is too subtle for a blind interpretation. These data define the tanks in the east/west direction but allow for variation in their north/south position. The midline between the tanks is at 14E.

Central pit (C0). Placing boundaries for the central pit based on resistivity data alone would be difficult. Figure 1 has the pit located between two structures, the trenches on the east side of the site and the General's Tanks on the west. Given that there is a zone of unexcavated Bandelier Tuff separating the tanks from the pit, there is only one location that will accommodate the 52.4- x 40.8- x 6.7-m pit (C0) described in the Introduction. There is a discrepancy between the central pit location as placed in Fig. 1 and as placed by the resistivity data (Fig. 25). The resistivity data have the pit displaced 5 m to the east of the location presented on the engineering drawing of Fig. 1.

Trenches (B1 and B2). The trenches (B1 and B2) are characterized by two separate (>70-ohm-m) resistive anomalies. These two anomalies are located exactly as indicated relative to the central pit on Fig. 1. That is, they are also displaced 5 m from the positions shown on Fig. 1.

It is surprising that the excavations would be more resistive than the hosting Bandelier Tuff, but the geometry is compelling. They must be filled with very resistive material and/or contain significantly less water in their pore spaces than does the surrounding rock. A very dry filler could cause this anomaly.

Other (D2). The area east of the trenches is characterized by one resistivity high (D2). The feature is circular with a diameter of about 8 m and is similar in amplitude to the trenches (B1 and B2). D2 probably results from a very resistive (>1000-ohm-m) object such as a concrete plug, pad, or fill material like that found in the trenches. Resistivity is the only technique that identified this anomaly.

3. SELF-POTENTIAL

An SP study was performed at Area A to investigate electrochemical potentials related to variations in soil chemistry due to leaking containers, the oxidation of metallic material, or changes in the type of soil used to cover the site. Electrokinetic potential resulting from the movement of fluid through porous media is another source of SP voltage but is not considered an important mechanism at Area A.

SP is not normally used for waste site characterization but was performed because it has the potential to locate corroding material and variation in soil chemistry. Anomalies are often associated with oxidizing metallic mineral deposits (Sato and Mooney 1960). The SP technique should be integrated with geology, hydrology, and other geophysical methods to determine the appropriate source mechanism for a given anomaly.

Streaming potential is the voltage created as water flows through porous media such as fluid moving through a crack in a dam. Essentially, mechanical energy is converted to

electrical energy. The magnitude of the voltage will depend on the resistivities of the fluid and porous media, the pressure drop, and the composition of the solid material.

Electrochemical effects result in measurable voltage when metallic objects span different oxidation potentials. Metallic mineral deposits have been discovered by mapping naturally occurring voltages (SP) in areas of interest. Large voltages (up to 1 V) result when a mineral deposit spans oxidizing (surface water) and reducing (deeper water) environments, thereby causing the mineral deposit to corrode.

3.1 Equipment and Calibration

The equipment used to perform the SP survey consisted of two nonpolarizing copper/copper sulfate porous pot electrodes (Tinker and Rasor, San Gabriel, California), 18-gauge copper wire, a wire reel, and a Model 8022B Fluke digital voltmeter (John Fluke Manufacturing Co., Inc., PO Box C9090, Everett, WA 98206) with an input impedance of 1 Mohm.

The digital voltmeter (DVM) calibration was checked at the beginning and end of each day by monitoring both the resistance and voltage scales with a set of calibration resistors and a known voltage source. The voltage source was manufactured by Datel Interstel, serial number 342-00183. In all cases the DVM showed less than 1% error.

Voltage differences due to slight differences in electrode chemistry were monitored by placing the electrodes in a solution of copper sulfate and measuring the voltage between them. Mixing the copper sulfate solutions of the two electrodes together or replacing the solutions of both electrodes reduced the voltage difference to less than 2 mV.

The voltage for one station on all lines (A-V) was measured at the beginning of the survey to ensure that each line had a reference voltage from which any daily DC offsets could be detected and then corrected. Repeatability of the data was monitored by reoccupying stations during the day and by repeating measurements from one day to the next. When repeated measurements differed by more than 5 mV, the entire line was redone.

All voltages measured at Area A were done with respect to a point chosen to minimize reoccupation errors. This was accomplished by locating an area where the voltage gradient was close to zero and choosing a point (30S,40E) in the middle of that area. The reference electrode was installed at the beginning of the survey and then left in place for the duration of the survey. Changes in the absolute potential at this point were monitored by repeating previous measurements at the beginning, middle, and end of each day.

3.2 Results

Figure 32 presents the SP measured at Area A contoured at a 15-mV interval. These data were filtered to reduce the jitter and create an image more easily deciphered. The filter used to create Fig. 33 is a five-point mask that averages a data point with its closest four neighbors; the central value is weighted twice the surrounding values. All features observed in the filtered data can be observed in the unfiltered data, but they are more clearly presented.

The electrical and chemical environments in waste disposal areas have not been studied sufficiently to predict or to unambiguously interpret the effects noted. Now that strong SP effects have been measured, there should be follow-up to determine source mechanisms. The interpretations given below are provided with considerable reservation.

Soil cap. The eastern side of Area A, where the cap thins and then terminates, is the only region where any effect due to the presence or absence of the dirt cap could be discerned. Nothing in the data could be interpreted as being a transition zone in this sense. There is nothing in the SP data that shows variations in soil cap composition. The anomaly amplitudes are larger than one would expect from soil variations and most are also delineated by geophysical properties (conductivity, etc.) that are not related to the cap material. For these reasons the soil cap is considered homogeneous in terms of SP.

General's Tanks (A1 and A2). There is no reason to believe that the tanks are corroding because there is no strong SP negative anomaly directly associated with them. There is, however, a strong SP anomaly very close to them (D3). This anomaly may be associated with ancillary equipment surrounding the tanks. It is well outside the pit boundary and only a few meters east of the closest tank.

There are four small positive SP perturbations directly over the north and south ends of both storage tanks. If one were to seek a corrosion interpretation for these anomalies, it would be that the tanks are oxidizing in the central portion between the two ends.

Central pit area (C0). There are three SP anomalies within the central pit area (C0), all associated with magnetic or EMI responses. The northern side of C1 has a 26-mV response, the southwestern portion of C2 has a 26-mV response, and there is a 66-mV anomaly at C4. All of these anomalies, with the exception of C2, are contained within the pit boundary as interpreted on Fig. 25. C2 is open to the south and may result from something just outside of the gridded area. If one were to interpret these anomalies in the classic mineral exploration sense, these data indicate that there is oxidation of the metallic objects at these locations.

measurements made in the presence of strong gradients are readily identified. The magnetometers are designed to identify and to flag these questionable data.

A factory engineer was consulted about the gradient problem and corrective action was taken. The magnetometer power supply voltage was increased from 12 to 18 V and the integration time used by the magnetometer was reduced. These changes decreased the sensitivity of the magnetometer to "several" gammas but also greatly increased its tolerance to spatial gradients. Measurements at Area A show that the modifications substantially improved the data quality even though they did not completely correct the problem.

To maintain control of diurnal drift, we deployed the G-866 magnetometer at station 26S,40E and recorded diurnal variations (a measurement was made every 5 s). To maintain control on instrument function and operator performance, we reoccupied a field base station (20S,40E) at regular intervals throughout the survey. Figure 34 presents data recorded at the field base station and at the diurnal base station. Not all the G-866 diurnal data are plotted because they were not digitally recorded. The G-866 data were selected to faithfully represent the shape of the diurnal drift curve as plotted by the magnetometer. The overall precision of the survey is about 50 gammas.

4.2 Results

Base station reoccupations show variations of up to 30 gammas of change. These variations result from moving the sensor to determine the maximum variation that could reasonably result from operator "inattention." The magnetic gradient at the field base station is about 125 gammas/m; sensor movement could reasonably account for about 20-gamma variations. The remainder of the variation in base station readings results from high-frequency variations of up to 10 gammas as was monitored on the diurnal monitor.

The diurnal monitor showed the magnetic field changing smoothly at about 8 gammas/h with approximately 10 gammas of high-frequency noise. The total diurnal drift contained in these data is about 50 gammas. Figure 34 shows the diurnal variation of the earth's magnetic field with the base station reoccupations superposed.

It was not possible to make accurate measurements in the vicinity of the storage tanks (A1 and A2) because we could not completely eliminate the problem with strong gradients. However, this lack of accuracy should not be considered overly detrimental to the survey results. The fact that questionable data exist indicates the presence of highly magnetic material. The lack of accuracy means that quantitative analysis cannot be used for interpretation and that interpretation must be based on a good understanding of the way magnetic objects perturb the earth's field.

Trenches (B1 and B2). There are no discernible SP effects in the vicinity of the trenches.

Other (D3). D3 is defined by approximately 18 points of SP data. None of the other geophysical techniques registers anomalous response. The SP data taken by itself could indicate corrosion of a metallic object, but the fact that there is no indication of an associated metallic object in either the EMI or magnetics makes this interpretation tenuous at best.

4. MAGNETICS

A total-field magnetic survey was performed to look for variations in the magnetic susceptibility of the ground created by burying magnetic material or removing naturally occurring magnetic minerals by excavation. The combination of magnetic measurements with EMI measurements provides a way to distinguish between magnetic metals such as steel drums and nonmagnetic metals such as aluminum sheets. Magnetic field strengths were recorded on 2-m centers with the sensor 2 m above the ground. This eliminates many high-amplitude, high-frequency anomalies associated with small metallic objects near or on the surface of the ground (nails, bottle caps, etc.).

At Los Alamos, New Mexico, the declination and inclination of the earth's magnetic field are 11.5° east and 63° respectively. Averaging several days of field measurements shows the regional field strength in the Los Alamos area to be about 51 900 gammas. Magnetically susceptible objects subject to the earth's field create secondary fields, which then sum with the earth's field; it is the magnitude of the sum of the primary and secondary fields that is measured.

4.1 Equipment and Calibration

The survey utilized two proton precession magnetometers produced by EG&G Geometrics, 395 Java Drive, Sunnyvale, CA 94089, (408)-734-4616. Model G-866 outputs total magnetic field readings on a paper strip chart and was used to monitor diurnal changes in the magnetic field. Model G-856X records and stores data in internal memory and has the capability to upload the stored data to a computer for processing. The G-856X was used for all data acquisition on the grid.

The above magnetometers are said to have an absolute field measurement accuracy to 0.5 gamma. However, they are not designed to measure magnetic field strengths in areas with strong spatial gradients, such as found at Area A. Results from preliminary work indicated that gradients of over 5000 gammas/m made it impossible to measure magnetic field strength to even within several thousands of gammas. Fortunately,

The survey was decisive in its ability to discriminate targets. The smallest anomaly interpreted is over 200 gammas, and the smallest contour interval is 100 gammas. Thus, 50 gammas of noise does not seriously detract from the results. None of the data presented in this section have been filtered except that 50 000 gammas has been subtracted from all data to aid in presentation. These data have such large variation that it is necessary to have two contour intervals. The contour interval west of 88E is 1000 gammas; the contour interval east of this line is 100 gammas (Figs. 35 and 36).

Area A can be divided into three distinctive regions with different magnetic signatures. The first of these zones extends from the western boundary to 30E. It is characterized by one very strong dipolar anomaly with a peak-to-peak amplitude in excess of 14 000 gammas. This number is a minimum since the gradients became so strong that the magnetometer was not capable of making an accurate measurement.

The second distinct zone extends from about 30E to 100E. It is characterized by intermediate-amplitude responses that are also typically dipolar in nature.

The third zone extends from about 100E to the eastern boundary of Area A. In order to see any structure at all in this area, the contour interval must be reduced to 100 gammas. Figure 36 is the same as Fig. 35 except that a 100-gamma contour interval has been superposed.

Soil cap. There is no magnetic response that can be attributed to the presence of the dirt cap. The only location where any effect could be discerned in the eastern side is where the cap thins to no cap at all. Nothing in these data could be interpreted as being a transition zone in this sense. There is no reason to believe that the cap should have a magnetic response. Neither the naturally occurring soil nor the Bandelier Tuff contains much magnetic material.

General's Tanks (A1 and A2). The locations of the two General's Tanks are clearly depicted with the magnetic data. The locations of the two storage tanks based on the magnetic data are marked on Fig. 25 (A1 and A2) and are the same locations as shown on Figs. 1 and 2.

Points at which the strong gradients caused data "dropouts" can be seen at coordinates 10E,26S and 20E,26S. The fact that these data are "bad" indicates that the gradients are stronger at these locations than at any other locations in the vicinity and therefore indicates the presence of two magnetic objects rather than one large object. This is a case in which the data dropouts are part of the key to resolving two objects instead of one. A hint of two objects may also be seen at the northern end of the dipolar anomaly (16E,9S).

Central pit area (C0). The region extending from about 30E out to approximately 90E is characterized by a relatively complex structure of intermediate (>1000 gamma) anomalies. These anomalies are interpreted as resulting from objects placed in the central pit (C0). To encompass all the magnetic anomalies in this region using the pit dimensions given in the Introduction, C0 must be placed as shown on Fig. 25. These dimensions are the smallest dimensions that could surround all the anomalies in this region.

Within C0, there are various large magnetic objects (drums, sheet metal, etc.). It looks as if there are basically three dipolar anomalies within the central zone. They have been marked C1, C2, and C3 on Fig. 25. This should not be considered more than a very rough estimate of the general geometry of objects within the central zone. It would be a mistake to consider these as "three magnetic objects." It is more likely that the three zones represent the combined effect of a variety of highly magnetic objects at each of these locations.

Trenches (B1 and B2). The third region (the area to the east of 90E) is characterized by no response whatsoever with a 1000-gamma contour interval. To interpret this zone, the data are presented on Fig. 36 with a 100-gamma contour interval. There are two parallel, east/west-trending, 200-gamma, dipolar anomalies that represent the two trenches at Area A. Figure 25 shows the location of these trenches as placed by all the geophysical criteria.

Other (D1). The last distinctive feature is a 300-gammma feature (D1) located at 131E,5S. This feature would be consistent with the southern end of a magnetic object extending to the south from outside the gridded area. It could also represent a buried magnetic object such as a steel drum or have something to do with the power line terminus.

5. RADAR

An impulse radar survey of Area A was performed because it had the potential for much higher resolution and depth discrimination than any other technique. Radar is sensitive to changes in the dielectric constant (clay and water primarily). It is dependent on transmission frequency, ground resistivity, and dielectric contrast between the ground and targets.

Commercial ground-penetrating radar (GPR) systems have been developed to locate relatively shallow targets with simple geometries such as buried pipes. We felt it was worth a try given the potential for much higher resolution and the possibility for depth determination.

Impulse radar profiling consists of pulsing the ground with a radar frequency electromagnetic signal and recording the return signals. The time delay between the source

pulse and the return pulse is the travel time from the transmitting antenna to the reflecting medium then back to the receiving antenna. Knowledge of the velocity of the pulse in the medium is necessary to compute the depth to the reflector. The velocity of the medium may be measured directly if there is an object buried at a known depth in that medium or if the dielectric constant of the medium through which the pulse travels is known. Figure 37 depicts a typical radar profile.

The Radar Survey Data at Area A consist of 45 north-to-south data rows 4 m apart. All records start with the radar antenna located at the south boundary fence and proceed to the north. A 0.4-m^2 metal plate was placed under the radar antenna at the beginning and end of each row. These metal reflectors provide a ground surface reference time for each record. A fiducial was placed on the radar strip-chart record when the rear wheel of the radar antenna was next to a stake. The radar antenna was positioned on the west side of the row of stakes. The soil moisture changed from damp in the morning to dry in the afternoon.

5.1 Equipment and Calibration

The radar survey at Area A was performed using an analog Subsurface Interface Radar (SIR) system from Geophysical Survey Systems, Inc. (GSSI), 15 Flagstone Drive Hudson, NH 03051, (603) 889-4841.

The system consists of a Model PR-8304 profiling recorder and a 300-MHz radar antenna/receiver. The SIR's profiling recorder outputs a continuous high-speed strip chart. The strip-chart gray-scale intensity is adjustable with the amplifier and filter controls. The vertical axis of the strip chart represents time in nanoseconds and is adjustable from 0 to 1000 ns.

The penetration of radar signals into soil varies with radar frequency and soil conductivity. Typically, items of known shape and size are buried at a specific depth and located with the radar system in order to determine the attenuation and the velocity of the medium. At Area A, there was no response from any known object and, as such, this type of depth calibration was not possible. Two measurements were performed with the SIR equipment to verify system performance in air and to determine the velocity of unaltered host rock.

Radar reflection and transit time calibration measurements were done using a 3.2-m-thick Bandelier Tuff boulder that had rolled away from the cliff face in the vicinity of Area A. Bandelier Tuff is the rock formation into which waste disposal Area A is cut. The fill material used to close the site is pulverized Bandelier Tuff. The velocity obtained from

this experiment is expected to be similar to the velocity of dry fill material at Area A. Damp fill material will have lower velocities.

The radar unit was turned on its side and laid against the boulder, which had reasonably flat faces. The radar unit was also turned on its back to shoot straight up at the air and at an aluminum sheet placed about 1.8 m above the radar source. This same aluminum sheet was placed on the backside of the boulder in contact with it and at variable distances. Figure 38 illustrates the geometry used. Figure 39 contains the following data:

Column 1 - The radar unit shooting straight up into the air
Column 2 - The radar unit shooting straight up into the air at the aluminum sheet 1.8 m above.
Column 3 - The radar unit against the rock face to find the reflection from the far side of the boulder.
Column 4 - Same as column 3, except that the aluminum plate has been placed against the far face of the rock.
Column 5 - The timing calibration pulses and delay times in nanoseconds.
Column 6 - Same as column 3.
Column 7 - Same as column 4.
Column 8 - Here the plate is not in contact with the rock; it is approximately 0.5 m from the back side of the boulder.
Column 9 - Same as column 8 except that the plate is approximately 1 m from the backside of the boulder.
Column 10 - Same as 8 and 9 with the plate at approximately 2 m.
Column 11 - Same as columns 4 and 7.
Column 12 - Same as columns 3 and 6.

These data indicate 30 cm/ns velocity for the aluminum plate in the air and illustrate that the aluminum sheet could not be detected when it was on the other side of the boulder. Figure 40 presents data with the amplifier and filter setting changed to suppress the first arrival and to enhance the later arrivals. With these data, one does see the arrivals from behind the rock that indicate a velocity through the Bandelier Tuff of 20 cm/ns. Figure 40 contains the following data:

Column 1 - The radar unit against the rock face to find the reflection from the far side of the boulder.
Column 2 - Same as column 3 except that the aluminum plate has been placed against the far face of the rock.
Column 3 - Here the plate is not in contact with the rock; it is approximately 0.5 m from the backside of the boulder.
Column 4 - Same as column 8 except that the plate is approximately 1 m from the backside of the boulder.
Column 5 - Same as 8 and 9 with the plate at approximately 2 m.
Column 6 - Same as 2.
Column 7 - Same as 1.
Column 8 - Calibration pulse with delay times in nanoseconds.

Air radar calibration records were generated before and after the survey by using the west boundary fence as a reflector. The radar antenna was set up facing the 1.5-m-high, woven-wire boundary fence. The antenna was then moved from 0 ft to 18 ft, in increments of 6 ft, and then back again. Figure 41 shows the results of this calibration. The signal transit times were measured and agreed with the theoretical velocity of electromagnetic pulses in air. The columns in Fig. 41 are as follows:

Column 1 - Radar unit at 18 ft from the fence.
Column 2 - Radar unit at 12 ft from the fence.
Column 3 - Radar unit at 6 ft from the fence.
Column 4 - Radar unit at 0 ft from the fence.
Column 5 - Radar unit at 6 ft from the fence.
Column 6 - Radar unit at 12 ft from the fence.
Column 7 - Radar unit at 18 ft from the fence.

5.2 Results

Figures 39 and 40 indicate a signal velocity of 30 cm/ns for the aluminum plate in air and 20 cm/ns for the signal velocity through the Bandelier Tuff boulder. These data also indicate that the aluminum sheet could not be detected when it was on the backside of the calibration boulder without the filter and gain settings specifically adjusted to enhance that particular reflection.

From Figs. 39 and 40 one can see that the radar unit is very sensitive to the filter and gain settings, which must be set qualitatively by the operator in the field. At Area A we observed the reflection trace on an oscilloscope while passing over some of the easiest targets on site. We profiled directly over the large storage tanks and also the two trenches. There was nothing apparent either on the recorded traces or on the oscilloscope that would have helped us adjust the filter and gain settings for the overall site. Therefore, the settings used were our best guess, based on the oscilloscope information.

None of the major features present at Area A were detected with the radar survey. There are two explanations for this. First, the equipment is quite sensitive to the manner in which the gains and filters are set. There is no way to establish if these were adequate for Area A. We did observe the signal with an oscilloscope to determine if the metal storage tanks and the pits could be detected. We could find no combination of settings that detected the features. For this reason, we do not feel that the detection problem lies with the settings. Second, the conductivity of the ground was too high for the sensitivity of the machine. Both the resistivity and the EMI techniques indicate the cap and fill to be 60-70

ohm-m. The skin depth for this resistivity at 300 MHz is 0.2 m (approximately 43 dB/m), thereby limiting the depth of investigation of this radar system to approximately 1 m.

On the east side of the area, the cap is thin and it overlies highly resistive rock and resistive trenches. The only explanation we have for why the trenches were not detected is that the dielectric constant of the crushed Bandelier Tuff (fill material) and the *in situ* Bandelier Tuff is the same. If this is the case, then it is impossible for any radar system to detect pit edges in the Los Alamos waste disposal environment. It is difficult, however, to conceive of a geologic situation in which a large conductivity contrast will not also result in a change in the dielectric constant.

Figures 42-45 are profiles taken directly over the metal storage tanks (A1 and A2). Figure 46 is a profile taken in the region between the tanks and the central pit. There are no obvious differences between these profiles. Figures 47-49 are profiles taken directly over different parts of the two trenches on the east side of the area. There is nothing obvious in the data that indicates trenches. The profiles listed run north/south on grid lines and correspond to the following lines:

Figure	Run Number	Profile
42	6	12E
43	7	16E
44	8	20E
45	9	24E
46	10	28E
47	28	100E
48	31	112E
49	32	116E

Careful inspection of the profiles shows 300-MHz impulse radar to be ill suited for Area A (and in general the Los Alamos environment) in terms of penetration depth and ability to locate pit and trench boundaries. The system was plagued with problems during the survey. For instance, the system as it came from the factory contained enough metal to create a severe ringing problem. This has since been remedied. Other problems are inherent in the design of the system. It appears to be very sensitive to exactly how the operator "tweaks" the gain and filter controls. Radar may prove to be useful in the future, but the field procedures and equipment used at Area A did not result in useful data.

For this type of work, 300 MHz is too high a frequency; 80 MHz is more appropriate. Data should not be taken in continuous mode; instead, a single measurement should be taken at each sample point for a short period of time. This procedure should reduce the noise in the data due to the sensors' motion and poor coupling to the ground. It would also make it easier to scale the data so that the records are easily compared. It would

be much better to use a unit that has a separate transmitter and receiver, thereby allowing velocity and depth to be measured directly over almost any detectable feature.

6. ELECTROMAGNETIC INDUCTION

An EMI survey was performed at Area A to locate metallic conductors such as pipes, drums, and sheets of aluminum. Highly conductive regions such as those resulting from wet clay will also be located in this manner. The combination of EMI measurements with magnetic measurements provides a way to distinguish between magnetic metals such as steel drums and nonmagnetic metals such as aluminum sheets. The combination of EMI with resistivity covers the entire spectrum of electrical targets.

EMI techniques are those that induce an electromagnetic field into the target and observe its effect either as a function of time or as a function of phase distortion. The technique used at Area A is of the latter type and uses two horizontally oriented coils separated by 3.66 m. One coil produces the source (inducing) field and the other measures the induced field.

The quantity measured is the voltage induced in the receiving coil by both the transmitter source field and the fields generated in nearby materials by the source coil. The in-phase received voltage is normalized to the primary signal and presented in parts per thousand (ppt). The quadrature component (out-of-phase component) is converted to apparent conductivity and is presented in millisiemens per meter (mS/m), or the equivalent millimhos per meter (mmho/m).

At each measurement point, both the in-phase and out-of-phase (quadrature) components were measured in the vertical dipole configuration (horizontal coplanar coils). The instrument was held at hip level (approximately 1 m). Measurements were made with the boom parallel to the grid line and centered directly over the plotted point. The instrument was always oriented such that the receiver coil was to grid east and the transmitter coil to the west. Data were recorded automatically in digital form for uploading to a computer.

6.1 Equipment and Calibration

The device used was the Geonics EM-31; it is manufactured by Geonics Limited, 1745 Meyerside Dr. Unit 8, Mississauga, Ontario, Canada L5T 1C5,(416) 676-9580. Geonics interfaced the EM-31 to a data-storage device, which enables the operator to monitor the analog display (apparent conductivity or in-phase amplitude) while the in-phase and quadrature voltages are automatically stored for transfer to a computer. Geonics software uploads the data from the polycorder storage device to the computer and converts

the stored voltages to apparent conductivity (mS/m) and normalized in-phase in ppt. The Polycorder Electronic Notebook is manufactured by Omnidata International, Inc., 750 West 200 North Logan, UT 84321, (801) 753-7760.

The EM-31 consists of a transmitting loop, which creates a 9.3-kHz primary field, and a receiver, which measures the induced field. The coils are separated by 3.66 m and were oriented horizontally.

Calibration was monitored in accordance with the operators manual at station 30S,40E. The receiver zero reading, zero compensation adjustment (in-phase), and the phase adjustment were checked at the beginning and end of each survey line. The equipment was stable and only minor adjustments (<5%) in the in-phase compensation were required. The data are accurate to about 5%. Lines E and I were surveyed twice to demonstrate repeatability (Figs. 50-53).

6.2 Results

The results of the EMI survey are presented in Figs. 54-58. Figure 54 shows the in-phase component measured in ppt. Figure 55 presents the quadrature data in units of conductivity (mmho/m). Figures 56 and 57 are the same data as in Figs. 54 and 55, but they have been gently filtered to smooth the response. The filter that has been applied is a five-point matrix mask that averages the value of the center point with its four closest neighbors. The central point is weighted twice the value of the other four points.

Figures 54-57 show three distinct zones. The zone west of 30E has the in-phase instrument response off scale and at its maximum (31.6 mS/m) because of the massive amounts of metal in the General's Tanks. Between 30E and 85E there is a zone that shows a complex response due to a variety of objects. The response east of 85E is flat with the exception of three east/west-oriented features. The western two features result from objects placed in the two trenches (Fig. 4).

We have deleted 8 out of the 1500 data values. These data are not considered bad measurements; they are individual measurements that do not fit with the surrounding ones. These points result from the presence of small objects (less than about 0.25 m in area) very near to the surface. We replaced each deleted value with the average of its closest three or four neighbors. This is equivalent to removing the inhomogeneity and presenting the data without it. All the deleted data points are listed below.

	Original Value		Replaced Value	
	Quadrature (mS/m)	In-phase (ppt)	Quadrature (mS/m)	In-phase (ppt)
28S,14E	2.34	11.9	24.1	11.9
30S,12E	-4.60	5.2	23.2	5.2
32S,12E	-9.46	3.9	25.6	3.9
34S,12E	-9.48	11.3	45.4	11.3
16S,96E	-3.90	-8.0	8.7	-1.8
16S,100E	-5.47	-9.4	5.5	-1.0
44S,138E	-9.57	13.4	66.7	13.4
44S,144E	-7.50	24.4	38.5	24.4

The sampling interval is too large to adequately define these objects. A finer grid in the vicinity of the points would accurately define them. The points on line 12E are adjacent and indicate the presence of a long thin disturbance.

Soil cap. The quadrature component of the EM-31 data shows the conductivity of the cap, in an area where there has been no excavation (vicinity of 25E,35S), to be about 15 mS/m (67 ohm-m). Over the central pit, the conductivity is approximately 22 mS/m (45 ohm-m). These data show that the fill material and cap material are more conductive than the undisturbed rock and that the cap is less conductive than the interior of the central pit.

General's Tanks (A1 and A2). The storage tanks were well delineated by both the in-phase component and quadrature components of the field. The responses were so strong that the instrument was not capable of an accurate reading. It would be impossible to delineate two storage tanks from one large metallic object with the in-phase component of the data, but the location of the outside perimeter of the tanks is decisive. These EMI data present the cleanest and clearest picture of the tanks. The quadrature component of the field is strongly distorted in the region surrounding the tanks and is capable of resolving two objects rather than one (Fig. 58). There is a conductive zone approximately over each tank and a resistive zone between them.

Central pit (C0). The central pit shows complex responses that, for the most part, indicate metallic conductors. The quadrature component of the data shows very little character as compared with the in-phase component. The boundary of the pit is delineated by the EMI data only in the sense that the pit must contain all the objects detected and that the overall electrical response of the pit area is distinctly different from the surrounding area. The pit location boundaries as depicted on Fig. 25 (C0) were calculated by requiring

that the boundaries encompass all the anomalies detected in the region. The pit size shown is the minimum size that meets these requirements.

The apparent conductivity of the pit region is about 22 mS/m (45 ohm-m) as compared with 15 mS/m (67 ohm-m) outside the pit area. Anomaly C1 corresponds to the large ductwork illustrated in the background of Figs. 12-15. Anomaly C2 corresponds nicely to the material dumped over the edge of the pit (Fig. 15). Anomaly C3 is located in the vicinity of the ductwork shown in the foreground of Figs. 12, 14, and 15; however, it does not have an associated in-phase anomaly. C3 probably does not result from the ductwork pictured in these figures.

Trenches (B1 and B2). The EM-31 survey shows the presence of two east/west-trending pits. These data do not, however, represent the true dimensions of the trenches. According to the EM-31 data, the lengths of the trenches are 17 m and 23 m (north and south respectively). The lengths of the pits from the magnetic and resistivity data and the engineering drawing (Fig. 2) are 30 m. EMI and resistivity techniques respond to different electrical regimes and should not be used interchangeably as demonstrated by the fact that the EMI did not detect the eastern side of the trenches, whereas the resistivity did.

7. CONCLUSIONS

At Area A, remote geophysical measurements were definitive in locating and characterizing all known targets as well as discovering several undocumented ones. With these data and the resulting Area A image, we can safely perform necessary remedial activities such as monitoring, drilling, and relocating material without the fear of breaching an unknown or misplaced storage facility. The following is a summary of important conclusions resulting from this work:

1. The location and geometry of the General's Tanks (A1 and A2) as documented and as presented in Figs. 1 and 2 is accurate.

2. The two trenches (B1 and B2) and pit (C0) are located about 5 m to the east of what is shown on Figs. 1 and 2. This discrepancy should be considered in any future activities concerning Area A.

3. There are three anomalies (D1, D2, and D3) that are not documented. These areas should receive special consideration when drilling, placing sensors for monitoring, or relocating material from or into Area A.

4. The velocity of radar propagation in unaltered Bandelier Tuff is 20 cm/ns and will attenuate a 300-MHz radar pulse at about 10 dB/m (1000 ohm-m).

5. The resistivity of the cap material (pulverized Bandelier Tuff) is about 65 ohm-m and will attenuate a 300-MHz radar signal at about 43 dB/m.

6. The GSSI 300-MHz radar system is too noisy and not capable of sufficient penetration to be useful at areas similar to Area A without significant modification of the equipment and/or field procedures.

7. Care must be taken with the Geometrics proton precession magnetometer in the presence of strong magnetic field gradients. Regular tuning is necessary and high gradients can compromise measurements.

The interpretation of these data is based on the the best fit between the dimensions and geometry of the expected targets as shown on Figs. 1 and 2 and the geometry and location of geophysical anomalies (resistivity, self-potential, magnetics, and electromagnetic induction). Ground-penetrating radar profiles were also obtained but did not provide useful information about the site. The geophysical image (Fig. 25) was obtained by combining the results of all the techniques except radar and determining the combination of regions that yields the simplest, physically plausible explanation.

It is, of course, much easier to image an area when one has specific targets than to image a completely unknown area. The geophysical techniques employed at Area A would have been definitive in locating the General's Tanks and the trenches even without the benefit of the engineering drawings (Figs. 1 and 2) or any other prior knowledge. The pit (C0) may not have been well identified. No definitive boundaries were found that would suggest a single entity rather than three separate targets.

Each of the geophysical techniques used at Area A resulted in information unique to that technique. The combination of electromagnetics, resistivity, and magnetics provided an image of the ground that is not available with any of the techniques individually. All three of these techniques were necessary to unambiguously locate the trenches (B1 and B2), and all three techniques were necessary to determine that the west and east ends of the trenches contain fundamentally different material.

Resistivity is the only technique that identified anomaly D2, which is a resistive target residing in a resistive environment. EMI failed to detect this feature at all. Resistivity provided the clearest image of the two trench locations and established the electrical environment in the pit (45-70 ohm-m).

Self-potential was performed to determine if the material buried in Area A perturbs the static electric field in the ground. Many of the metallic conductors at Area A are generating electric fields. Anomaly D3 is a strong SP anomaly that is transparent to the rest of the techniques and is in close proximity to the General's Tanks. The source mechanisms for these voltages are not well understood. With further research the technique may prove valuable in assessing the probability of corrosion in certain types of objects.

Magnetic field strength measurements were definitive in locating the General's Tanks and establishing that much of the material buried at Area A is composed of magnetic alloys. It was necessary to integrate the EMI with the magnetic data to characterize the central pit, and it was necessary to integrate the resistivity with the magnetic data to image the trenches. There were some difficulties obtaining reliable field strengths. Care must be taken with the Geometrics proton precession magnetometer in the presence of strong magnetic field gradients. Regular tuning is necessary to assure sufficiently high field strength for accurate measurement, and the strong gradients themselves can compromise accuracy.

Radar profiles show the promise of being able to determine depth to objects and delineate them with higher resolution than any other method. Unfortunately, the equipment and procedures used at Area A did not result in useful data. None of the targets were detected; no pit or trench boundaries were delineated. There are some fundamental problems with the radar system. The maximum depth of penetration, for the GSSI system used, is 1 m (43 dB/m), and the computed velocity through the Bandelier Tuff is 20 cm/ns. This implies that only the first 10 ns of data contains unambiguous information from the subsurface. Cross-coupling between the transmitter and receiver antennas is strong during the first 10 ns of data, thereby compromising the results. This difficulty seems to arise from an impedance mismatch between the antennas and the ground. Radar still has the potential for an effective role in waste disposal area evaluation but only in special circumstances with carefully chosen equipment.

Electromagnetic induction was definitive in locating the General's Tanks and played the most important role in establishing the three zones within the pit boundaries (C1, C2, and C3). EMI demonstrated that the western side of the trenches contains fundamentally different material than the eastern sides.

7.1 General's Tanks

A1	6.1S, 8.0E	6.1S,11.6E	25.3S,11.6E	25.3S, 8.0E
A2	6.1S,16.6E	6.1S,21.0E	25.3S,21.0E	25.3S,16.6E

The storage tanks at the eastern side of Area A are located exactly as they are pictured in Figs. 1 and 2. The resistivity, EMI, and magnetics are decisive in east/west positioning; the north/south uncertainty is about 2 m. The magnetic and EMI signatures were the most definitive, the in-phase component of the EMI for location, and the magnetic field for resolving two objects. The combination of magnetics and EMI indicates that the

tanks are steel and therefore susceptible to corrosion. There is a large negative SP anomaly (D3) adjacent to tank A2 but definitely displaced to the east. If a corrosive environment in close proximity to the tank is of concern, then this anomaly should be investigated further.

There is no reason to believe that the tanks themselves are corroding because there is no strong SP anomaly associated directly with them. Radar data taken in the vicinity of the tanks show no changes that could be attributed to the tanks themselves or to any structure related to the tanks.

7.2 Central Pit

C0	4.5S,37.0E	4.5S,90.0E	44.5S,90.0E	44.5S,37.0E
C1	6.0S,40.0E	5.0S,65.0E	12.0S,67.0E	21.0S,41.0E
C2	43.0S,43.0E	30.0S,50.0E	29.0S,58.0E	43.0S,70.0E
C3	9.0S,72.0E 29.0S,76.0E	9.0S,88.0E	30.0S,88.0E	27.0S,83.0E
C4	42.0S,77.0E	36.0S,79.0E	36.0S,86.0E	42.0S,84.0E

The central pit is displaced about 5 m to the east of the location shown in Fig. 1. The pit boundaries were not detected directly by any technique. The east/west boundaries in Fig. 25 were placed by superposing Fig. 2 and all the geophysical data to find the best fit. The north/south boundaries were located from photographs (Figs. 9 and 12). The pit geometry is best delineated with a combination of EMI and resistivity data.

Radar data did not detect any consistent changes that could be related to pit boundary locations, overburden thickness, or the depth to any of the targets within the pit.

Figure 17 shows the location of the western boundary of the central pit relative to the positions of the telephone poles. The position of the poles relative to the fence line and the relative distance between the poles themselves indicate that the poles in Fig. 17 are the same poles that exist today (Fig. 58). By this line of reasoning, the western edge of the pit is about 16 m west of the pole closest to C1, which is the location derived from the geophysical data. Figure 17 was not available until well after the geophysical interpretation had been made.

C1. C1 is a group of discrete electrically conductive, magnetic objects with an associated negative SP anomaly. At least some of these objects are magnetic material (i.e., steel). Objects at 51E,6S and 51E,15S are closest to the surface.

C2. C2 is another conductive zone similar to C1. It, too, has a strong magnetic signature and an SP low. The main conductors in this zone occur at points 48E,42S; 52E,35S; 54E,28S; and 64E,40S. The first of these objects is the nearest to the surface and is the only one that does not have a prominent magnetic response. This object is

probably a nonmagnetic metal. C2 corresponds to the material that was dumped into the pit from the south rim as pictured in Fig. 15.

C3. The last major conductor in the pit, it is relatively near the surface, not very magnetic, and has a negative SP anomaly associated with it.

7.3 Trenches

B1	13.0S,90.6E	13.0S,120.9E	17.6S,120.9E	17.6S,90.6E
B2	26.8S,90.6E	26.8S,120.9E	31.4S,120.9E	31.4S,90.6E

These two trenches are displaced 5 m to the east of what is presented in Fig. 1. The trenches are more resistive than the hosting Bandelier Tuff and contain small amounts of magnetic material scattered throughout. There is a distinct difference between the contents of the eastern and western halves of the trenches. The western halves contain metallic conductors, whereas the eastern sides do not. The conductors are probably embedded within a very resistive matrix and are nonmagnetic (i.e., aluminum).

The trenches were detected by all the geophysical techniques except radar and SP. The EMI data clearly show the presence of two east/west-trending pits. However, only the western halves were detected. According to the EM-31 data, the lengths of the trenches are only 17 m and 23 m (north and south respectively). The magnetic and resistivity data and the engineering drawing (Fig. 2) indicate 30-m lengths. This result clearly shows that the EMI and resistivity techniques are sensitive to different regimes and may not be used interchangeably.

Radar lines placed directly over the trenches failed to detect any consistent change in response that could be related either to the trenches themselves or to the transition from trench to Bandelier Tuff. It is unlikely that the cap thickness in this area exceeded 1 m. There is "character" in these profiles over the western side of the northern trench. However, there is character in many locations and one would not be able to find this target out of all the other clutter.

7.4 Other Features

D1	2.0S,132.0E	9.0S,131.0E	13.0S,129.0E	15.0S,129.0E
	15.0S,127.0E	9.0S,124.0E	2.0S,126.	
D2	34.3S,128.0E	31.0S,135.4E	36.0S,137.7E	39.0S,130.4E
D3	7.9S, 23.8E	11.1S, 28.9E	15.0S, 23.8E	11.1S, 21.3E

The features described in this section are geophysical anomalies that indicate the presence of undocumented objects. They are multipoint anomalies that locate real changes in the subsurface. It is unlikely that they occur as a part of the natural environment.

D1. This feature is associated with the terminus of the power line and is unconstrained to the north. The magnetic response of this anomaly could result from either the southern boundary of a horizontally oriented object or from objects of small lateral extent. There appear to be two discrete objects: one centered close to 9S,127E and another close to 2S,128E. The apparent resistivity response of D1 indicates a zone of increased resistivity (approximately 4 ohm-m above background). There is no associated EMI or SP response.

D2. This feature is defined only by resistivity data. For the object to affect resistivity and not the EMI data, it must be a highly resistive body sitting in a very resistive host environment.

D3. This anomaly is defined only by a negative SP signature. This anomaly should be investigated further if corrosion of the General's Tanks is considered a serious problem. The fact that the anomaly is slightly to the east of the tanks may indicate that the tanks are not involved.

7.5 Summary of Anomaly Coordinates

A1	6.1S, 8.0E	6.1S, 11.6E	25.3S, 11.6E	25.3S, 8.0E
A2	6.1S,16.6E	6.1S, 21.0E	25.3S, 21.0E	25.3S,16.6E
B1	13.0S,90.6E	13.0S,120.9E	17.6S,120.9E	17.6S,90.6E
B2	26.8S,90.6E	26.8S,120.9E	31.4S,120.9E	31.4S,90.6E
C1	6.0S,40.0E	5.0S, 65.0E	12.0S, 67.0E	21.0S,41.0E
C2	43.0S,43.0E	30.0S, 50.0E	29.0S, 58.0E	43.0S,70.0E
C3	9.0S,72.0E	9.0S, 88.0E	30.0S, 88.0E	27.0S,83.0E
	29.0S,76.0E			
C4	42.0S,77.0E	36.0S, 79.0E	36.0S, 86.0E	42.0S,84.0E

ACKNOWLEDGMENTS

The work presented here represents the time and effort of many people. We would like to thank C. L. Edwards (ESS-3, Group Leader) for supplying personnel to acquire data, Caroline Reynolds and Micheline Devaurs (HSE-12) for their patience and support during all phases of the work, Jay Wenzel (HSE-ER) for being a willing listener and supporter, and Rick Montoya, Dan Cash, Ken Green and Tim Long (ESS-3) for spending time in the field collecting data. Diane Baker (ESS-3) helped input much computer data. Thank you all.

REFERENCES

Bogoslovsky, V. V., and A. A. Ogilvy, 1973, Deformations of Natural Electric Fields Near Drainage Structures, Geophysical Prospecting, V. 21, pp. 716-723.

Christensen, E. L., R. Garde, and A. M. Valentine, 1975, Demolition of Building 12, An Old Plutonium Filter Facility, Los Alamos Scientific Laboratory report LA-5755, Los Alamos, NM.

Corwin, R. F., and D. Hoover, 1979, The Self-potential Method in Geothermal Exploration, Geophysics, V. 44, no. 2, pp. 226-245.

Greenhouse, J. P., and R. D. Harris, 1983, Migration of Contaminants in Groundwater at a Landfill: A Case Study, Journal of Hydrology, V. 63, pp. 177-197.

Greenhouse, J. P., and D. D. Slaine, 1986, Geophysical Modelling and Mapping of Contaminated Groundwater Around Three Waste Disposal Sites in Southern Ontario, Canadian Geotechnical Journal, V. 23, pp. 372-384.

Harper, J. R., and R. Garde, 1981, The Decommissioning of TA-21-153, A Contaminated Old Filter Building, Los Alamos National Laboratory report LA-9047-MS, Los Alamos, NM.

Koerner, R. M., A. R. Lord, Jr., S. Tyagi, and J. E. Brugger, 1982, Use of NDT Methods to Detect Buried Containers in Saturated Silty Clay Soil, Proc. of Management of Uncontrolled Waste Sites, 5th Nat. Conf., Washington, DC, pp. 12-16.

Koerner, R. M., and A. R. Lord, Jr., 1984, NDT Location of Containers Buried in Saline Contaminated Soils, Proc. of Management of Uncontrolled Waste Sites, 5th Nat. Conf., Washington, DC, pp. 158-161.

Lord, A. E., R. M. Koerner, and F. J. Freestone, 1982, The Identification and Location of Buried Containers via Non-destructive Testing Methods, Journal of Hazardous Materials, V. 5, pp. 221-233.

Lord, A. E., Jr., and R. M Koerner, 1986, Non-Destructive Testing (NDT) for Location of Plastic Containers Buried in Soil, Hazardous Material Spills Conf. Proc., St. Louis, Missouri, pp. 539-545.

McNeil, J. D., 1982, Electromagnetic Resistivity Mapping of Contaminant Plumes, Proc. Management of Uncontrolled Hazardous Waste Sites, Washington DC, pp. 1-6.

Olhoeft, G. R., 1986, Direct Detection of Hydrocarbon and Organic Chemicals with Ground Penetrating Radar and Complex Resistivity, Proc. of the National Water Well Assoc. Conf. on Petroleum Hydrocarbons and Organic Chemical in Ground Water, Houston, Texas, pp. 1-22.

Rogers, Margaret A., 1977, History and Environmental Settings of LASL Near-Surface Land Disposal Facilities for Radioactive Wastes (Areas A, B, C, D, E, F, G, and T), Los Alamos Scientific Laboratory report LA-6848-MS, Vol. 1,

Sato, M., and H. M. Mooney, 1960, The Electrochemical Mechanism of Sulfide Self-potentials, Geophysics, V. 25, no. 1, pp. 226-249.

Saunders, W. R., and R. M. Germeroth, 1985, Electromagnetic Measurements for Subsurface Hydrocarbon Investigations, Proc. of the Petroleum Hydrocarbon and Organic Chemicals in Ground Water, Houston, Texas, pp. 310-321.

Stanfill III, D. F., and K. S. McMillan, 1985, Inspection of Hazardous Waste Sites Using Ground-Penetrating Radar (GPR), Proc. of the Nat. Conf. on Hazardous Waste and Environmental Emergencies, Cincinnati, Ohio.

Telford, W. M., L. P. Geldart, R. E. Sheriff, and D. A. Keys, 1976, Applied Geophysics, Cambridge University Press.

Tyagi, S., A. E. Lord, Jr., and R. M. Koerner, 1983, Use of a Very-low-frequency Electromagnetic Method at 9.5 kHz to Detect Buried Drums in Sandy Soil, Journal of Hazardous Materials, V. 7, pp. 353-373.

Tsuneo, I., S. Toshihiko, and Takashi Kanemori, 1987, Use of Ground-probing Radar and Resistivity Surveys for Archaeological Investigations, Geophysics, V. 52, no. 2, pp. 137-150.

Walther, E. G., D. LaBrecque, D. D. Weber, R. B. Evans, and J. Jeffrey Vann EE, 1983, Proc. of Management of Uncontrolled Hazardous Waste Sites, Washington, DC, pp. 28-36.

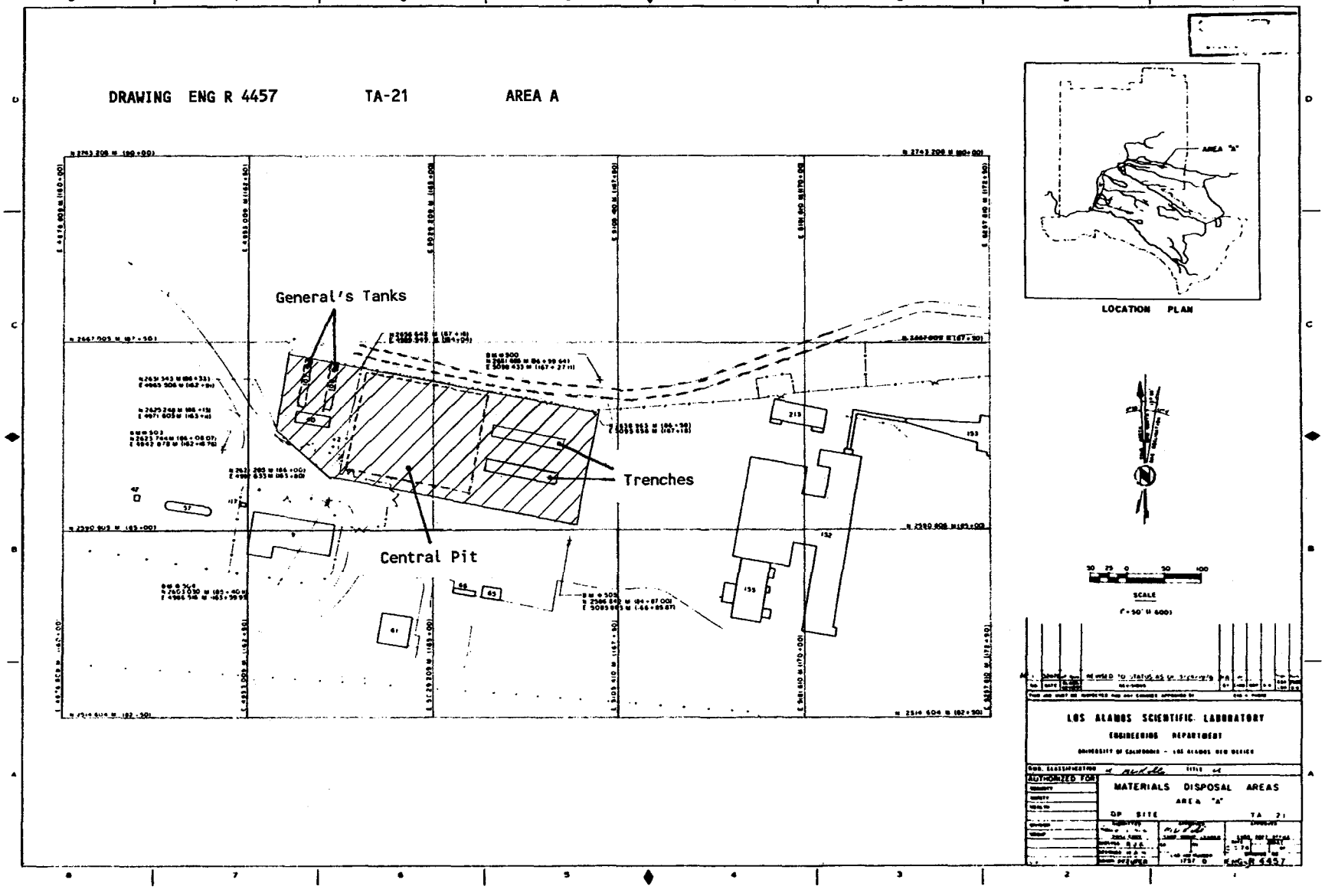

Fig. 1. Location map for TA-21 and materials disposal Area A (Rogers 1977).

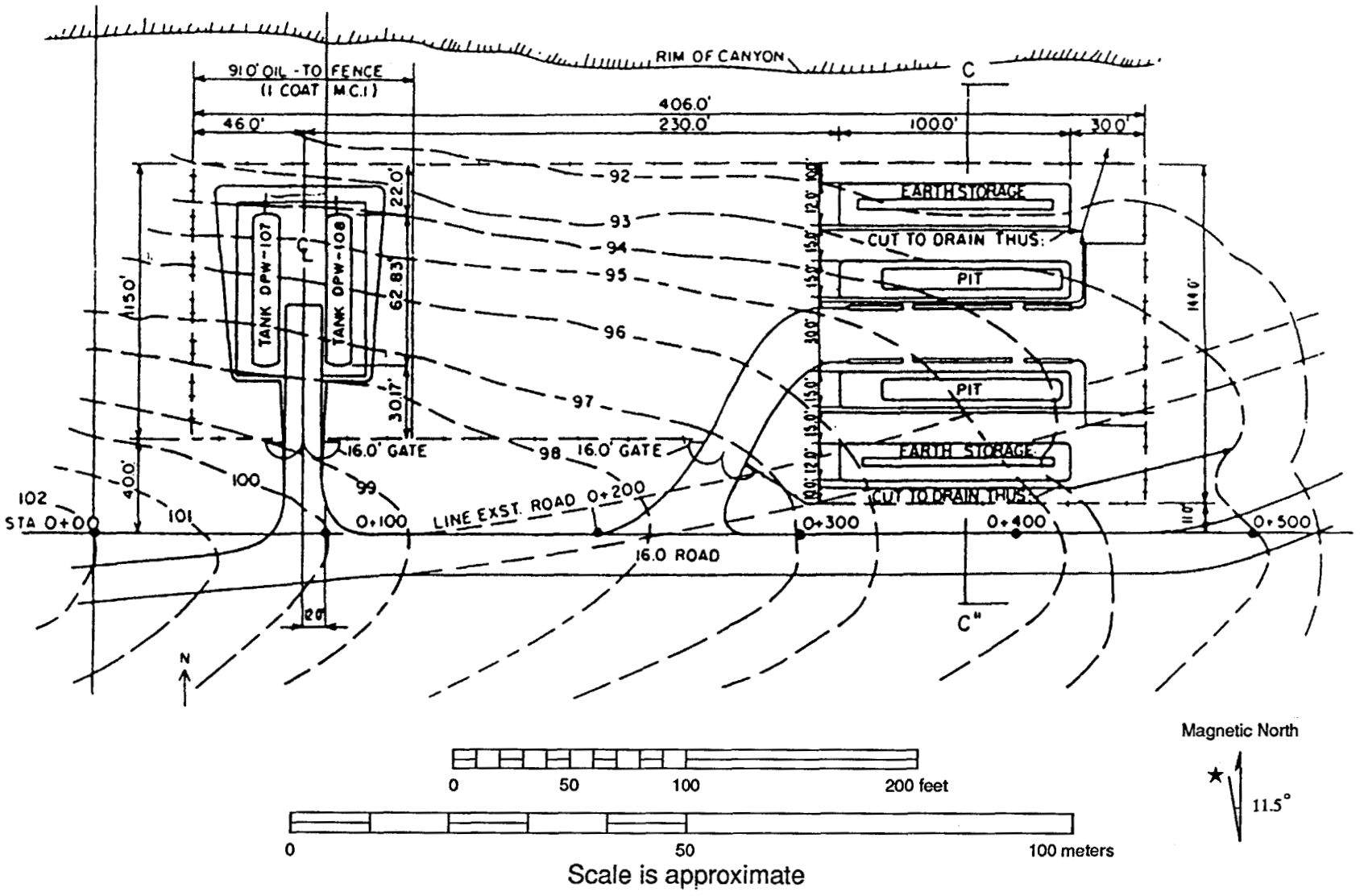

Fig. 2. Construction plan for Area A, January 24, 1945 (Rogers 1977).

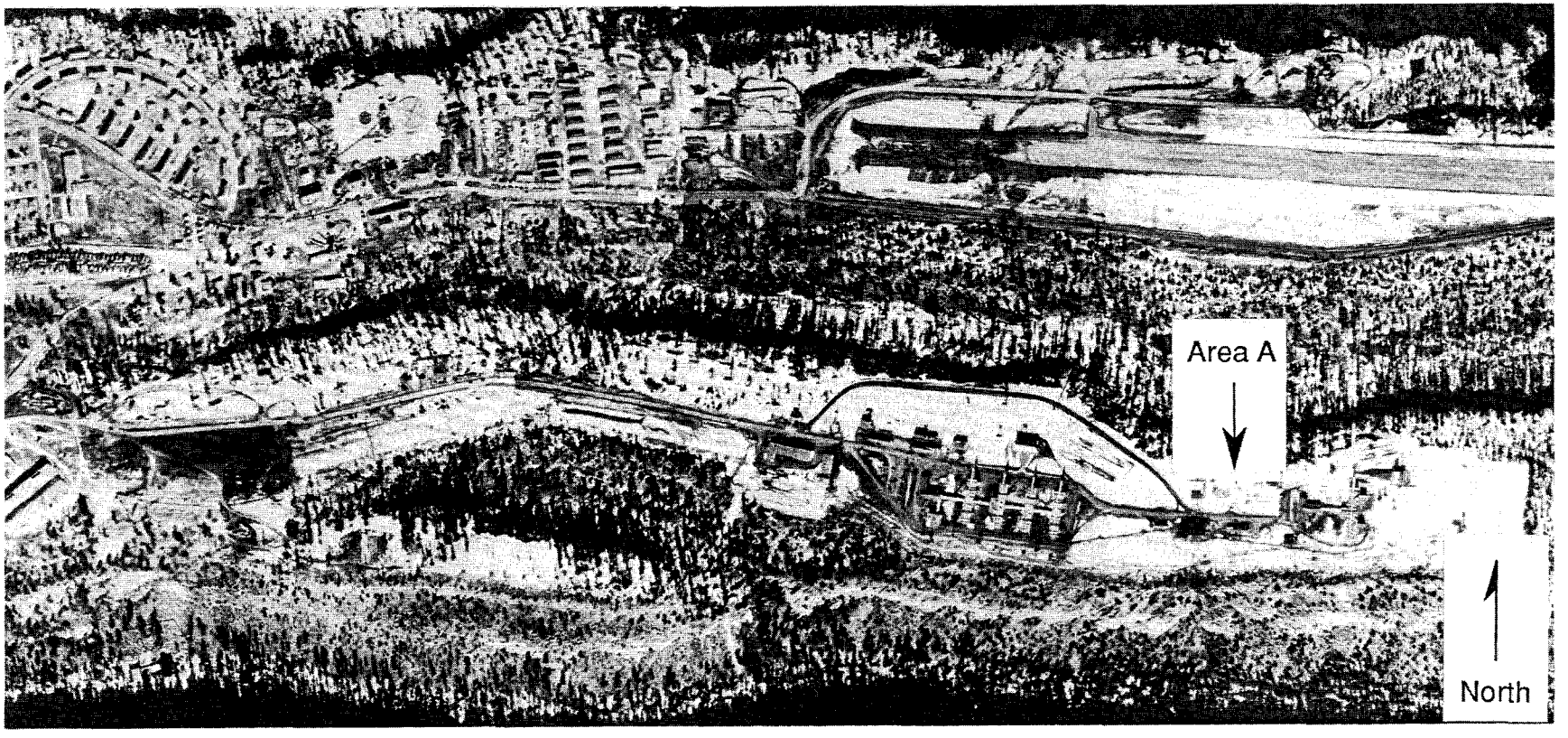

Fig. 3. Aerial photograph of TA-21 and Area A showing two trenches on the eastern side (1947).

Fig. 4. Photograph taken in 1948 showing waste in the two east side trenches. The small building and raised ground (background) are located above the General's Tanks.

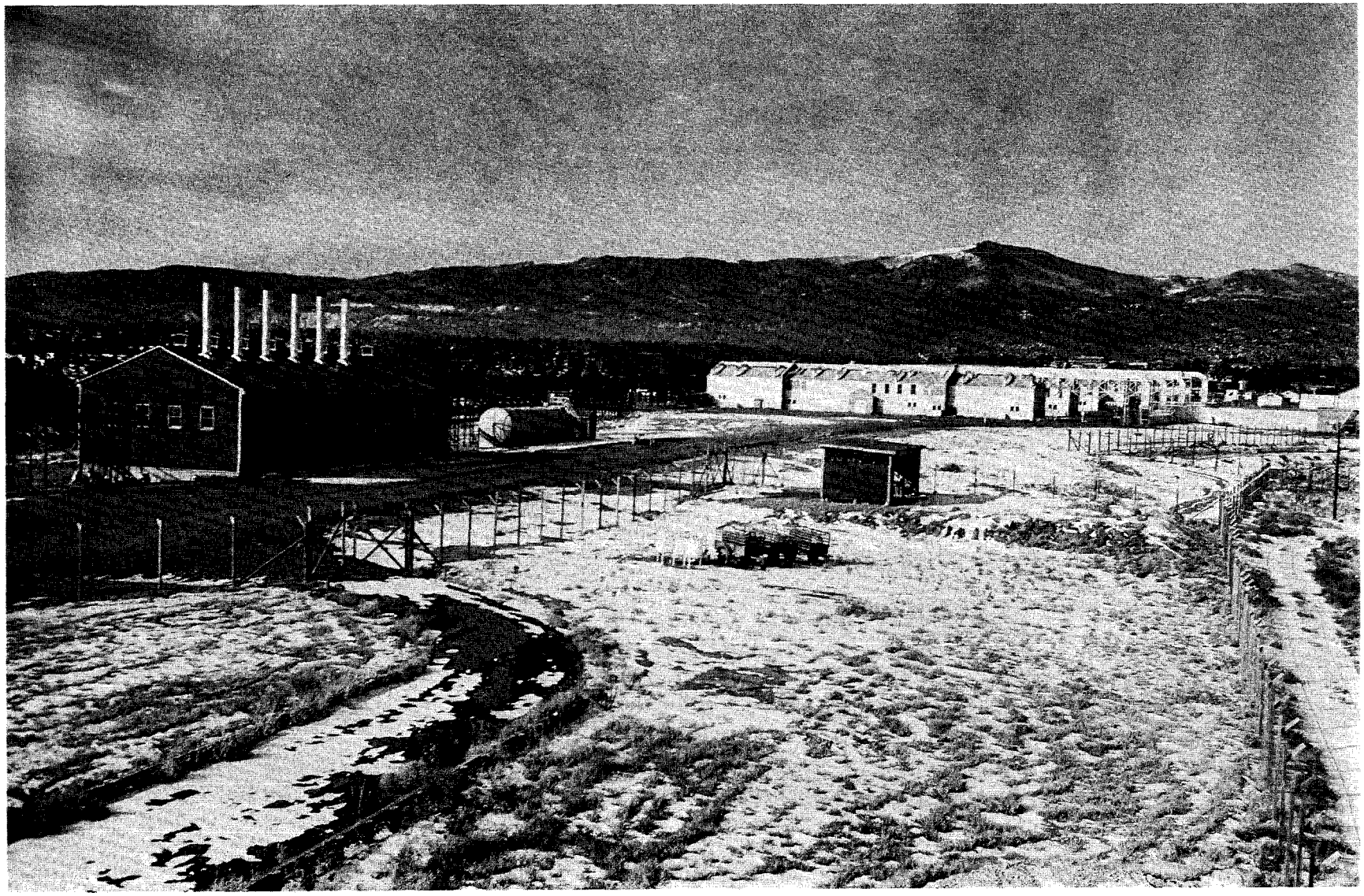

Fig. 5. Photograph of Area A taken between 1945 and 1948.

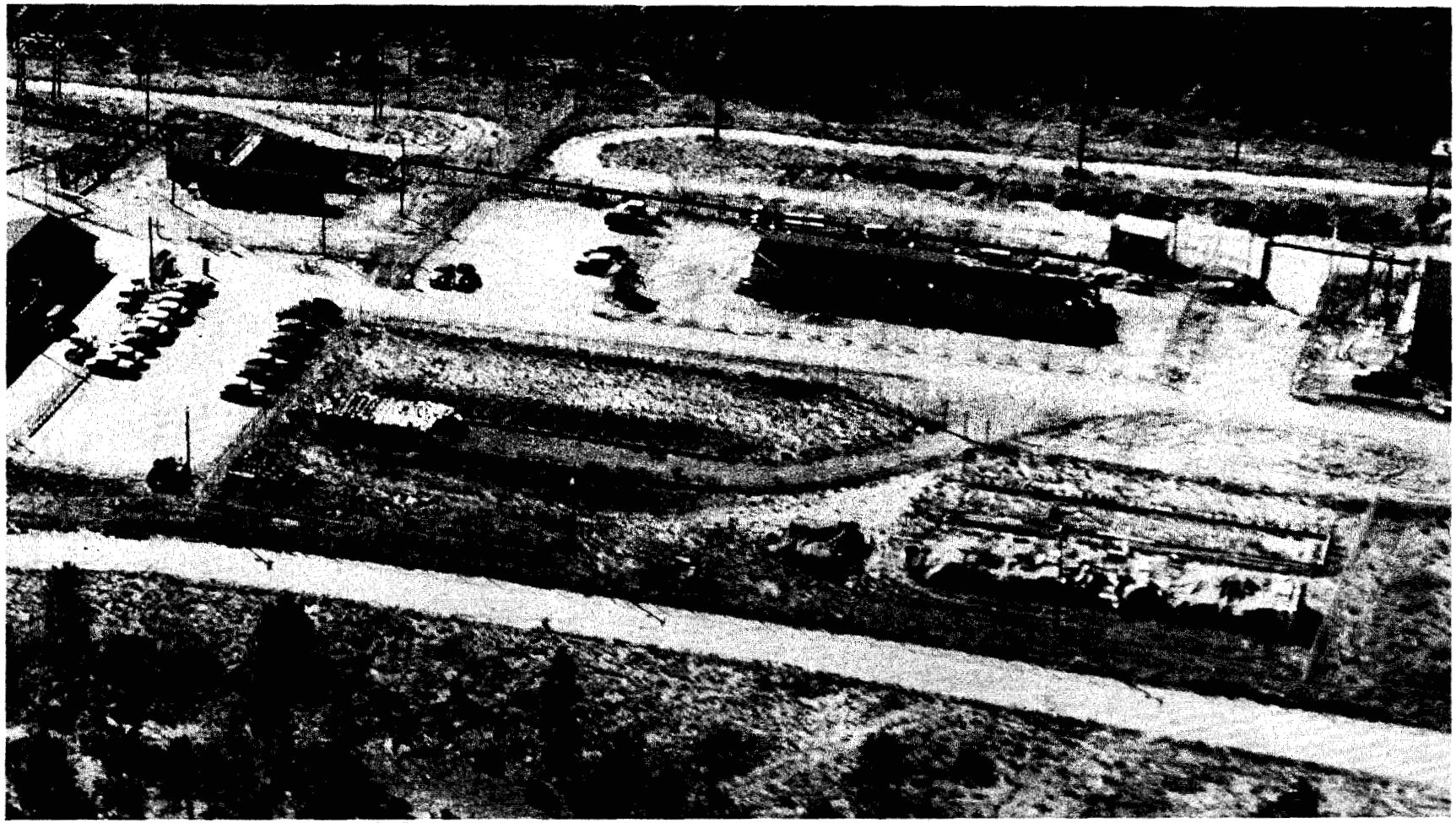

Fig. 6. Aerial photograph (January 1949) showing stored drums on the eastern third of the site (left side, next to parked automobiles).

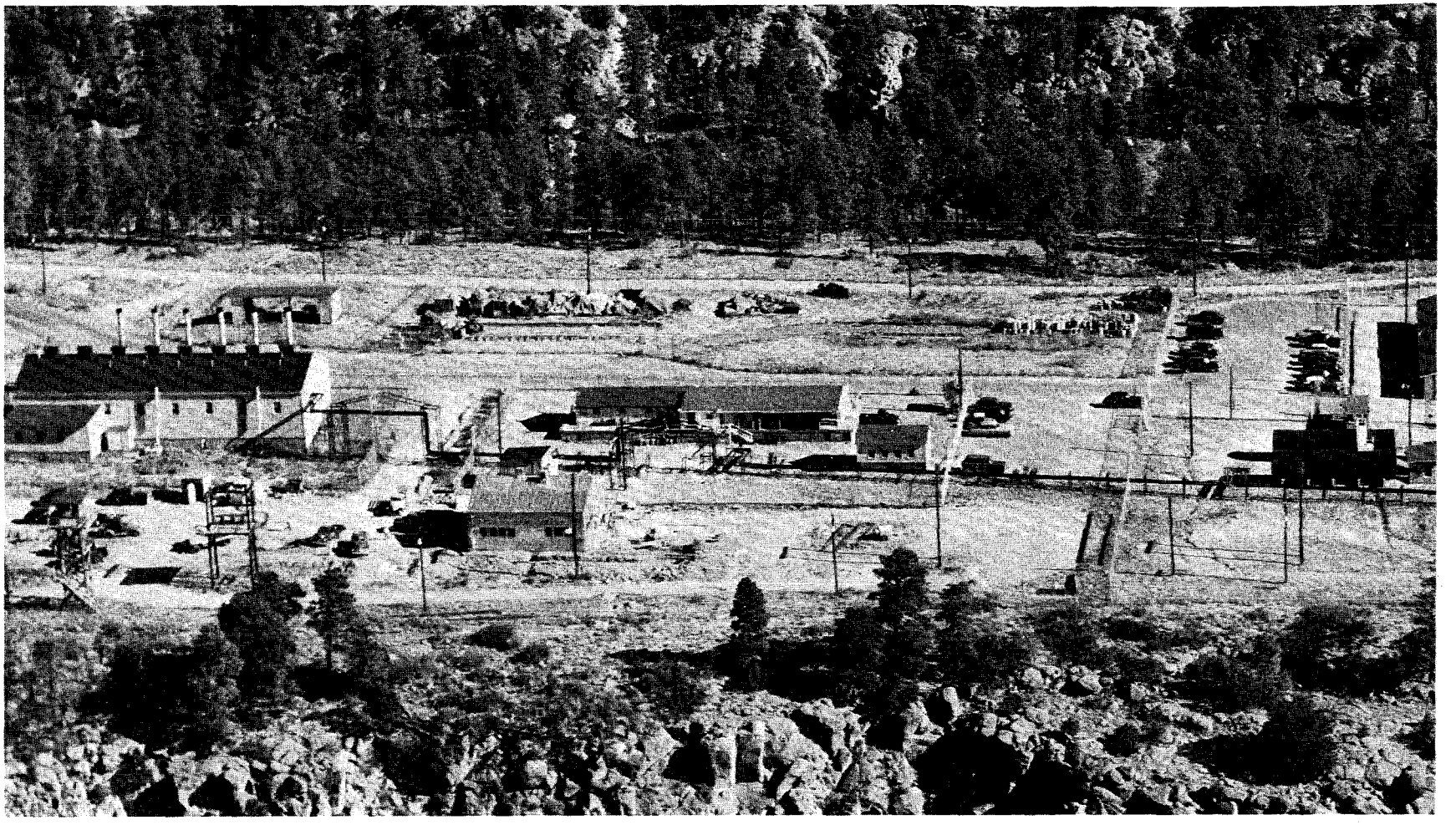

Fig. 7. Aerial photograph (September 1950).

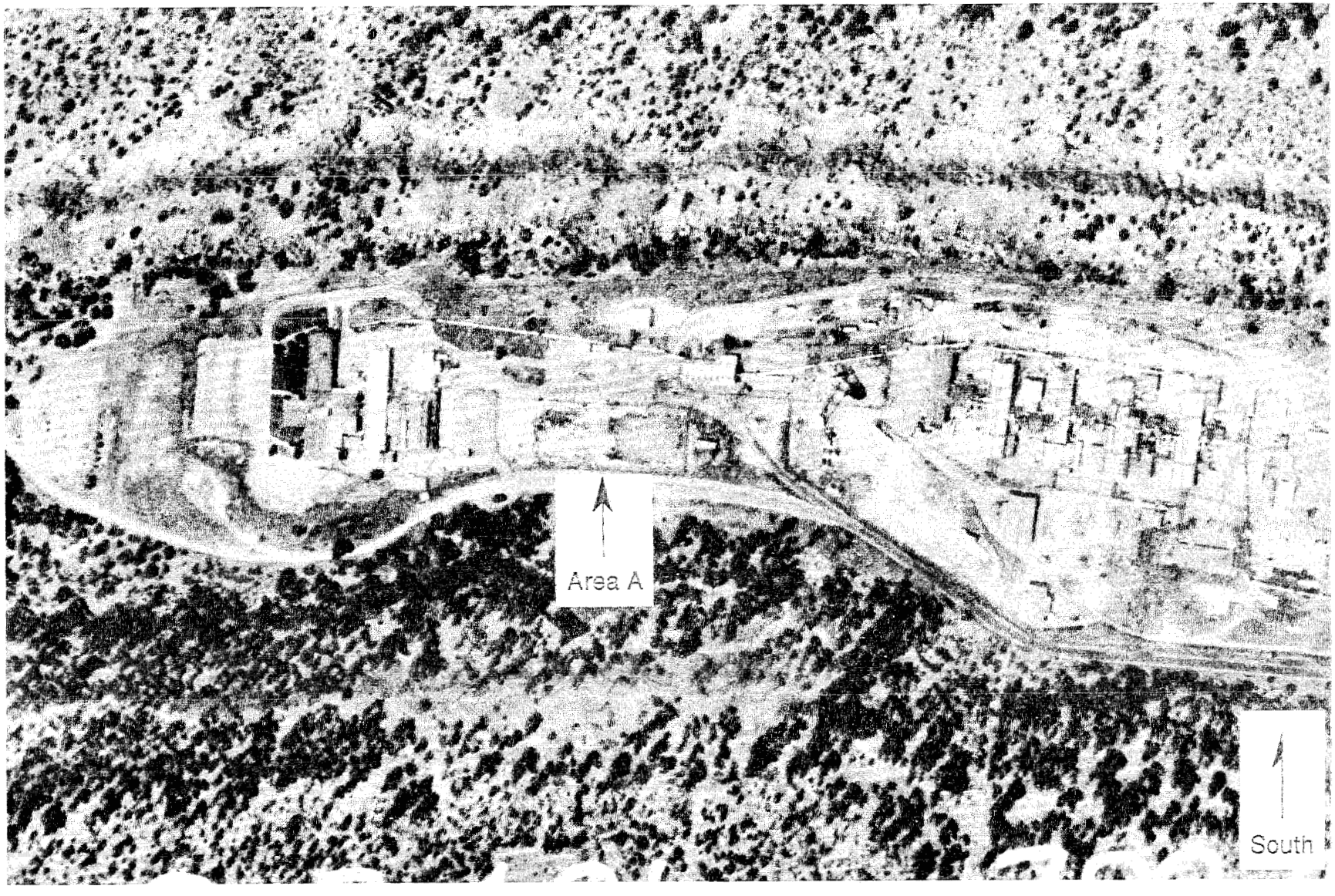

Fig. 8. Aerial photograph of TA-21 (1965).

Fig. 9. Photograph (1969) of the northern wall of the central disposal pit.

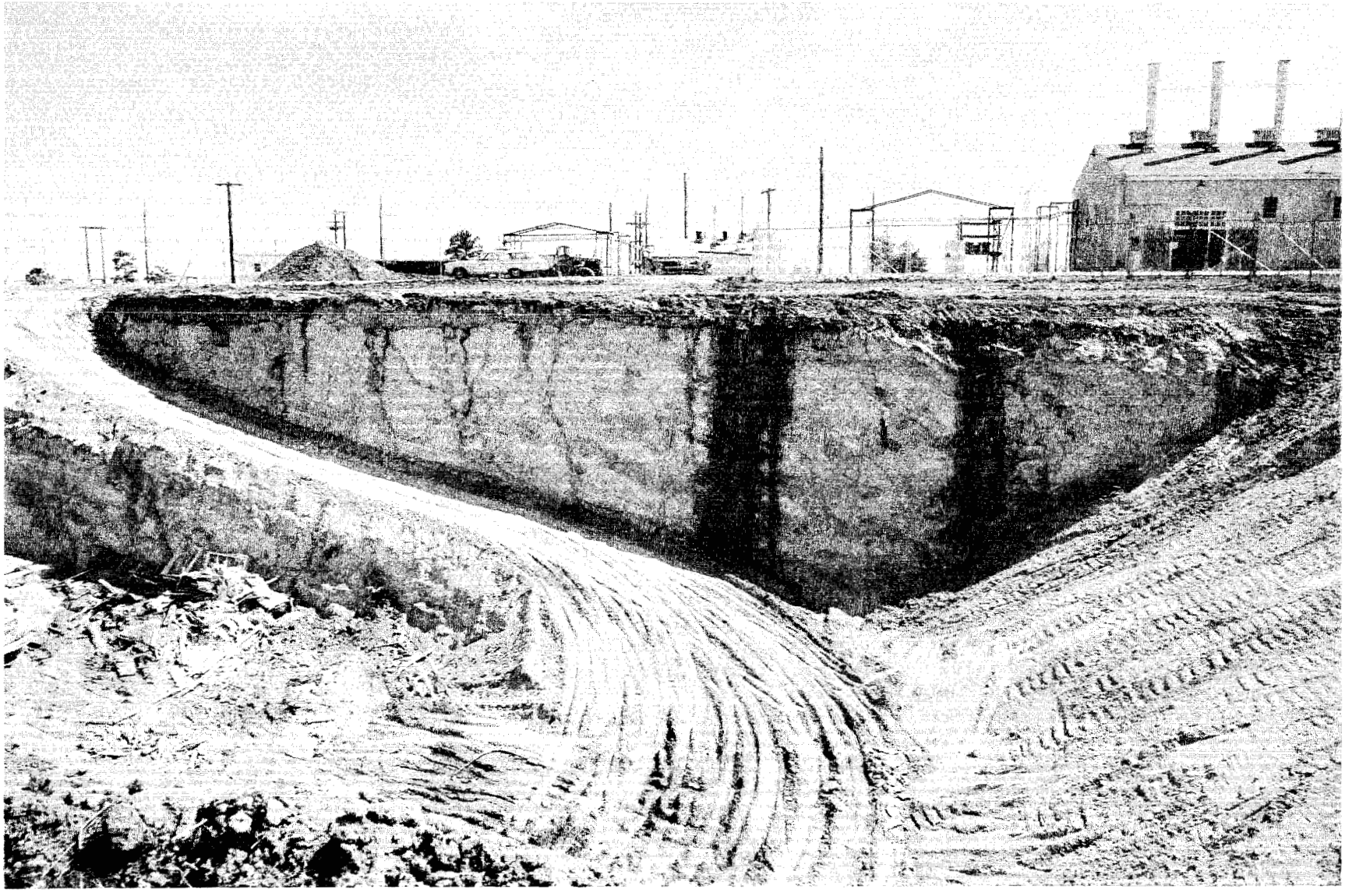

Fig. 10. Photograph (1969) of the southern wall of the central disposal pit.

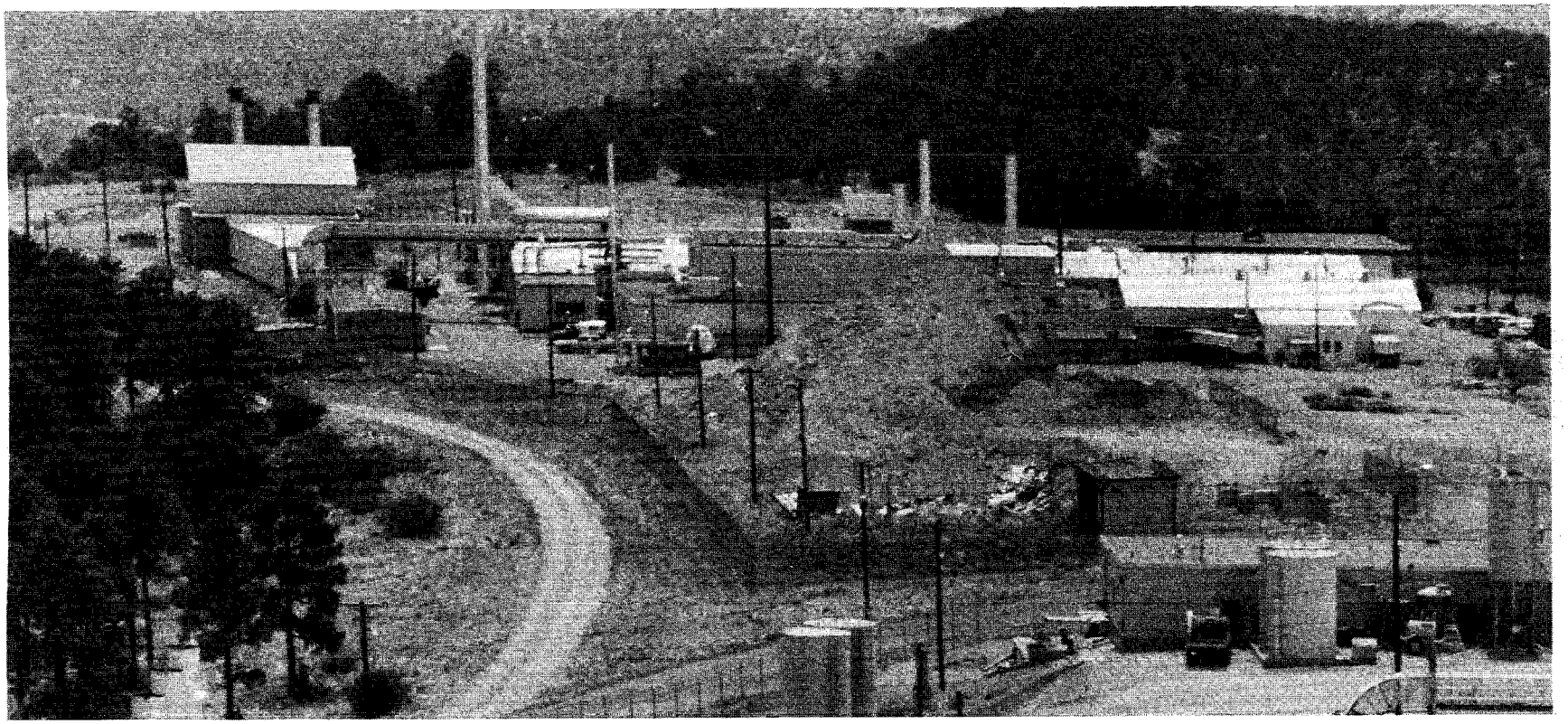

Fig. 11. Photograph (1971) showing backfill storage.

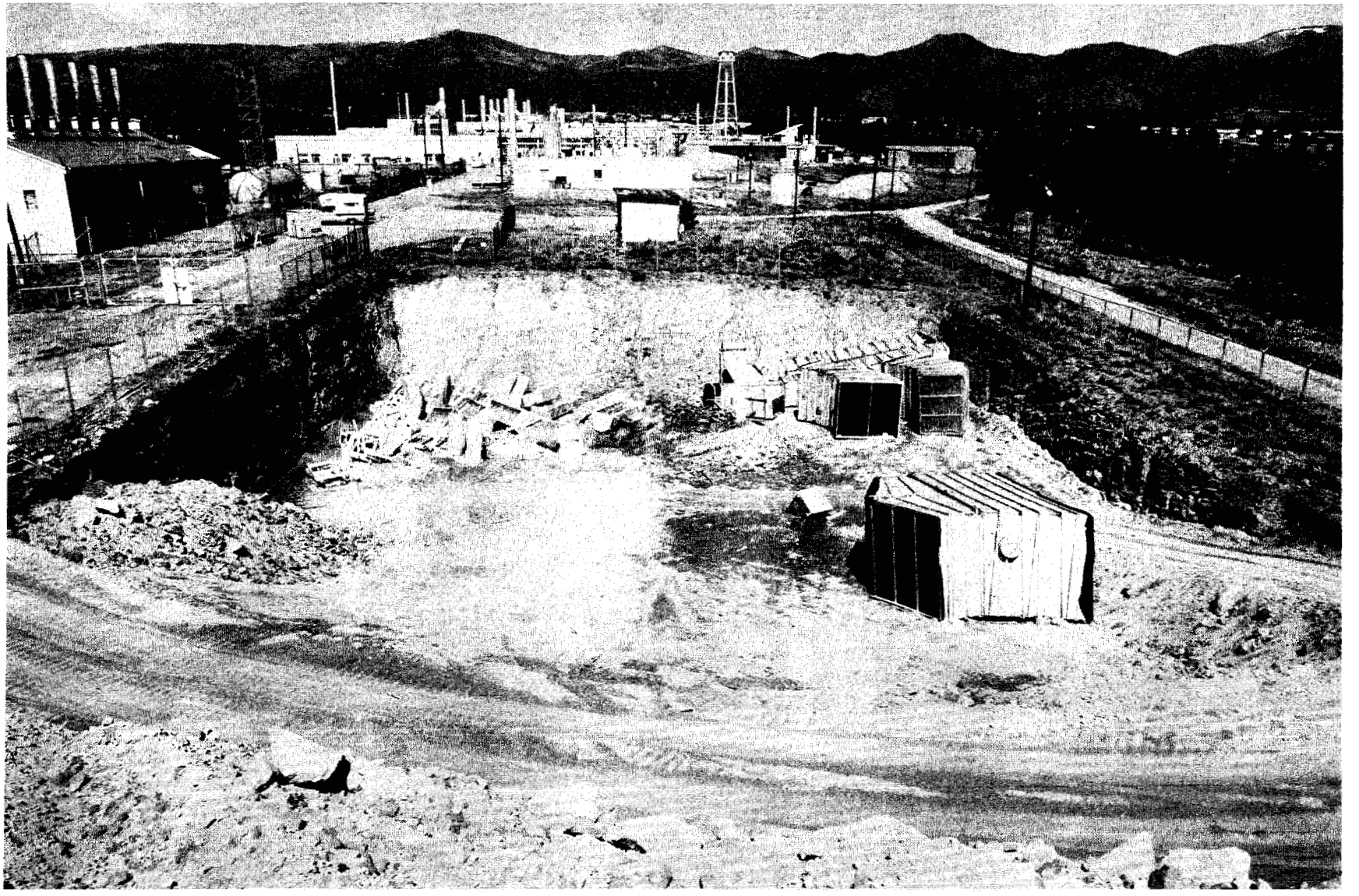

Fig. 12. Photograph (1973) showing burial of building demolition materials in the disposal pit.

Fig. 13. Photograph (1973) of the southeast corner of the pit showing hoods and other laboratory equipment being buried.

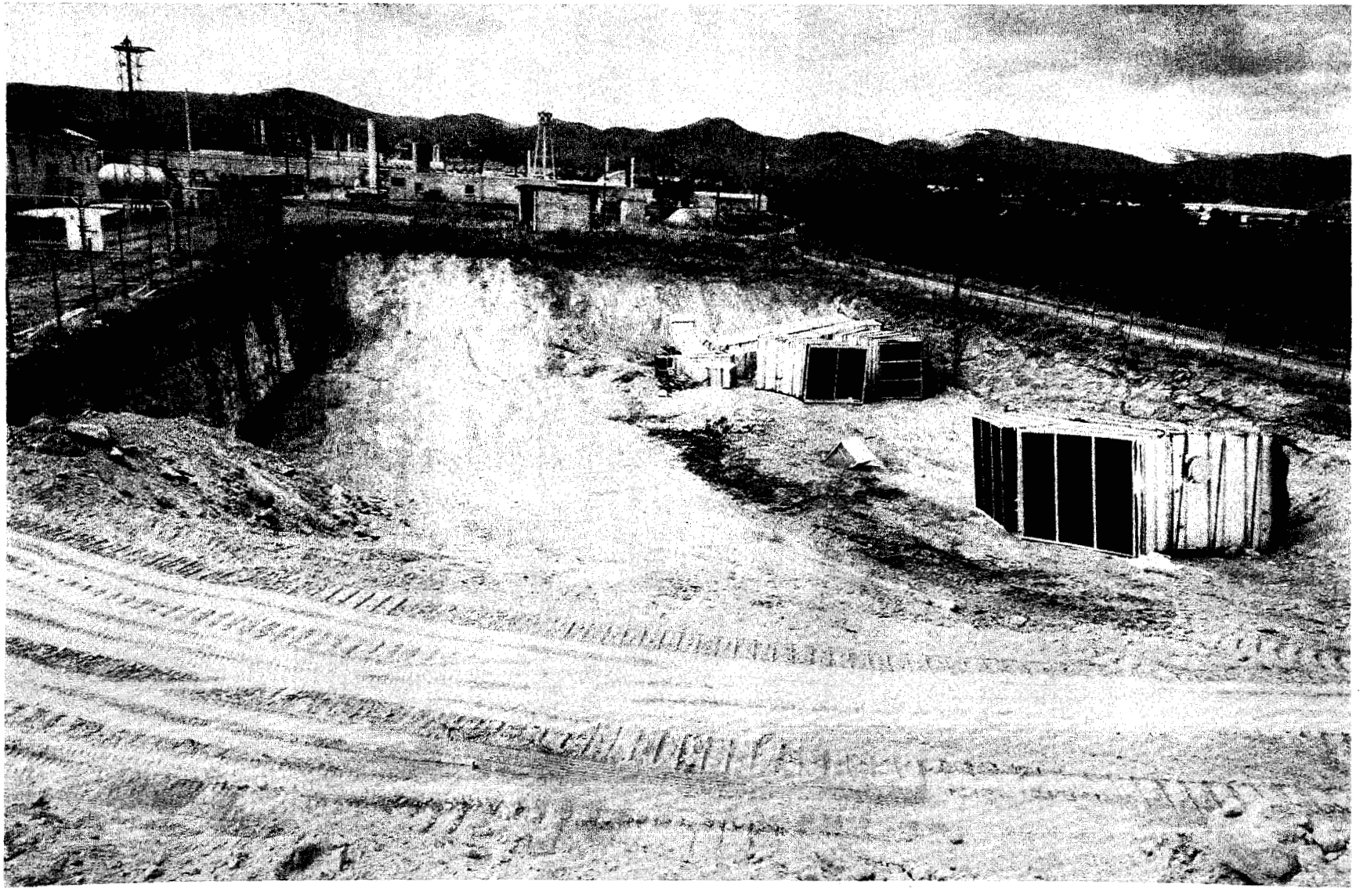

Fig. 14. Photograph (1973) showing building demolition materials being buried in the pit.

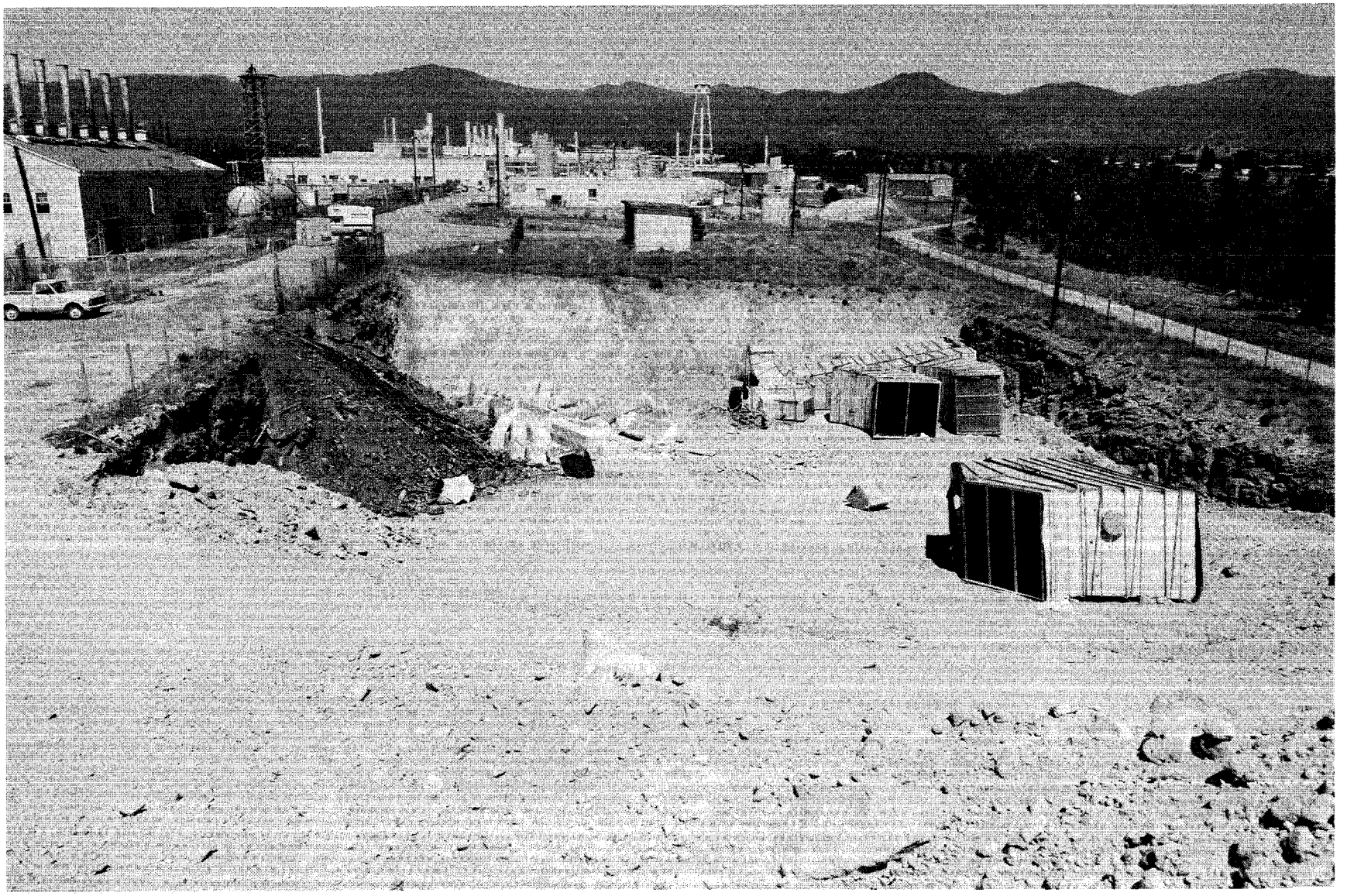

Fig. 15. Photograph (1973) showing material being pushed into the pit (left side).

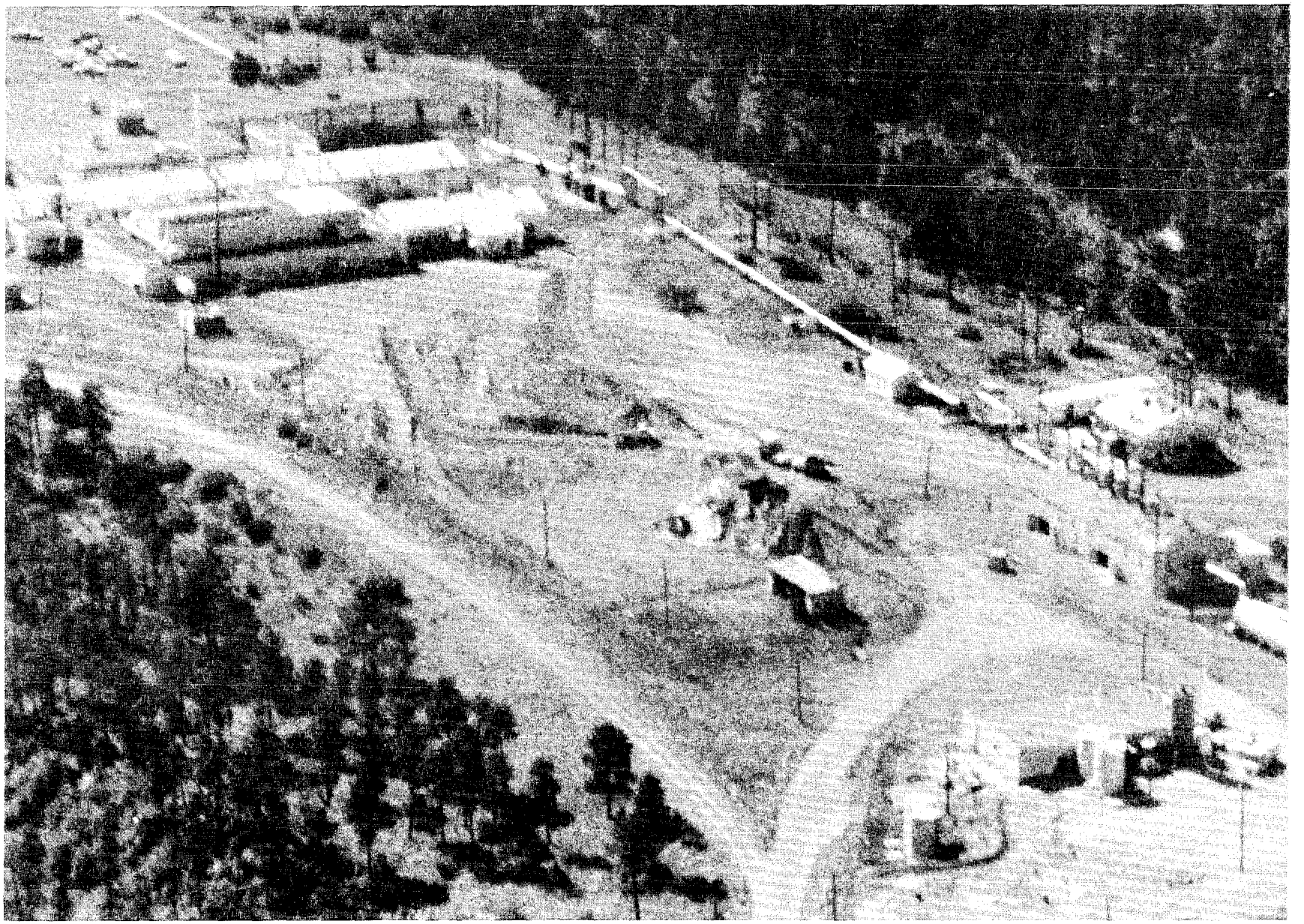

Fig. 16. Aerial photograph (1974) showing stockpiled backfill.

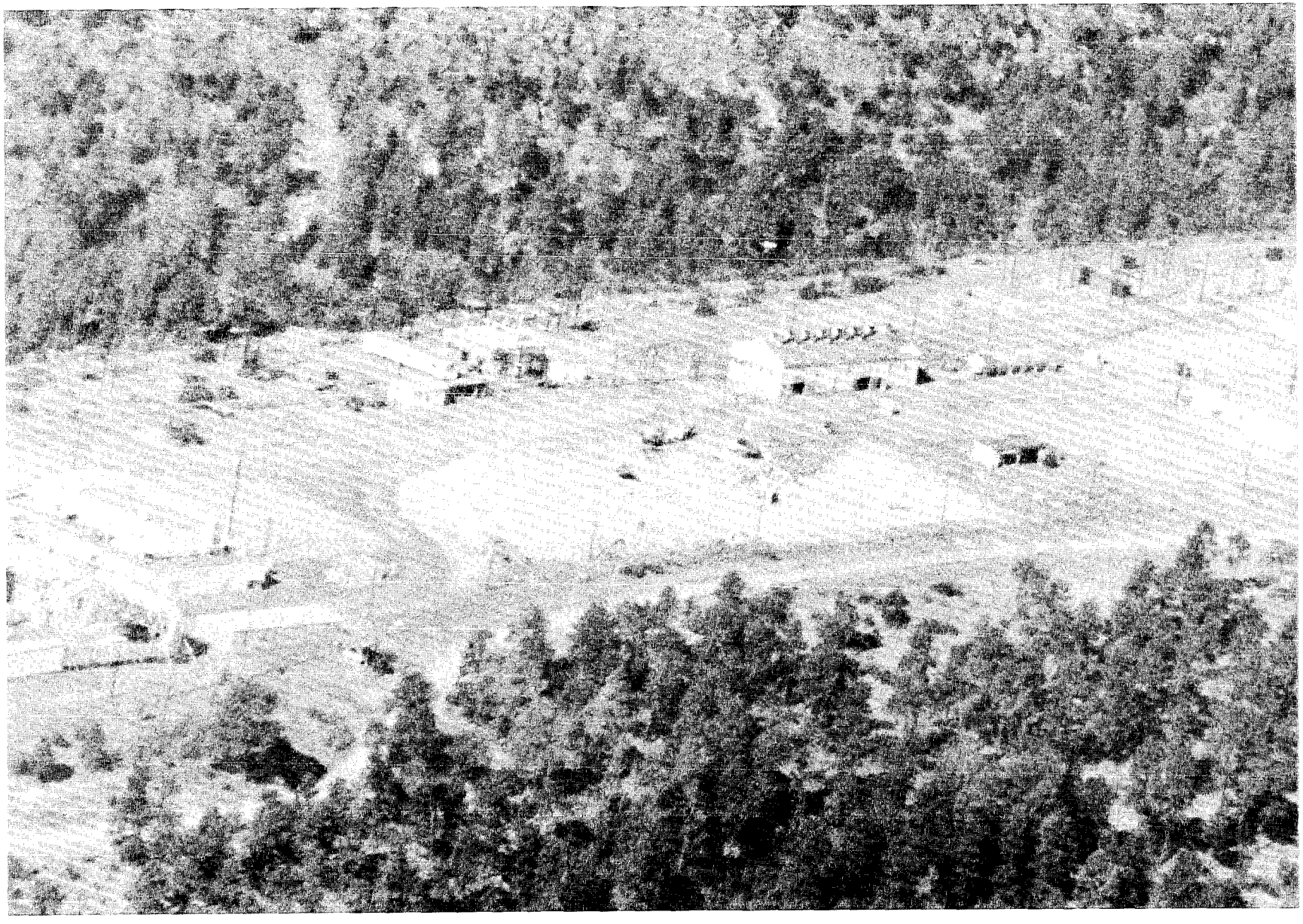

Fig. 17. Aerial photograph (1974) showing stockpiled backfill.

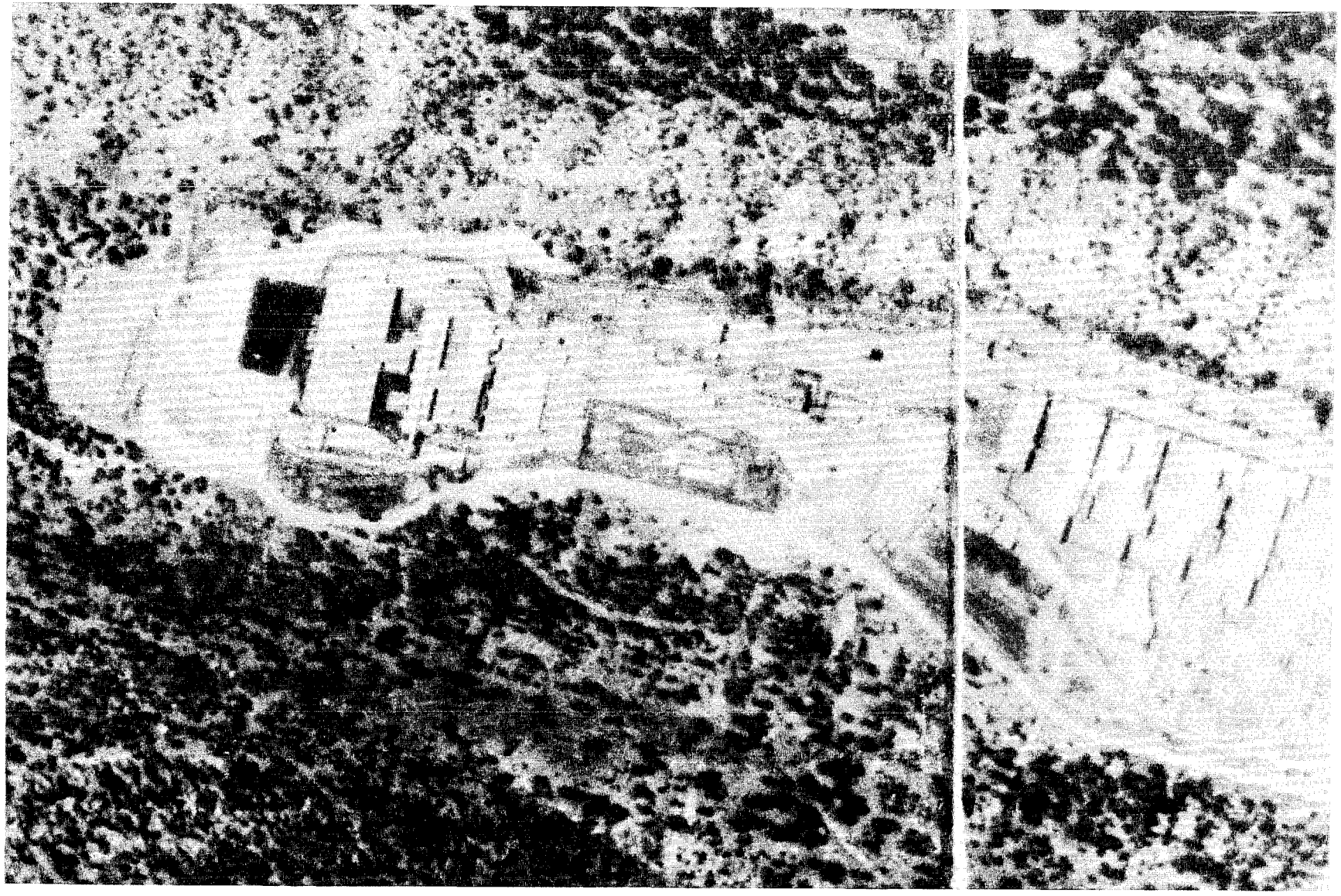

Fig. 18. Aerial photograph of TA-21 (1976).

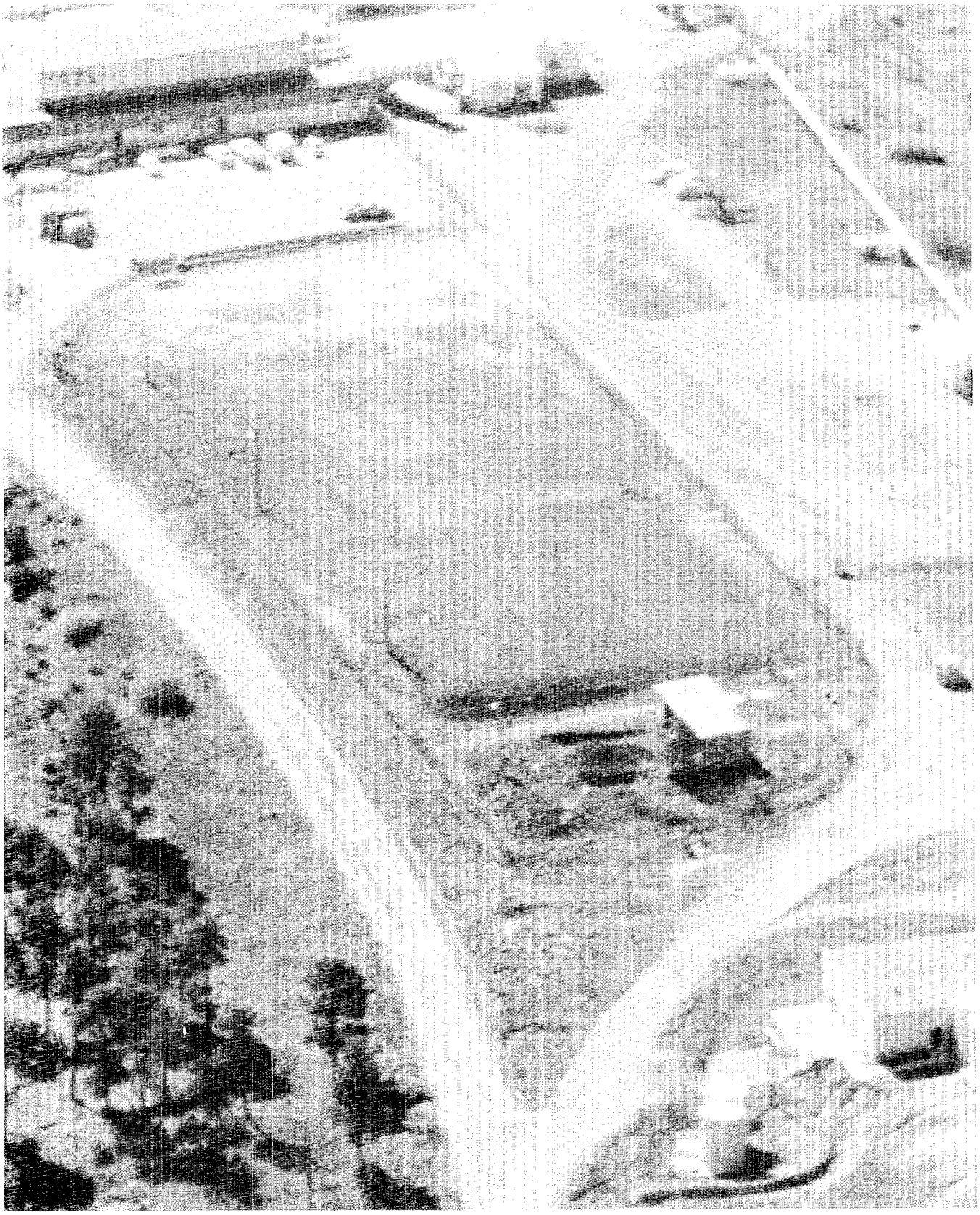

Fig. 19. Aerial photograph (1979) showing the surface characteristics of the site.

Fig. 20. Aerial photograph of TA-21 (1980).

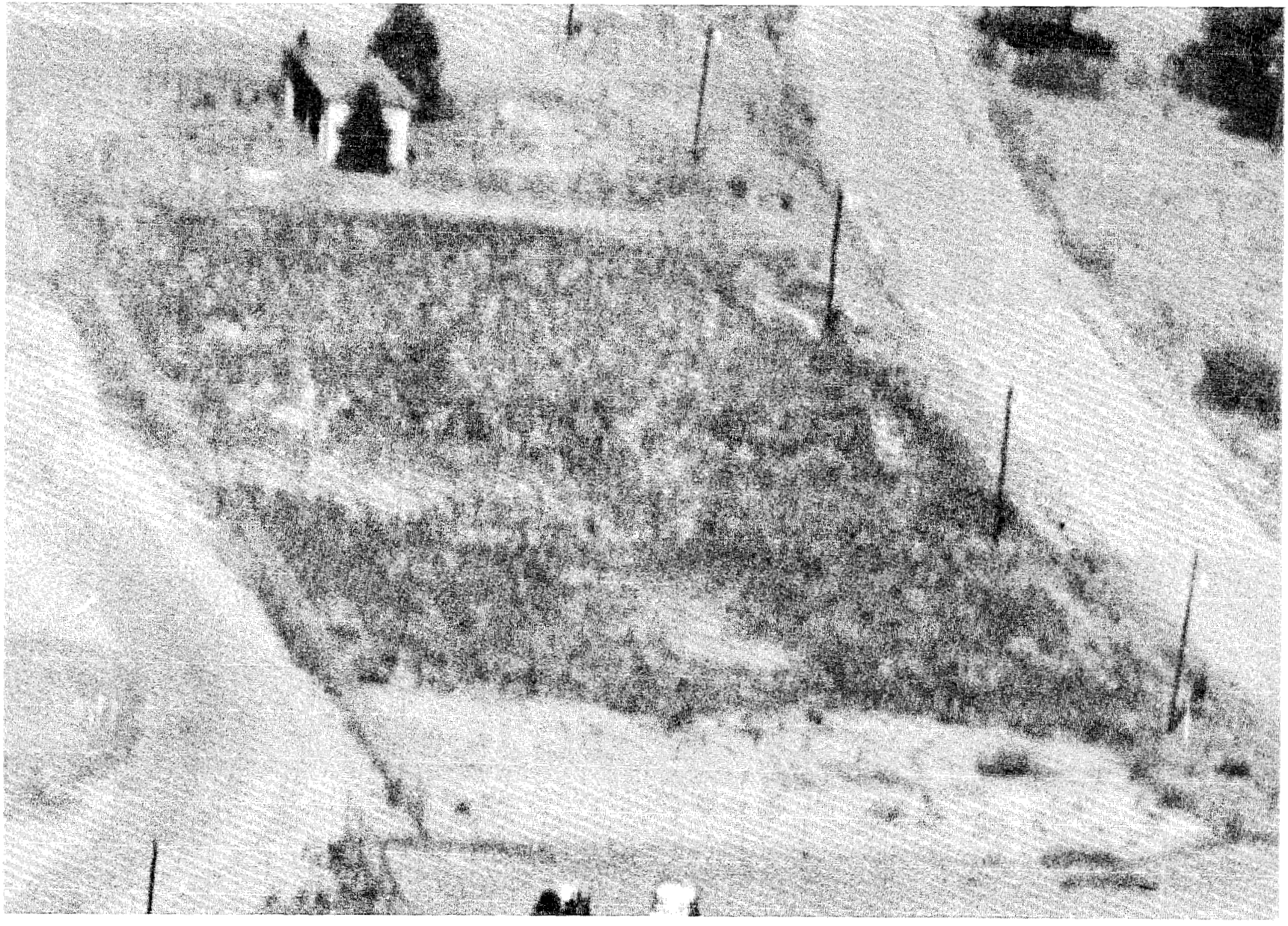

Fig. 21. Aerial photograph (1982) showing the surface characteristics of the site.

Fig. 22. Aerial photograph (1983) showing site vegetation.

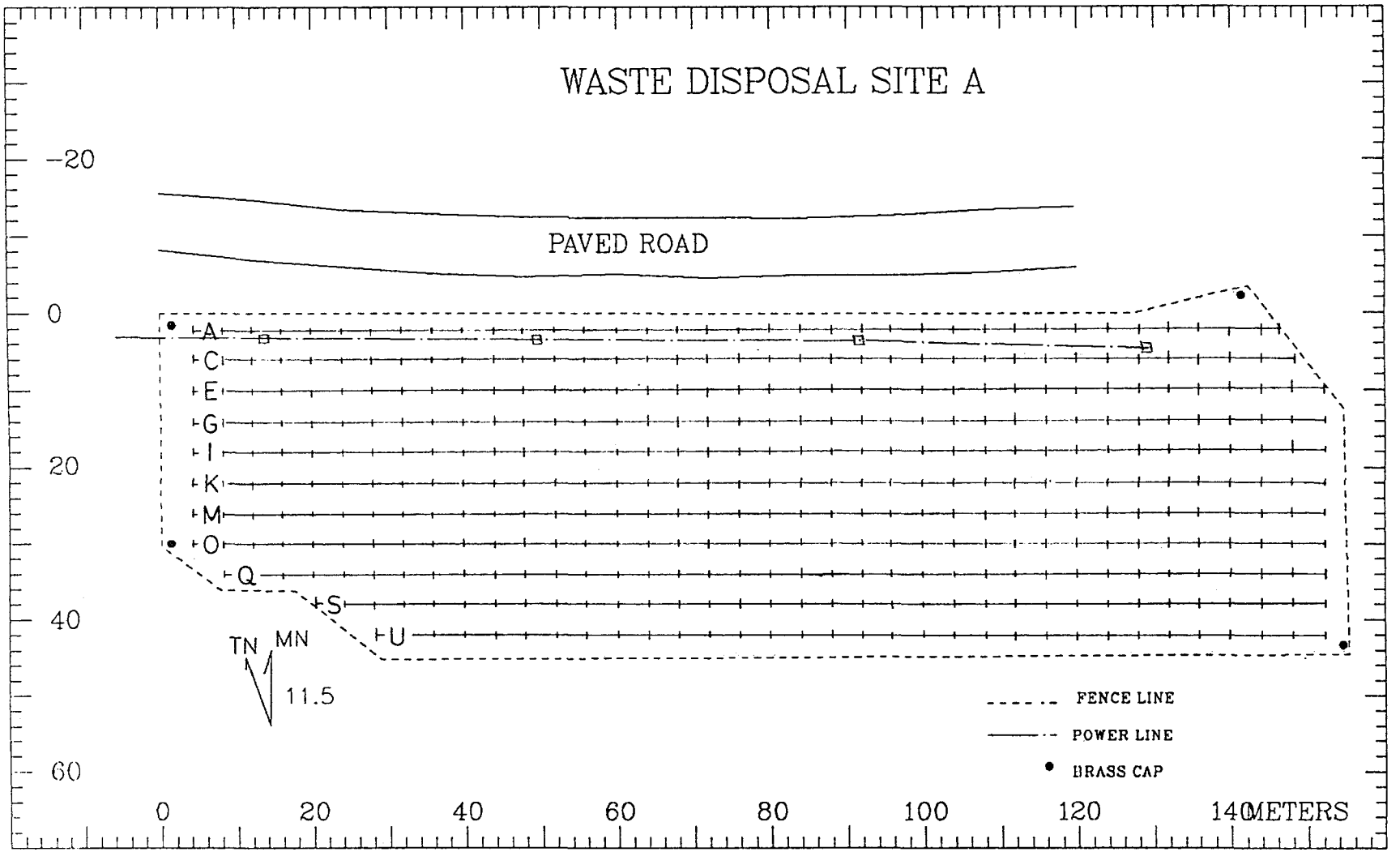

Fig. 23. The geophysical grid system with the road, fence, and telephone lines superposed as they exist now. Every second data line and every second data point are indicated.

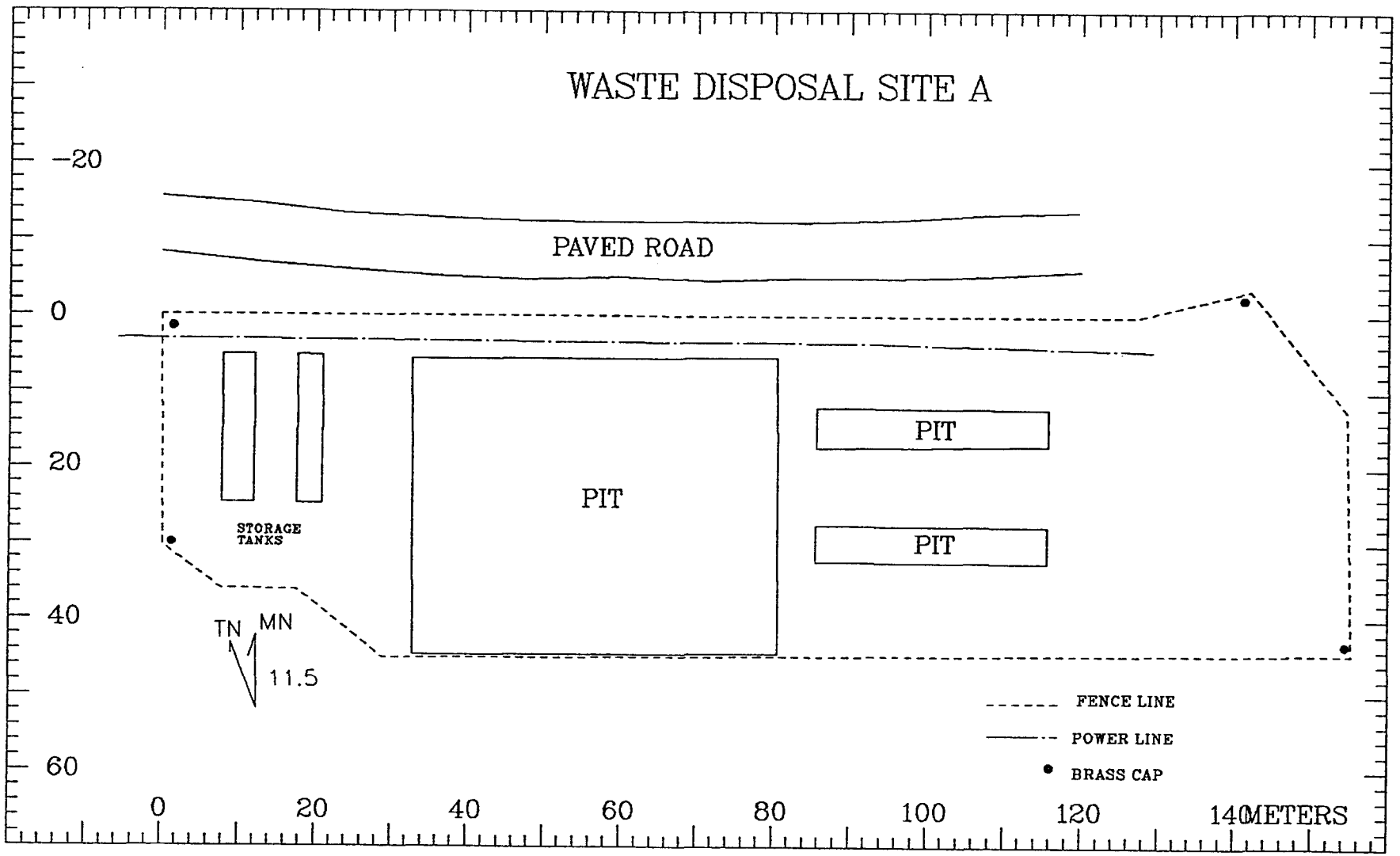

Fig. 24. The geophysical grid system with the storage tanks, pit, and trenches superposed. Locations are from Figs. 1 and 2.

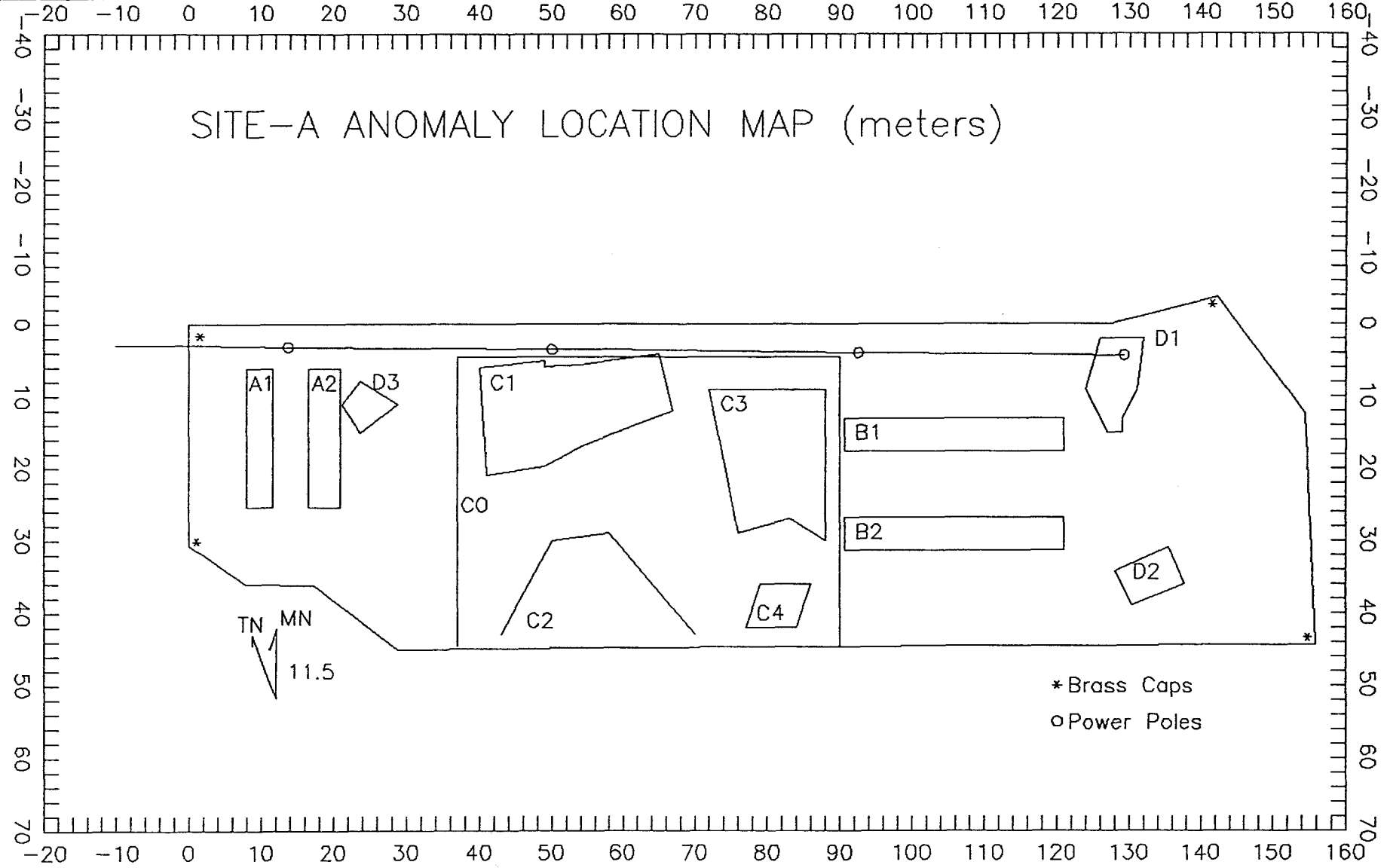

Fig. 25. The geophysical grid system with the storage tanks, pit, trenches and other targets superposed. Locations are based on geophysical data.

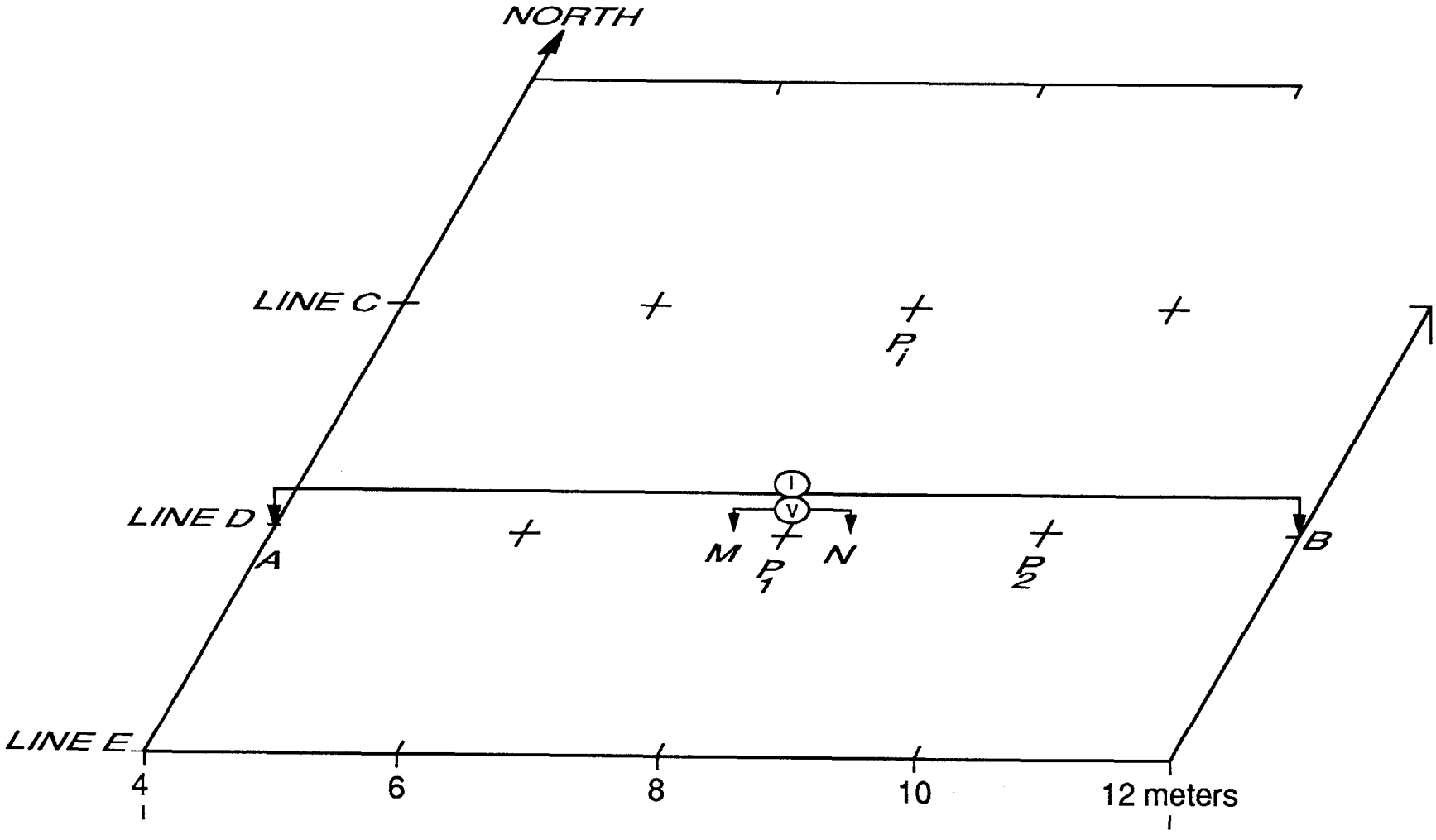

Fig. 26. Schematic representation of the Schlumberger array geometry. Measurements were made in this manner over the entire grid.

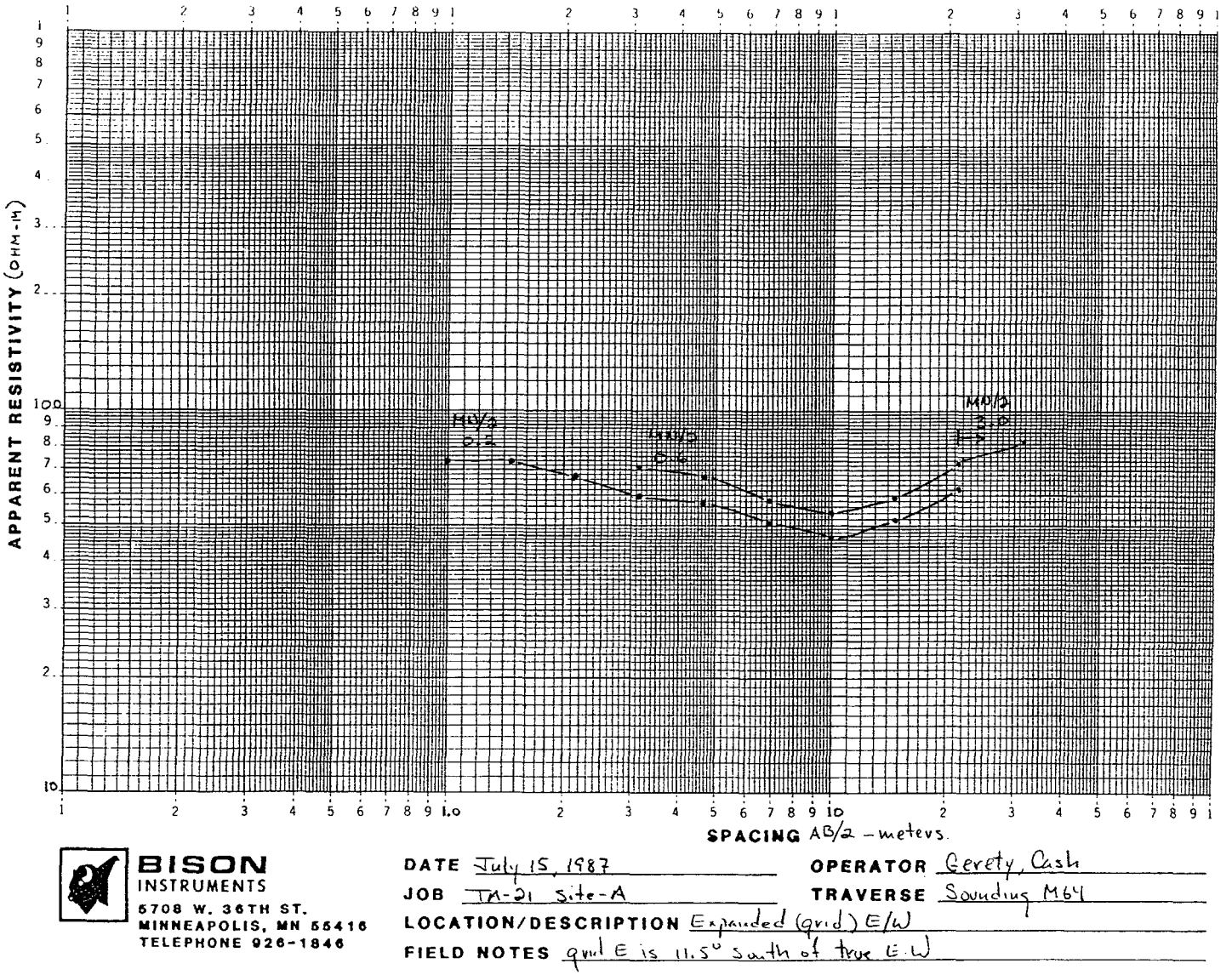

Fig. 27. Schlumberger sounding curve for station M64 (26S,64E) taken on July 15, 1987. The line is oriented east/west.

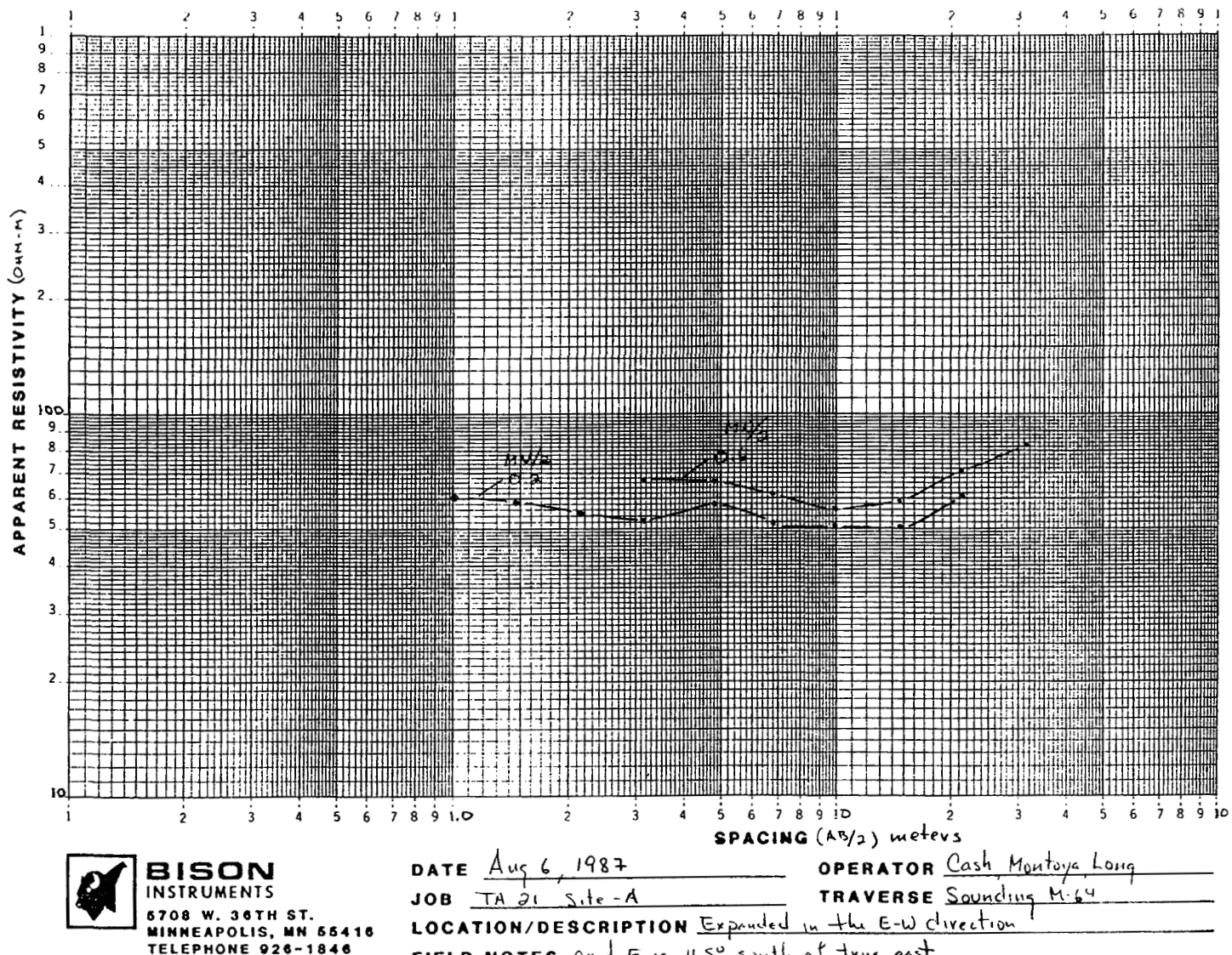

Fig. 28. Schlumberger sounding curve for station M64 (26S,64E) taken on August 6, 1987. The line is oriented east/west.

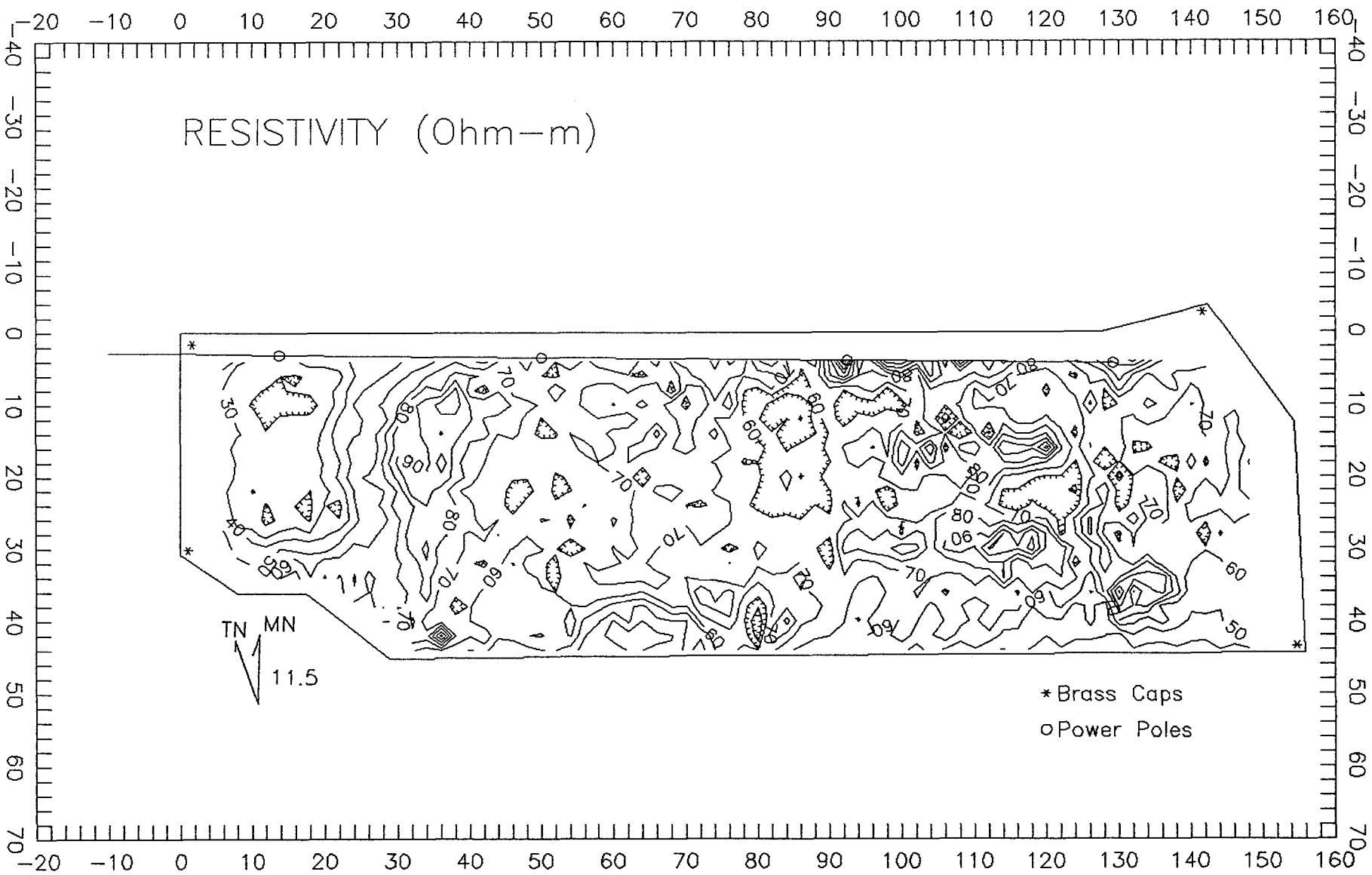

Fig. 29. Apparent resistivity contour map. The contour interval is 10 ohm-m.

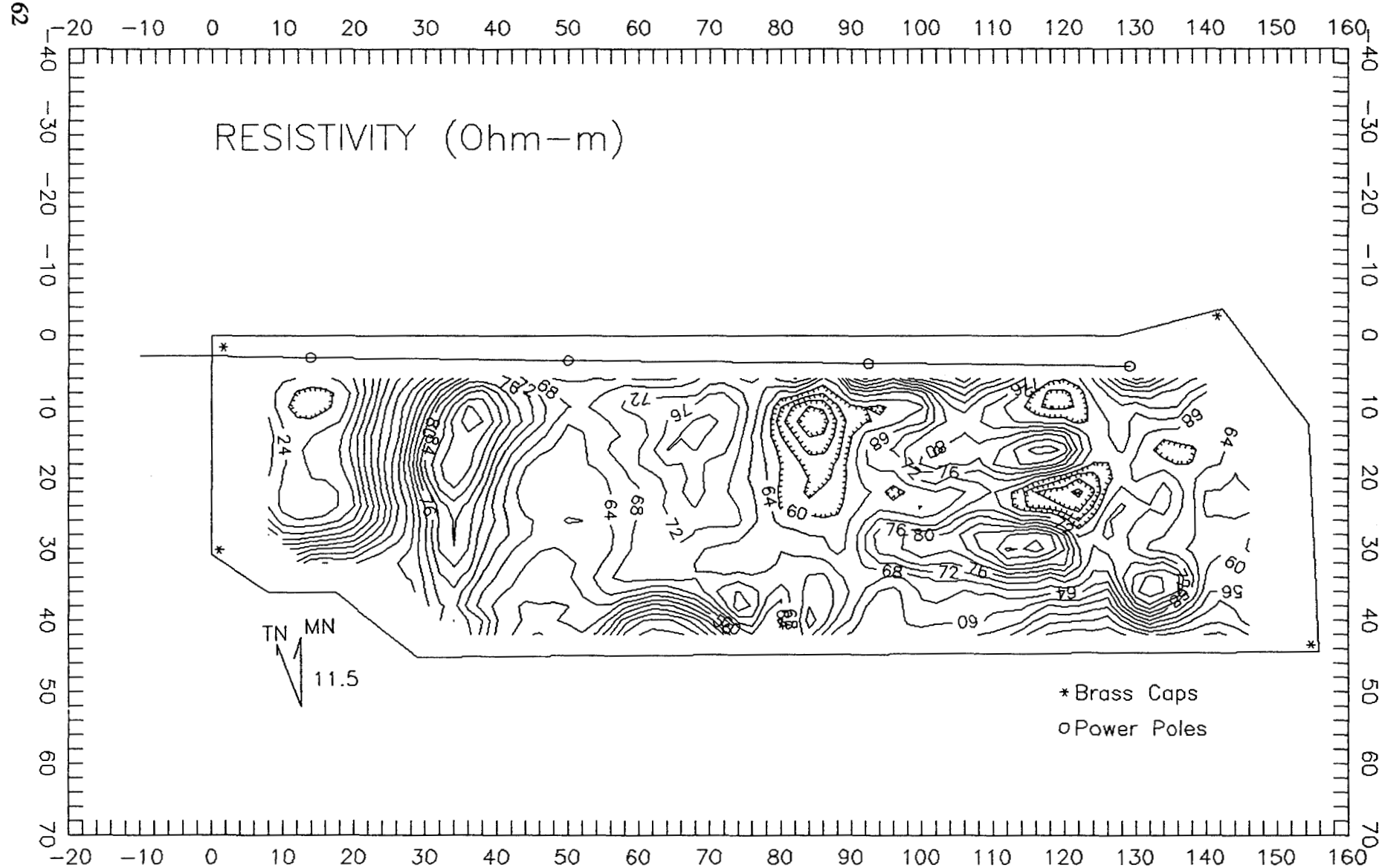

Fig. 30. Filtered apparent resistivity contour map. The contour interval is 4 ohm-m.

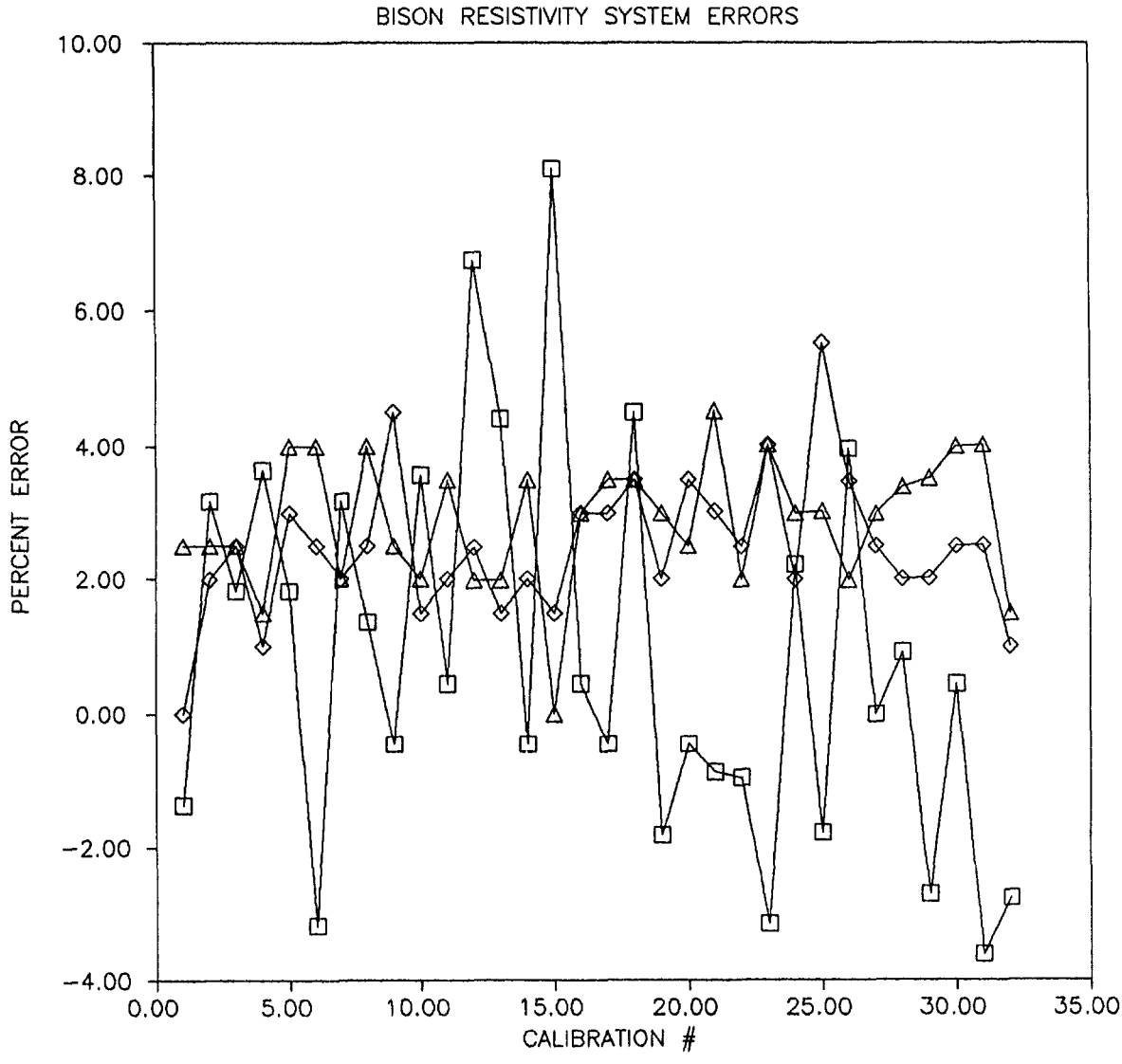

Fig. 31. Bison resistivity system errors measured during daily calibration. Squares, triangles, and diamonds indicate measurements through 0.11-ohm, 1.0-ohm, and 10.0-ohm resistors, respectively.

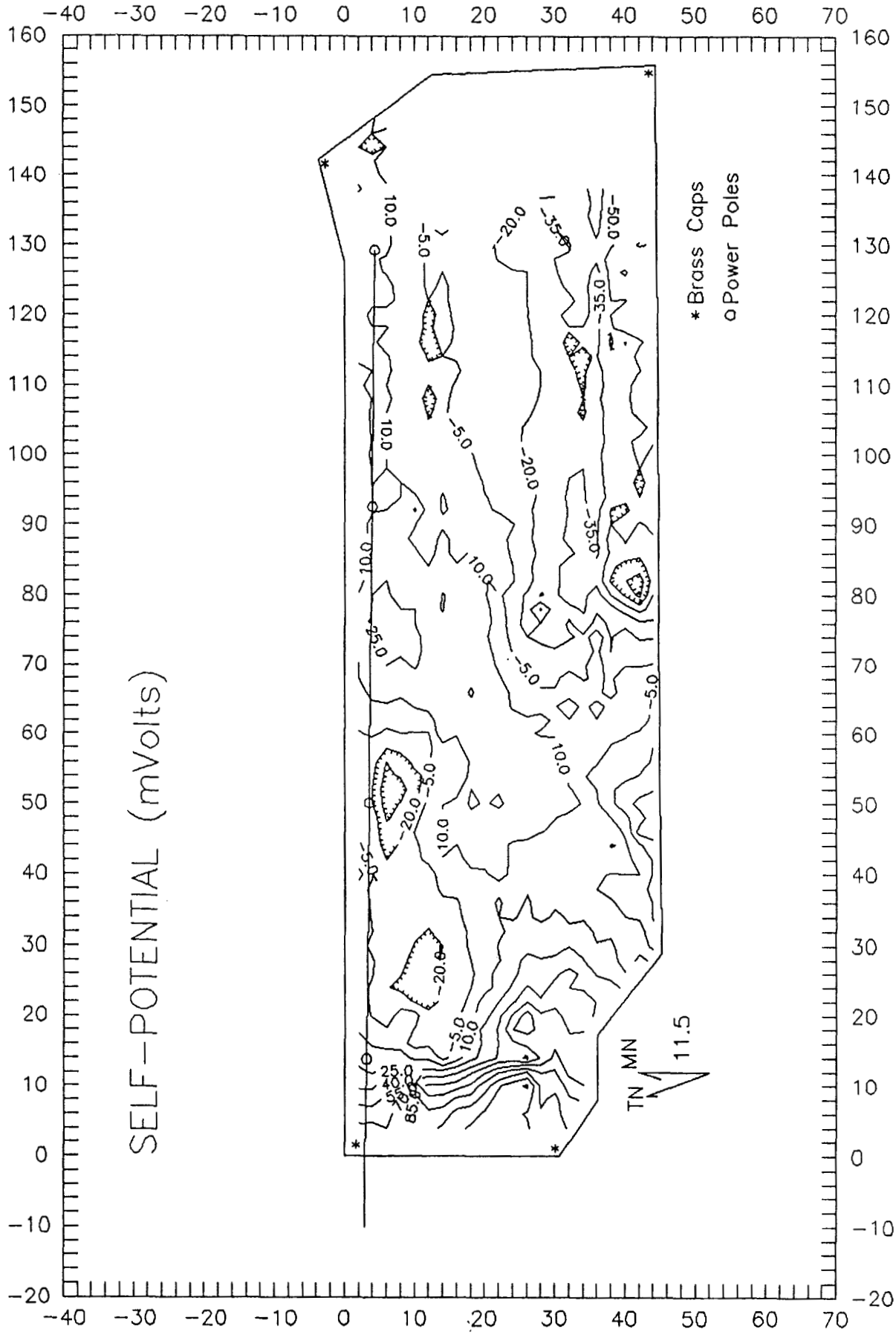

Fig. 32. SP contour map. The contour interval is 15 mV.

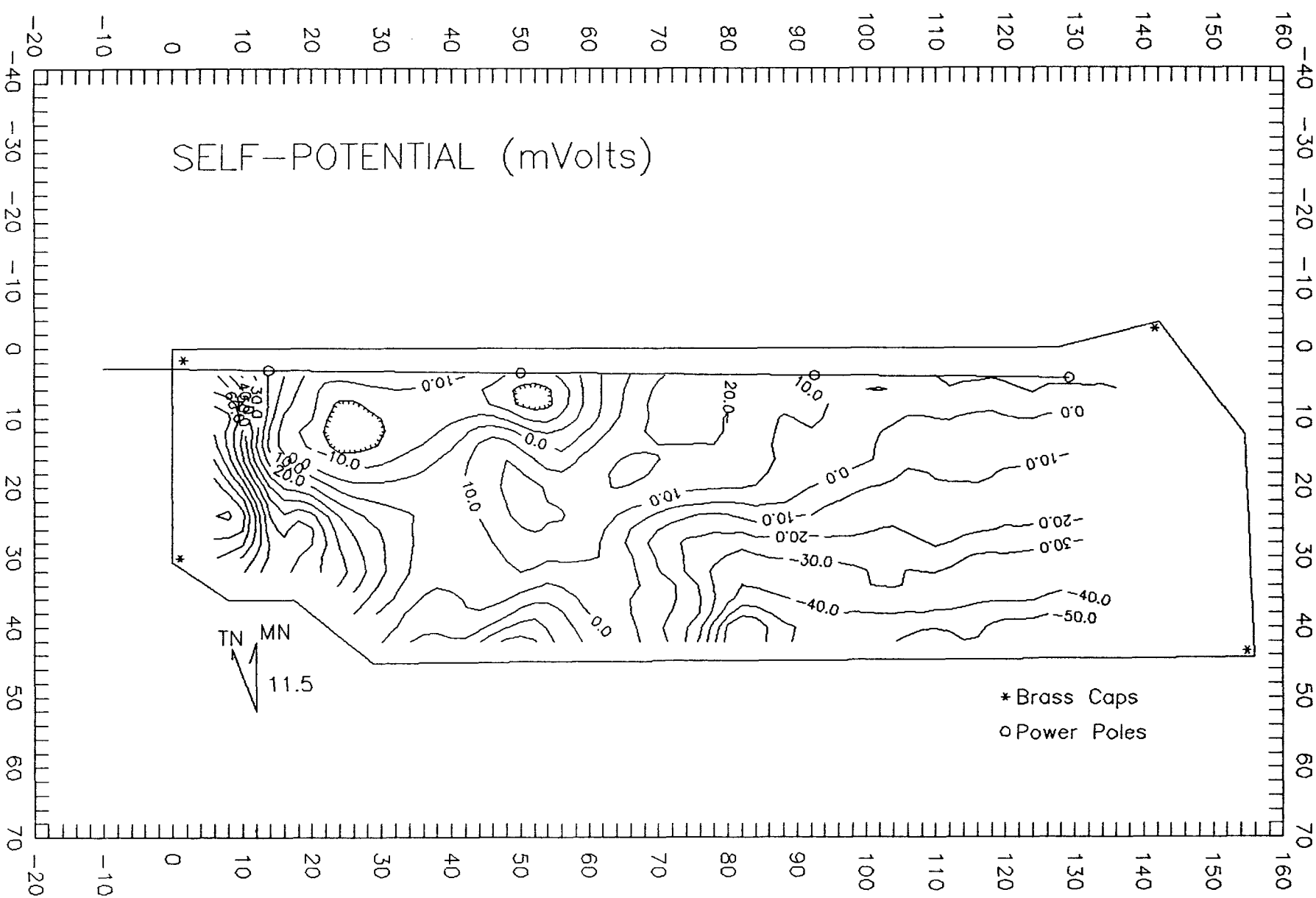

Fig. 33. Filtered SP contour map. The contour interval is 10 mV.

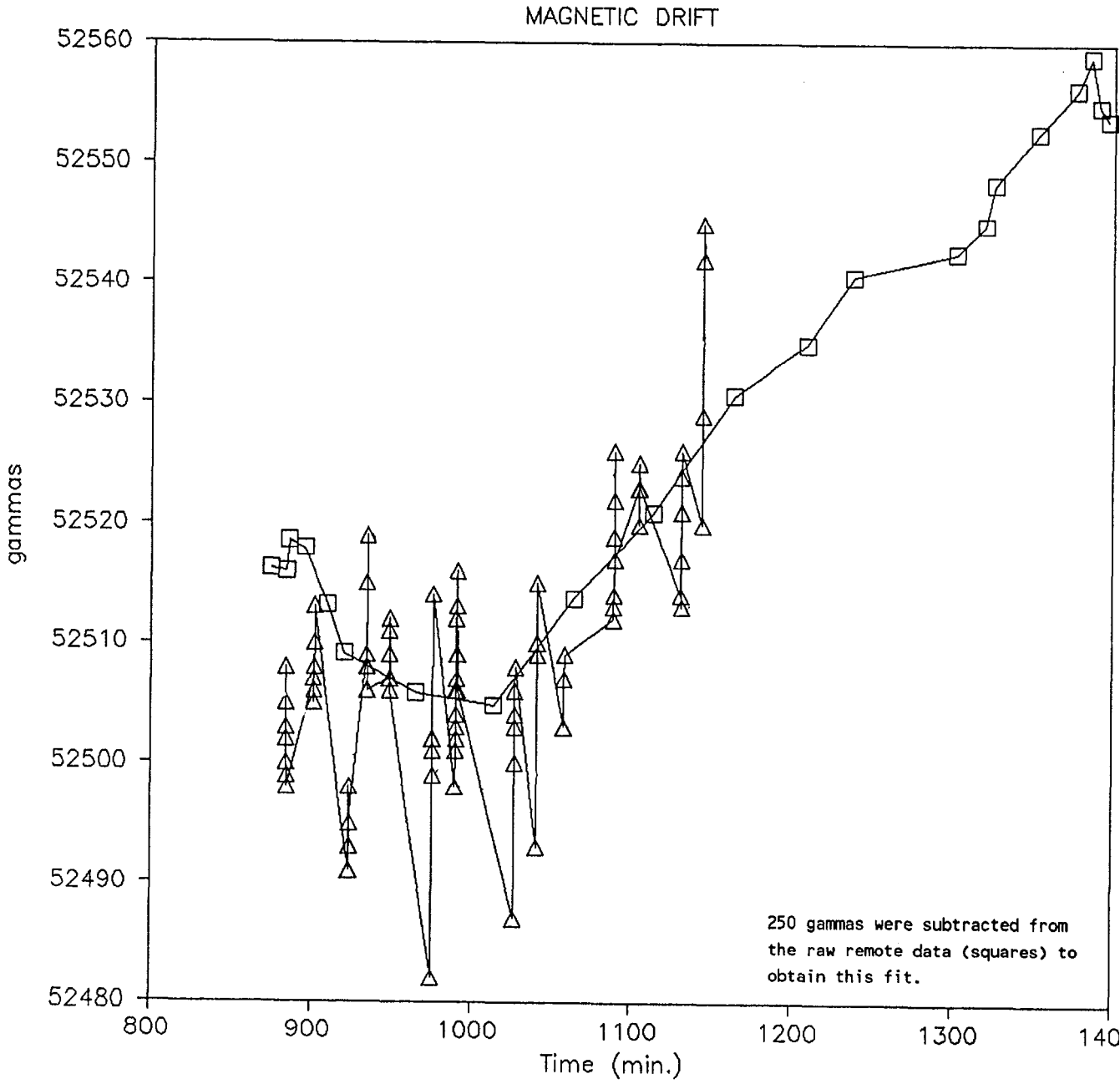

Fig. 34. Magnetic field diurnal drift measurements from station 20S,40E (squares) and diurnal drift measurements recorded during the reoccupations of station 26S,40E (triangles).

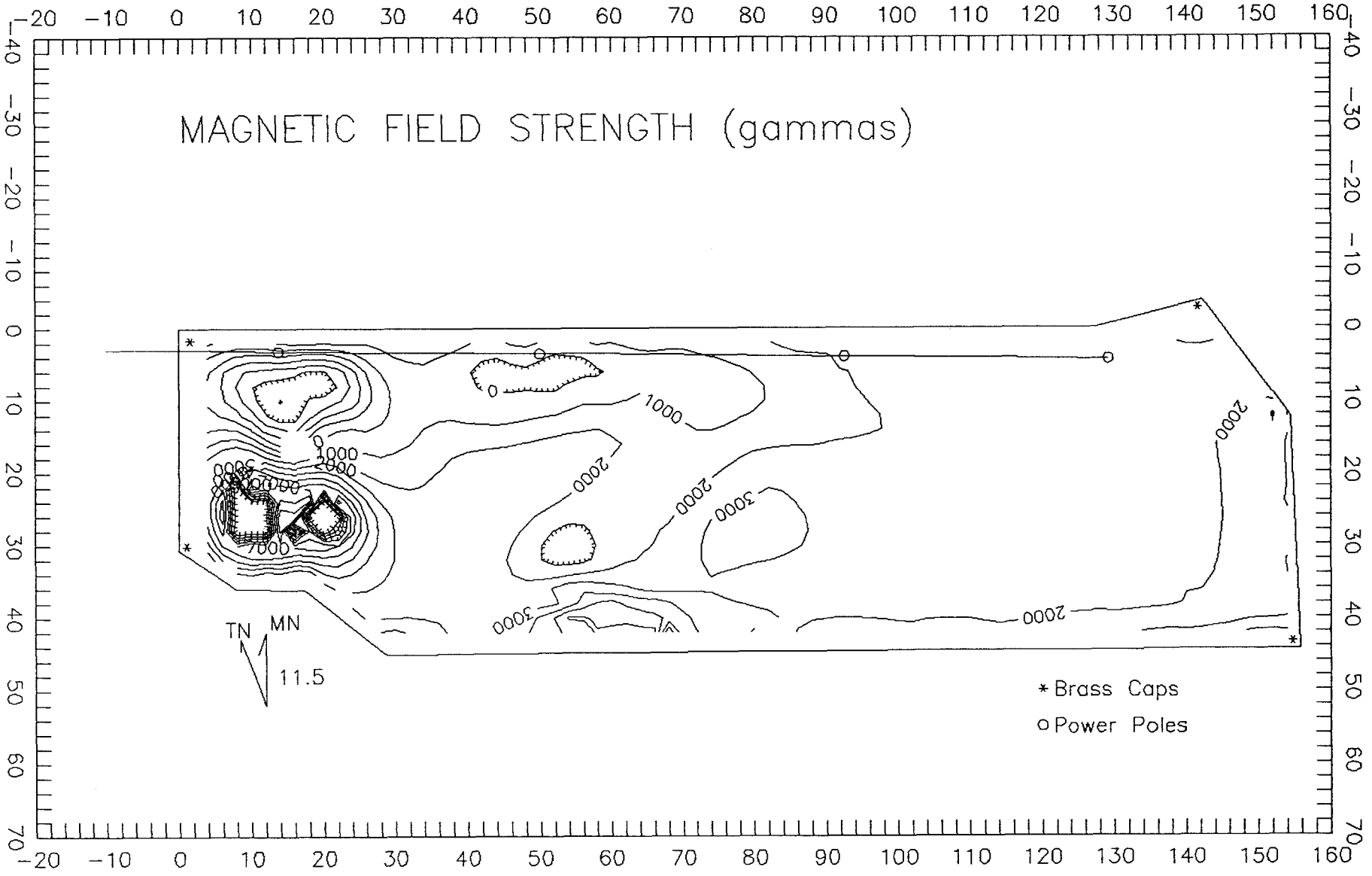

Fig. 35. Magnetic field strength (minus 50 000 gammas) contour map. The contour interval is 1000 gammas.

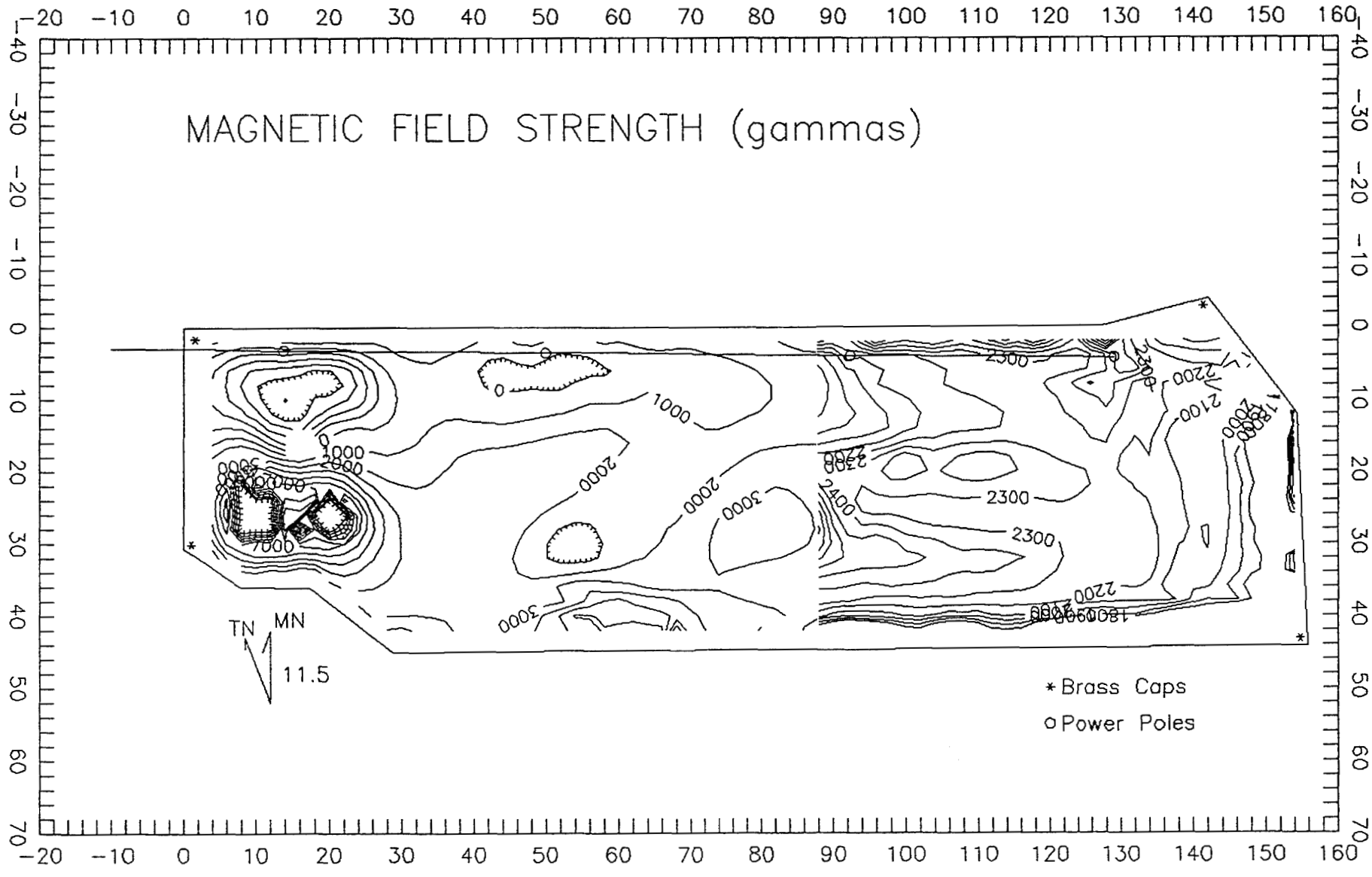

Fig. 36. Magnetic field strength (minus 50 000 gammas) contour map with two contour intervals (1000 and 100 gammas).

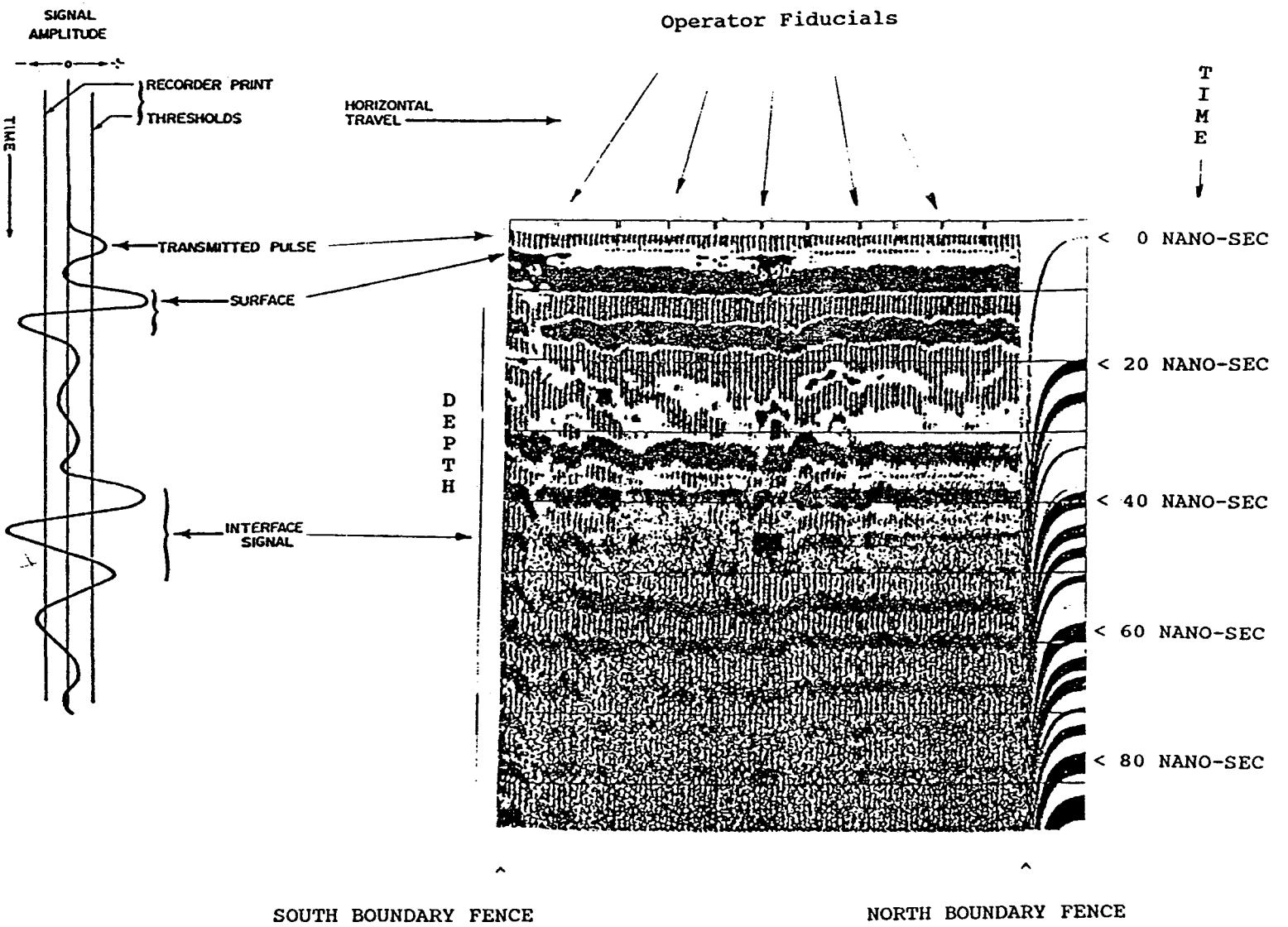

Fig. 37. Example of radar profile information as displayed by the radar system.

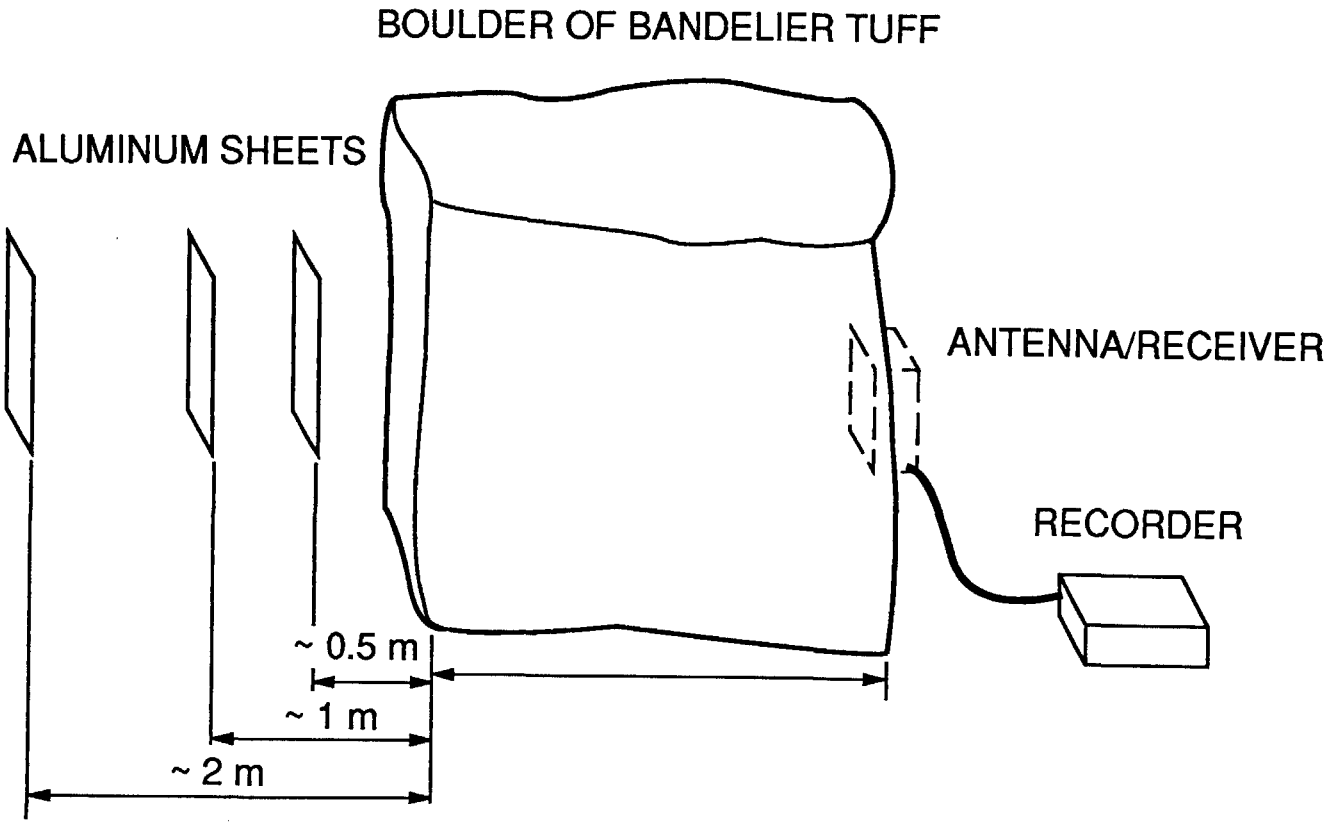

Fig. 38. Illustration of the geometry used to calibrate the radar unit.

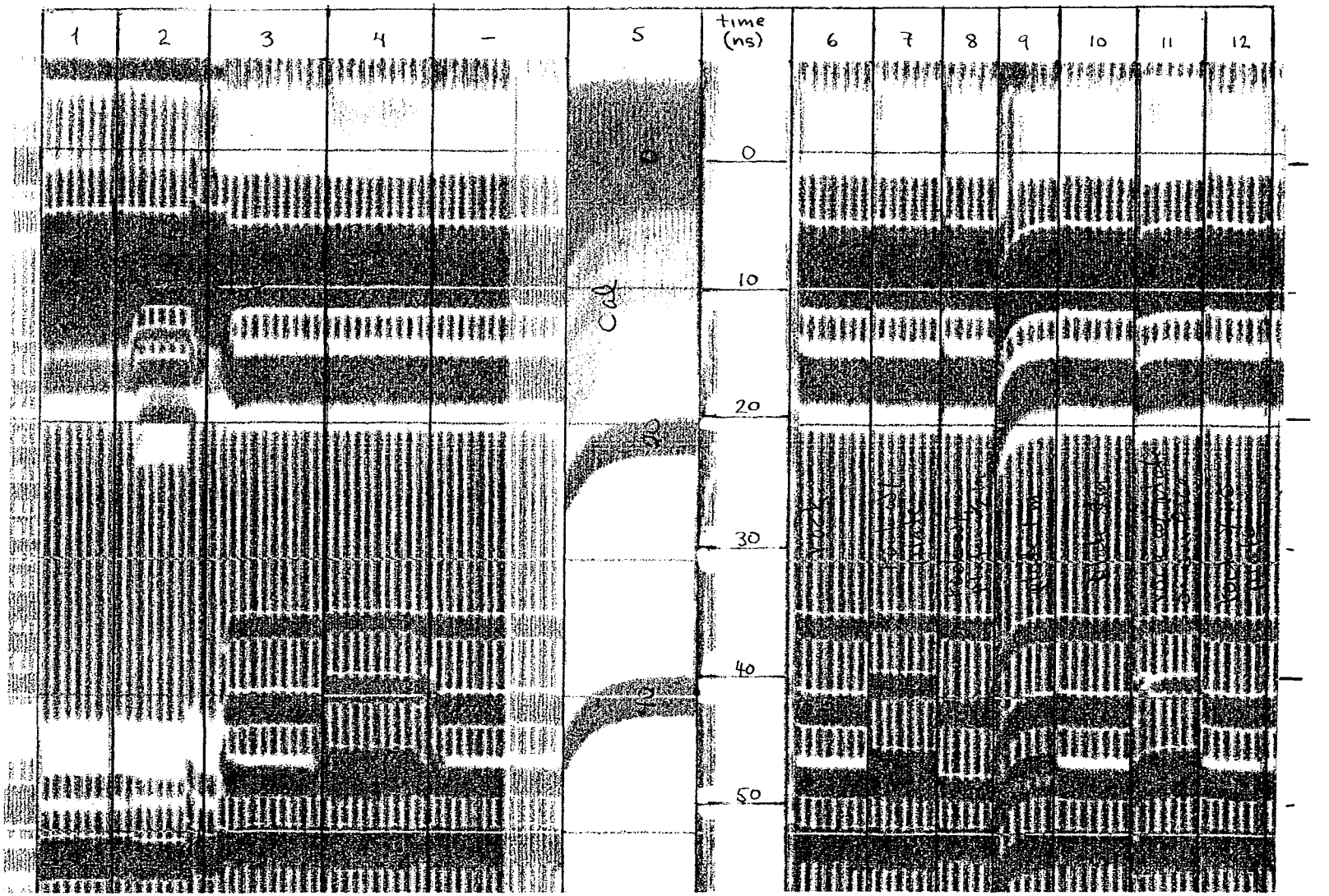

Fig. 39. Radar calibration data resulting from the geometry of Fig. 38.

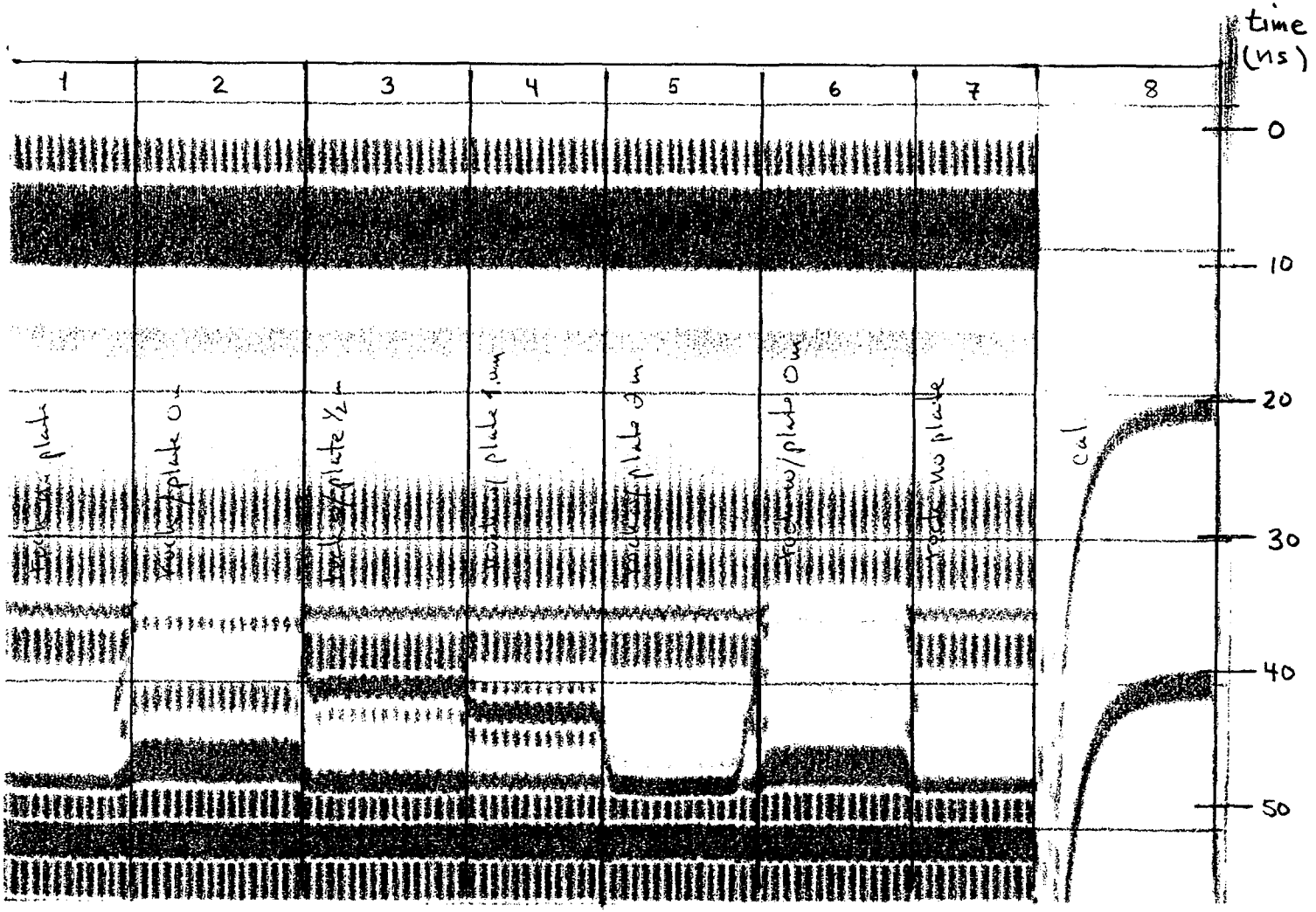

Fig. 40. Radar calibration data resulting from the geometry of Fig. 38. The gains and filter settings are different than used in Fig. 39.

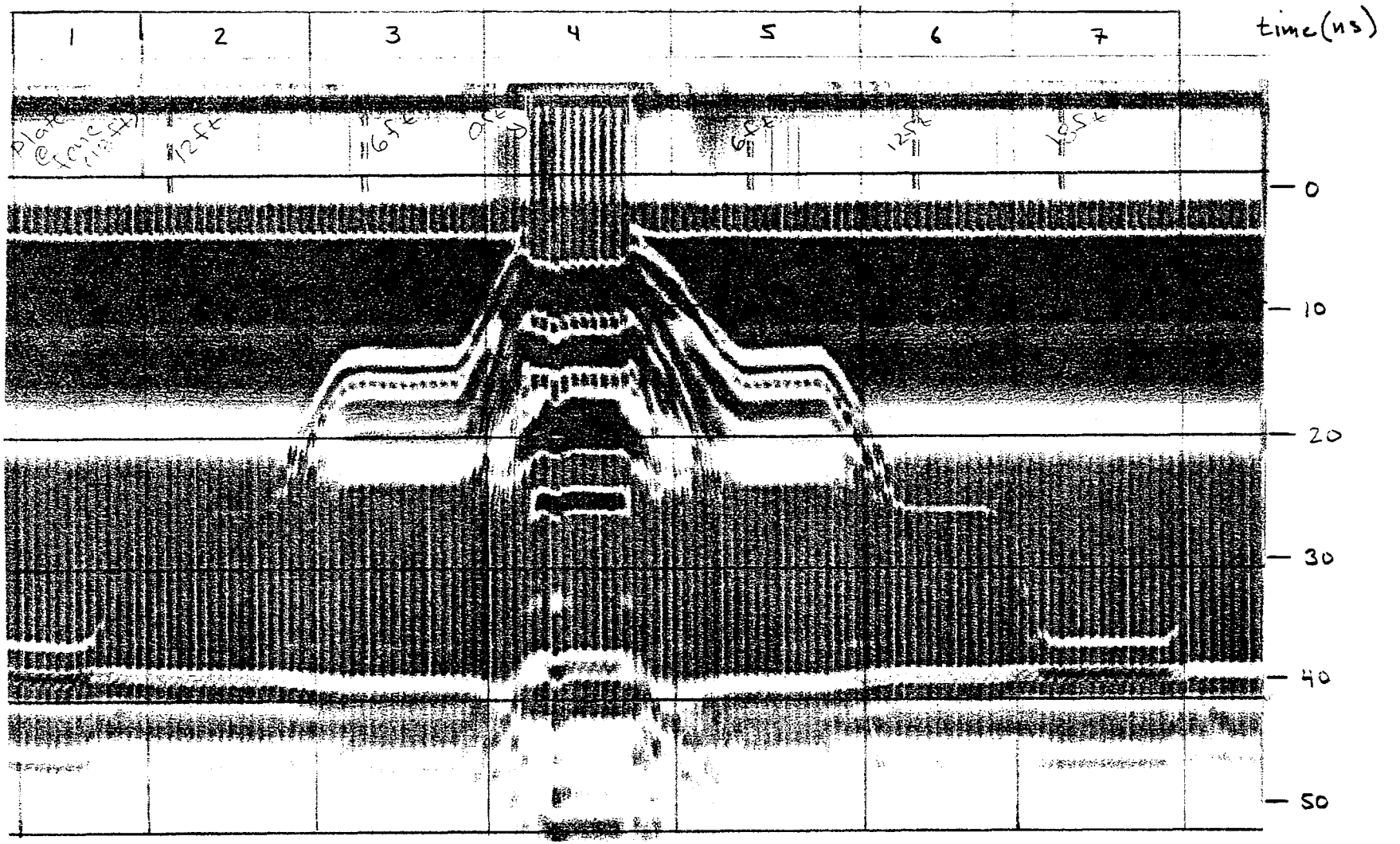

Fig. 41. Radar profiles of the data taken to calibrate the radar system on the fence surrounding Area A.

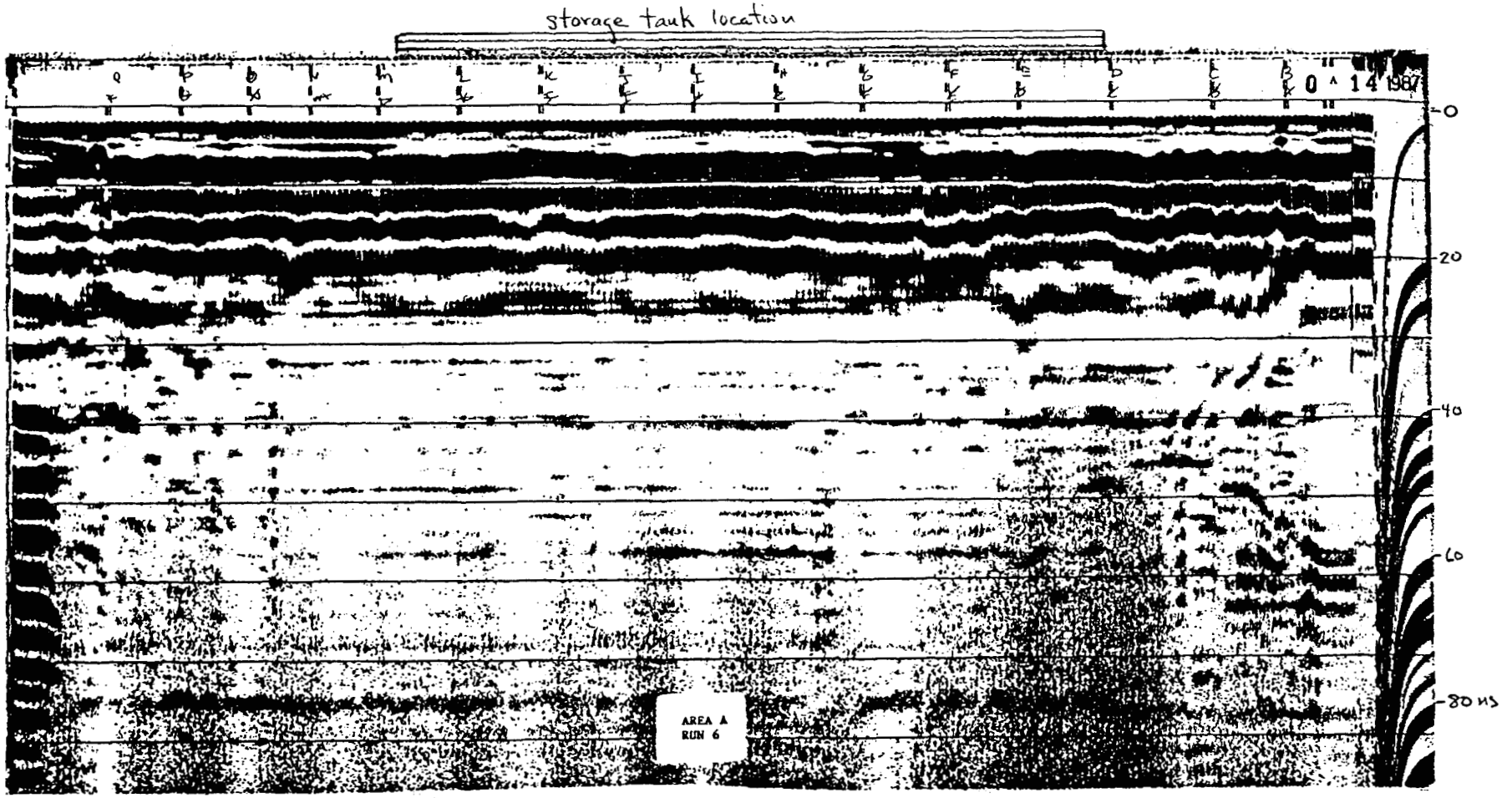

Fig. 42. Radar profile along line 12E over General's storage tank A1.

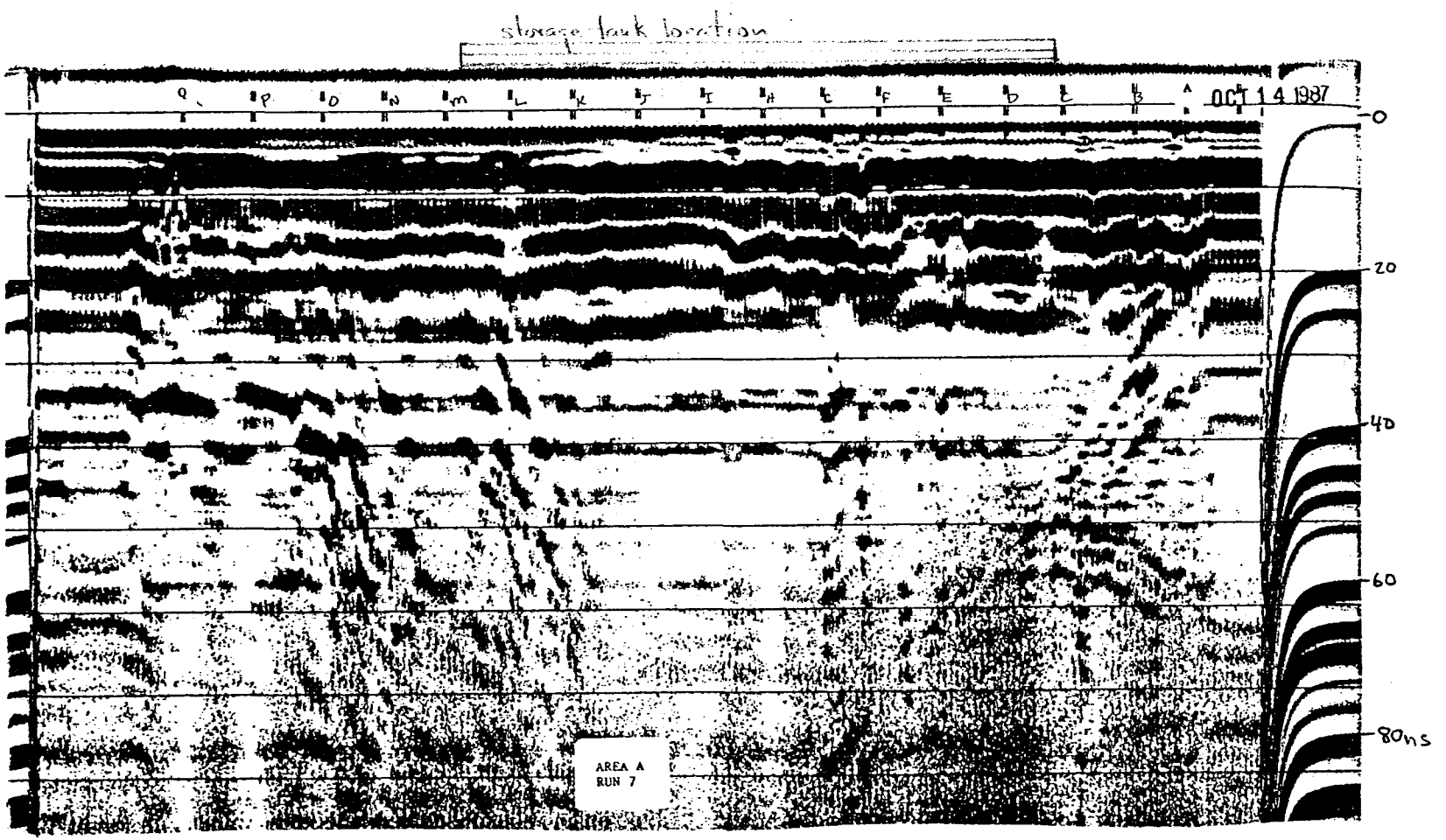

Fig. 43. Radar profile along line 16E over General's storage tank A2.

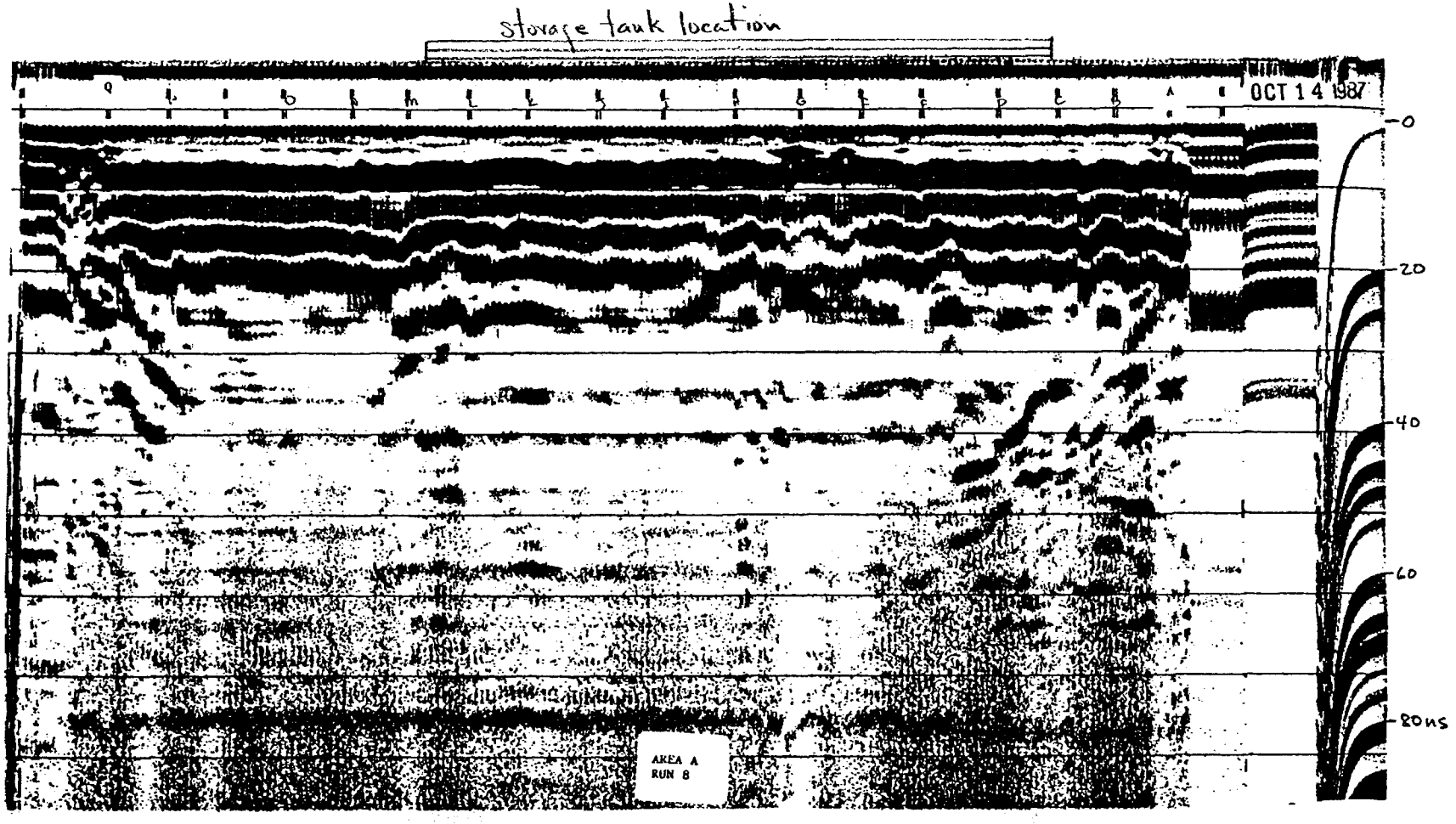

Fig. 44. Radar profile along line 20E over General's storage tank A2.

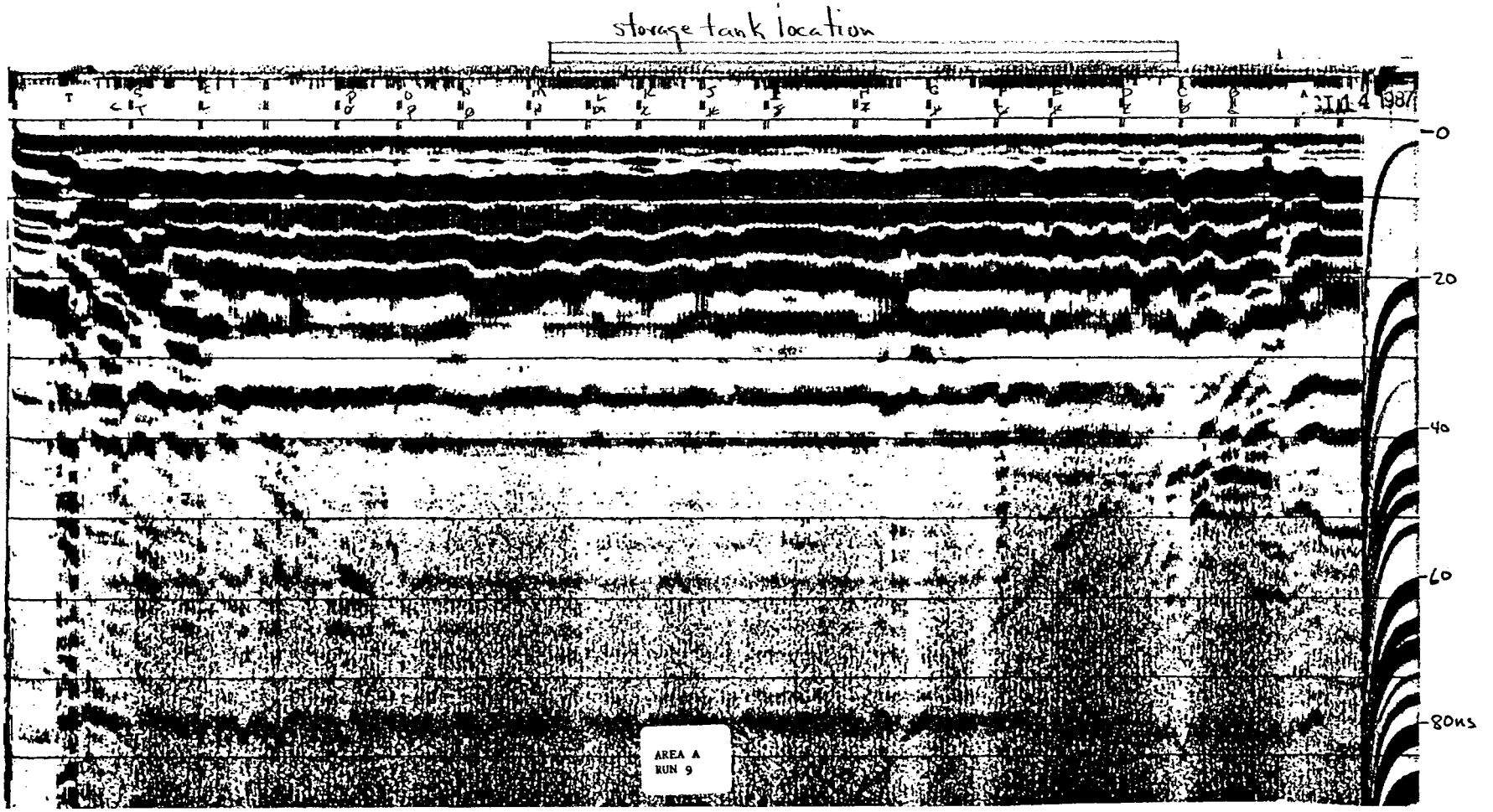

Fig. 45. Radar profile along line 24E over General's storage tank A2.

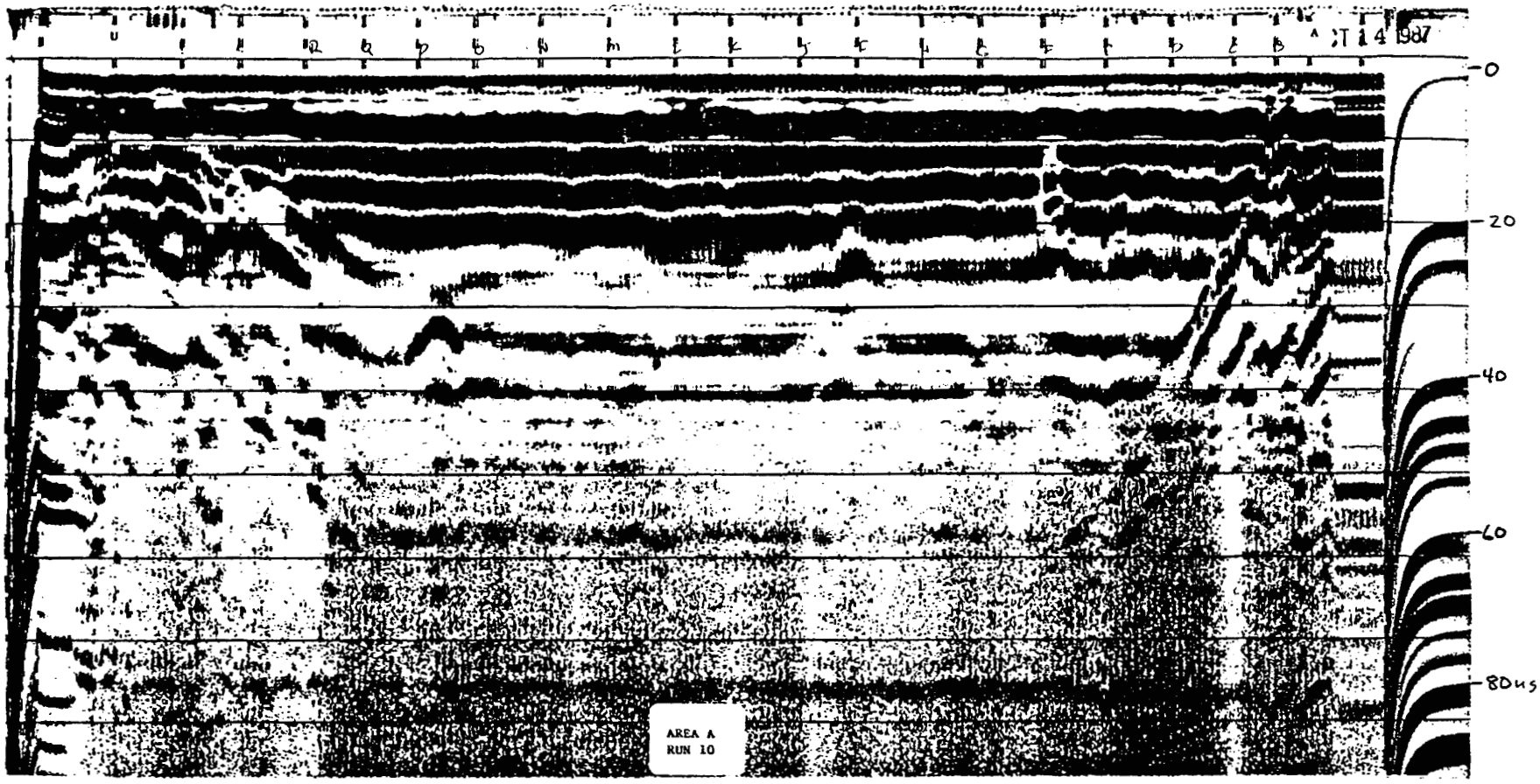

Fig. 46. Radar profile along line 28E. This profile does not pass over any known object, pit or trench.

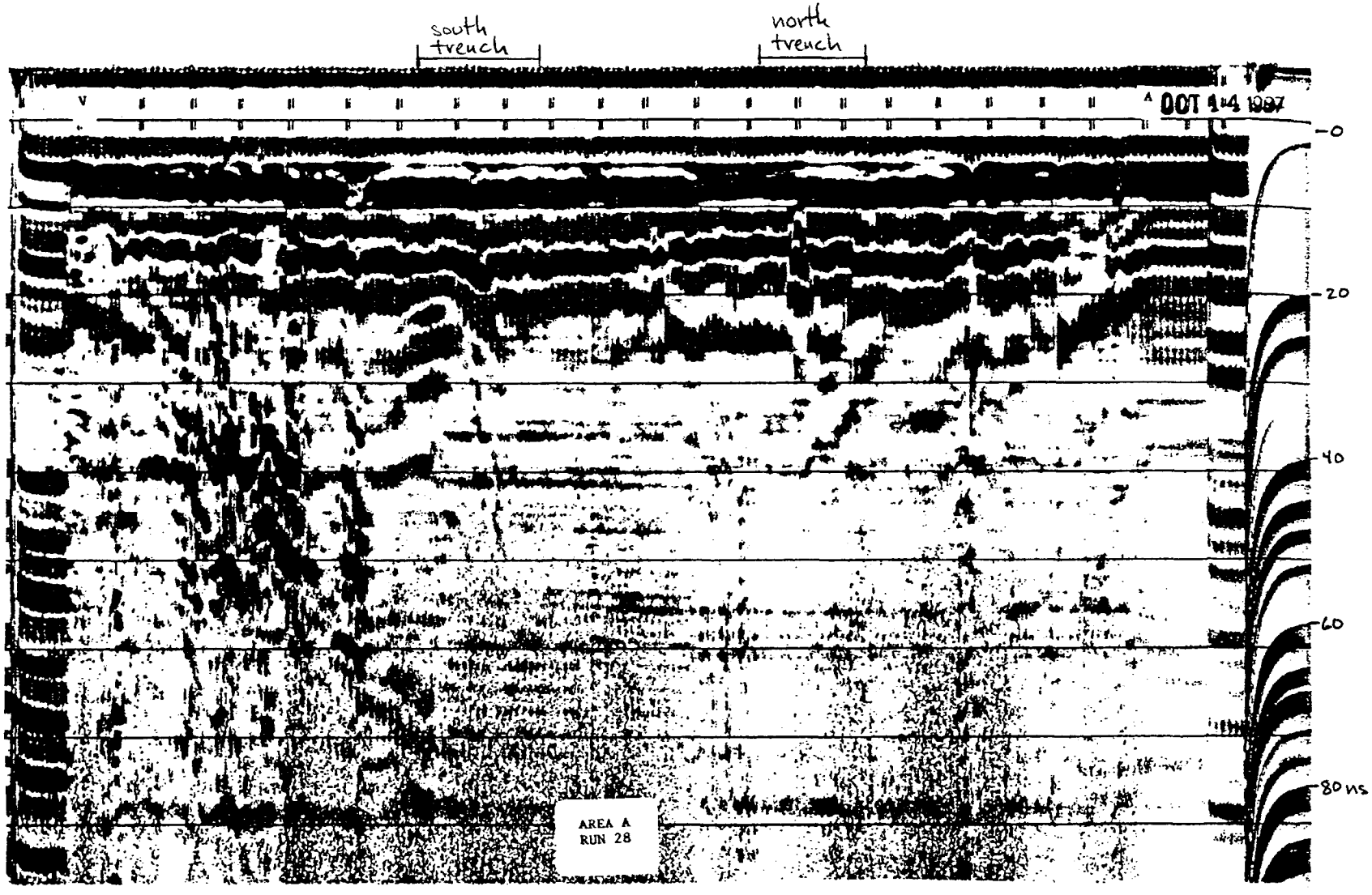

Fig. 47. Radar profile along line 100E over trenches B1 and B2.

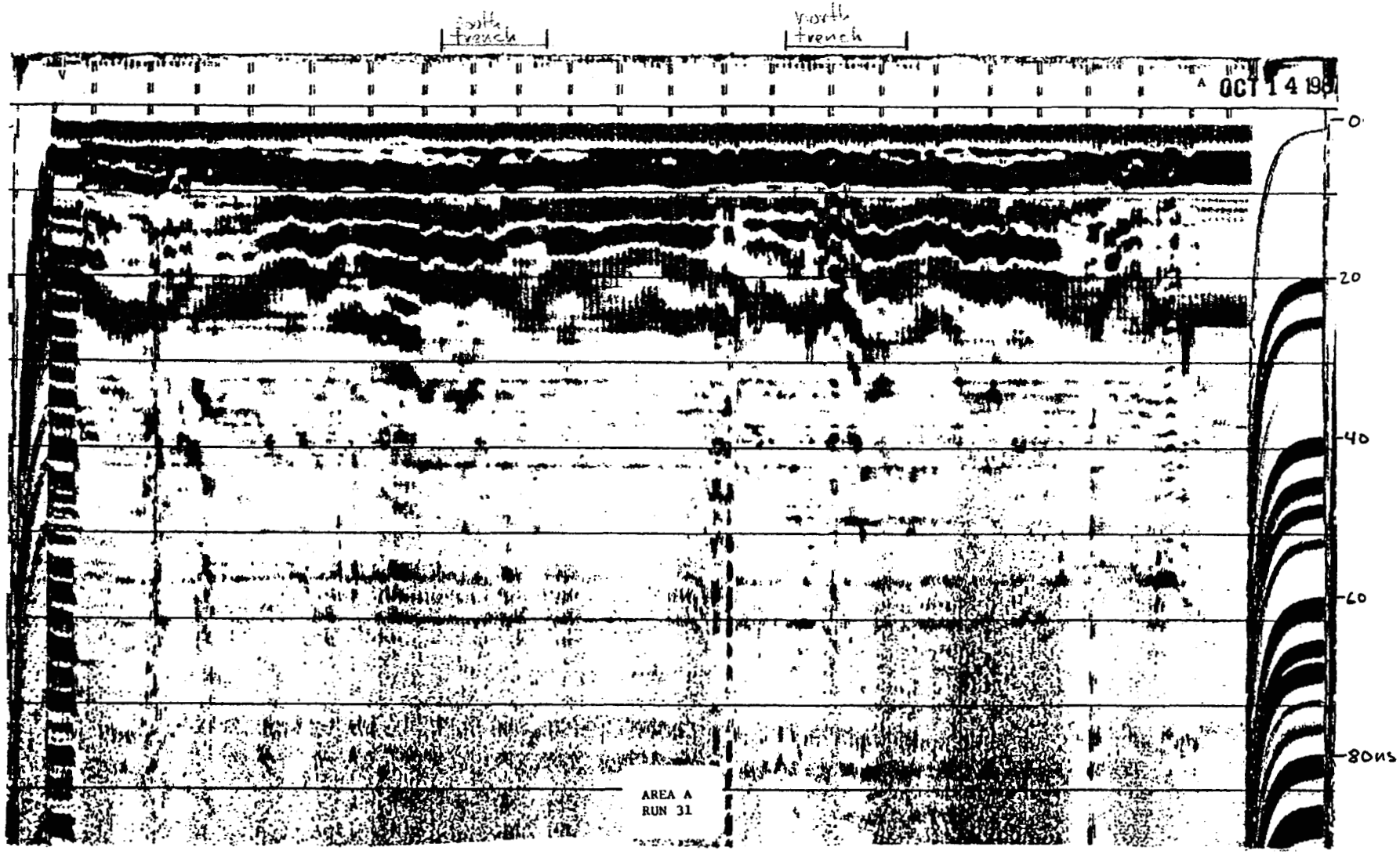

Fig. 48. Radar profile along line 112E over trenches B1 and B2.

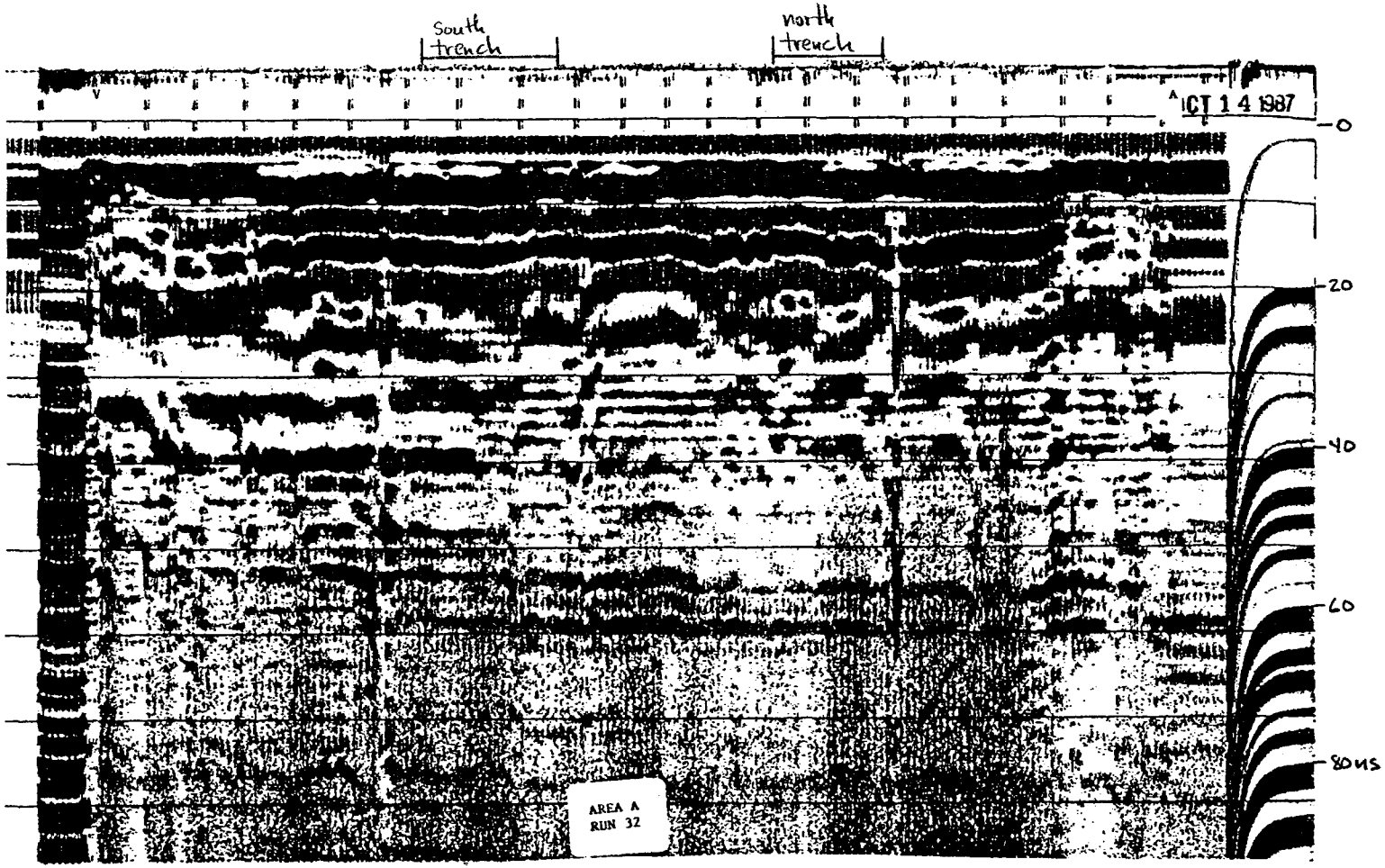

Fig. 49. Radar profile along line 116E over trenches B1 and B2.

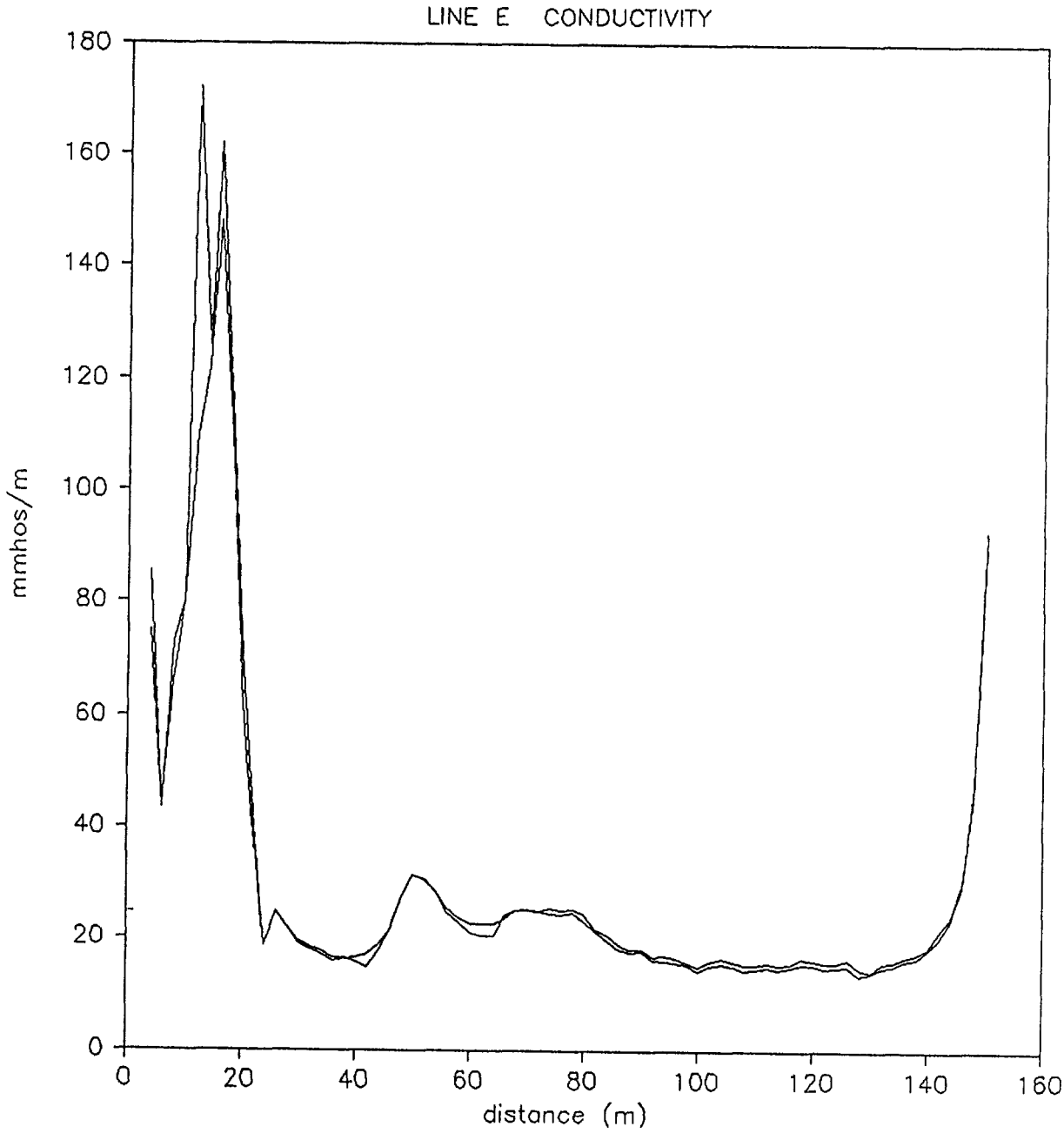

Fig. 50. EMI quadrature component profile line E (10S). Data were measured on two separate days to demonstrate repeatability.

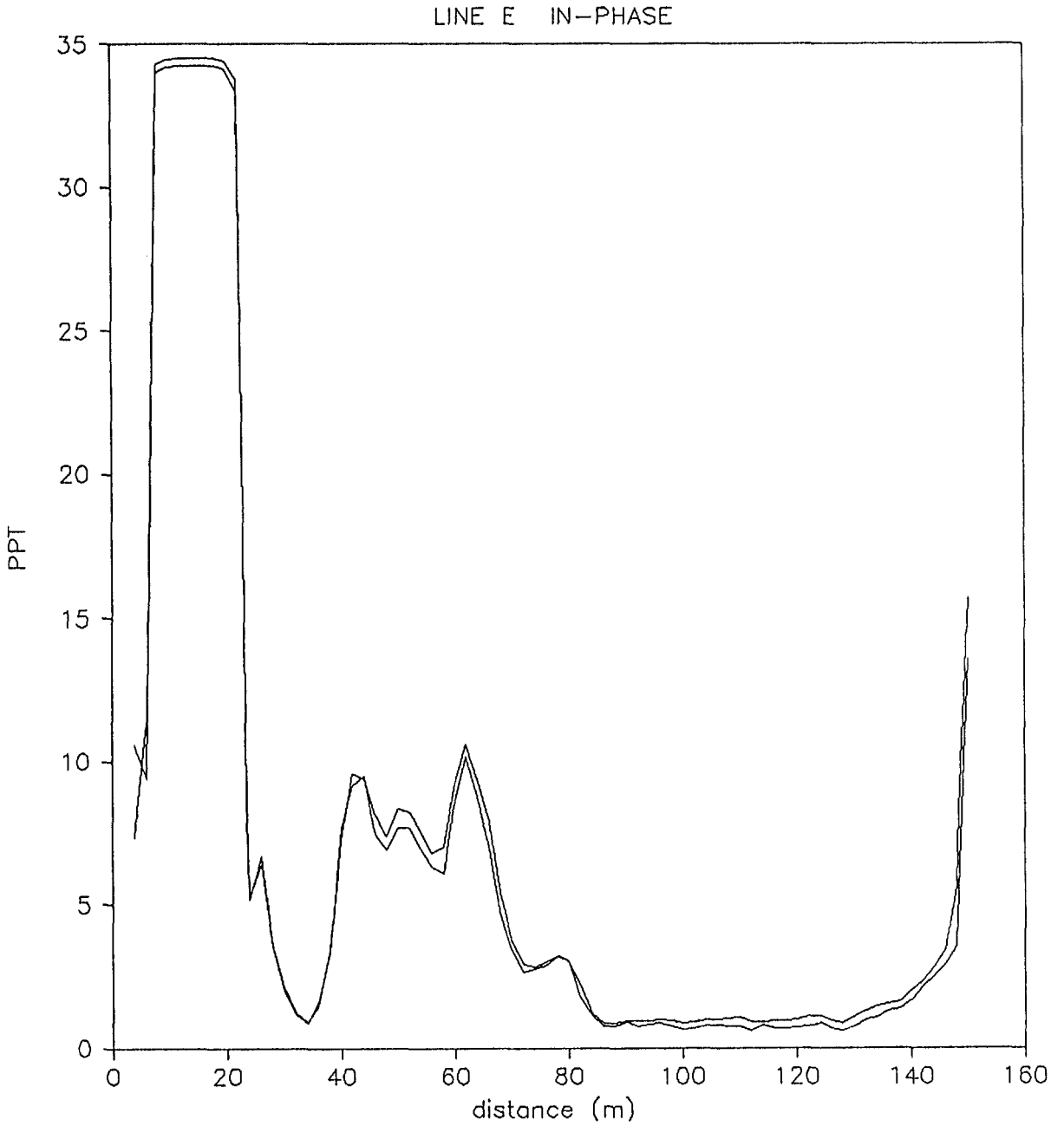

Fig. 51. EMI in-phase component profile line E (10S). Data were measured on two separate days to demonstrate repeatability.

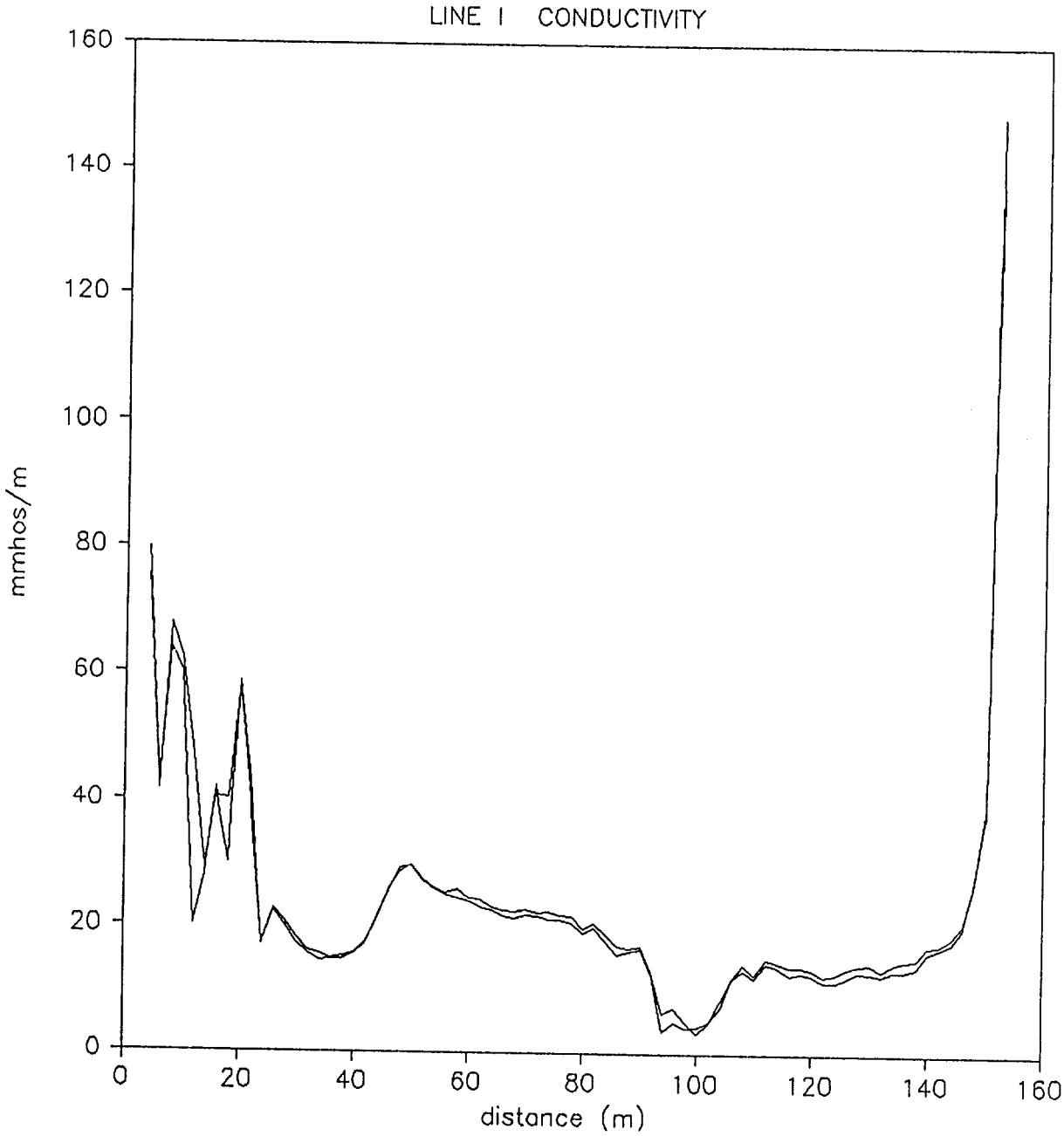

Fig. 52. EMI quadrature component profile line I (18S). Data were measured on two separate days to demonstrate repeatability.

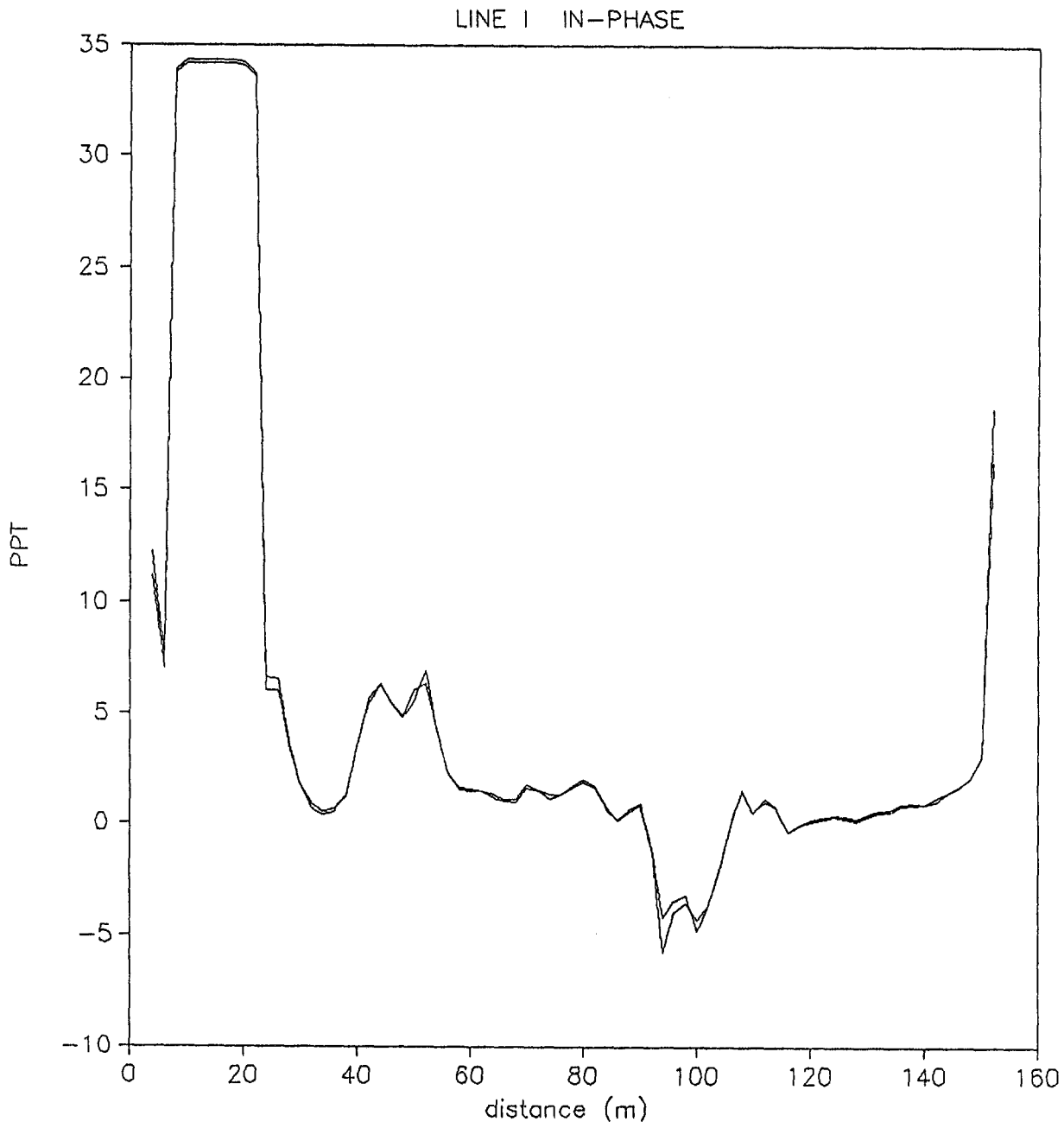

Fig. 53. EMI in-phase component profile line I (18S). Data were measured on two separate days to demonstrate repeatability.

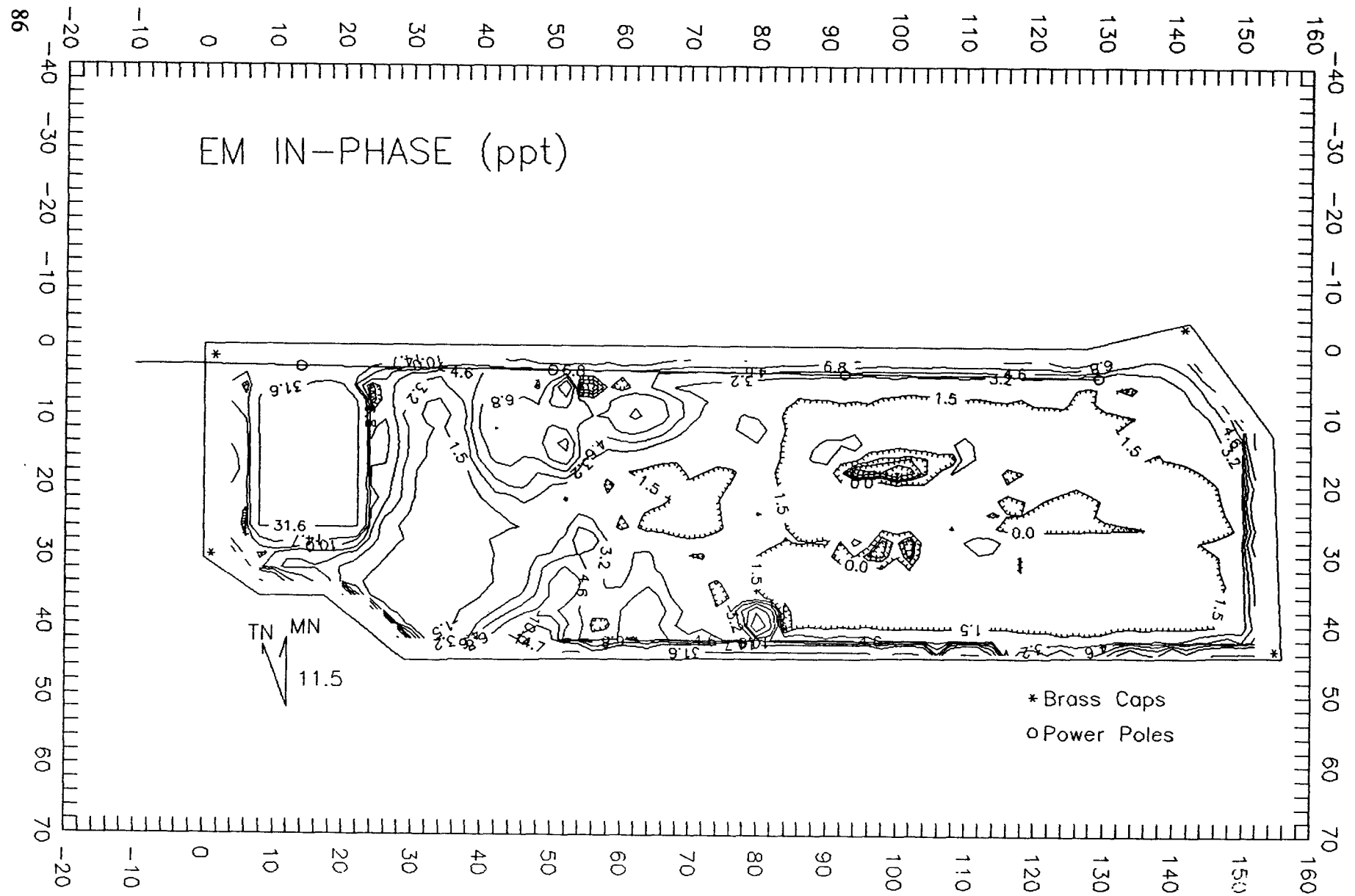

Fig. 54. EMI in-phase component contour map. The contour interval is logarithmic with six points per decade. Contour lines are placed at -10, -6.8, -4.64, -3.16, -2.15, -1.47, 0, 1.47, 3.16, 4.64, 6.8, 10, 14.7, 31.6, 46.4, 68, and 100 ppt.

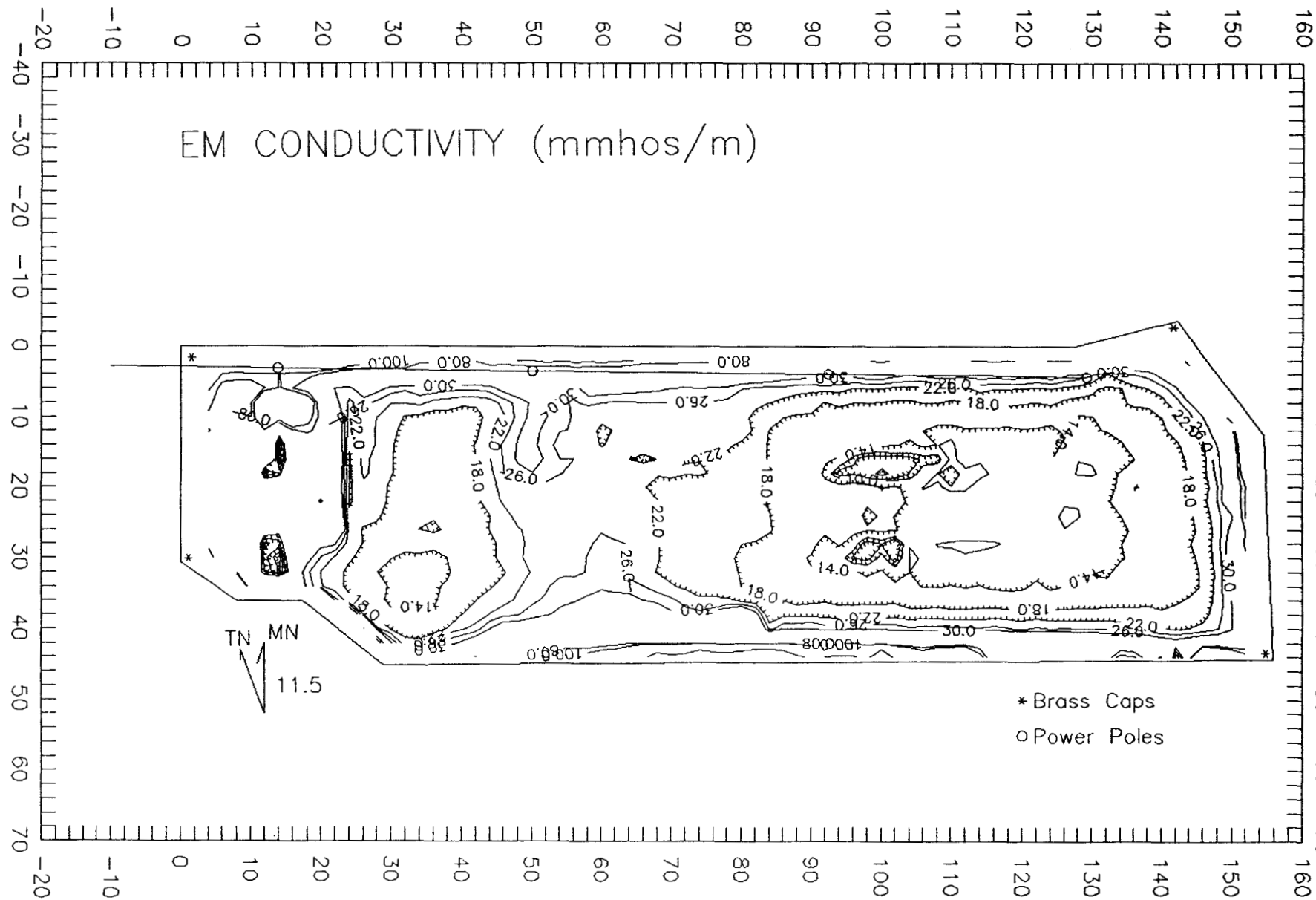

Fig. 55. EMI quadrature component contour map. The contour interval is irregular to detail the electrical structure of the data. Contour lines are placed at 0, 4, 8, 10, 14, 18, 22, 26, 30, 80, 100, and 400 mS/m.

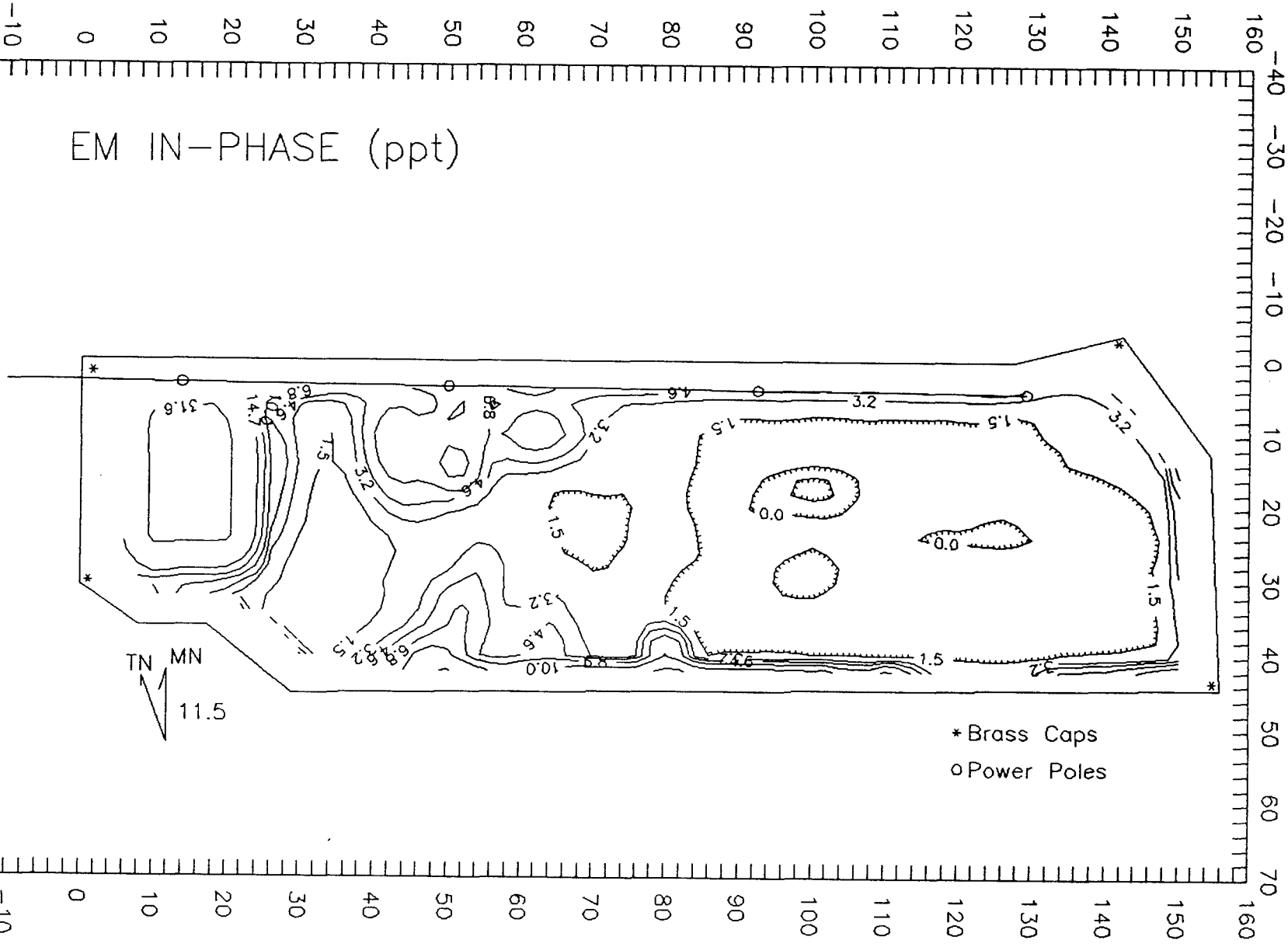

Fig. 56. Smoothed EMI in-phase component contour map. The contour interval is logarithmic with six points per decade. Contour lines are placed at -10, -6.8, -4.64, -3.16, -2.15, -1.47, 0, 1.47, 3.16, 4.64, 6.8, 10.0, 14.7, 31.6, 46.4, 68,

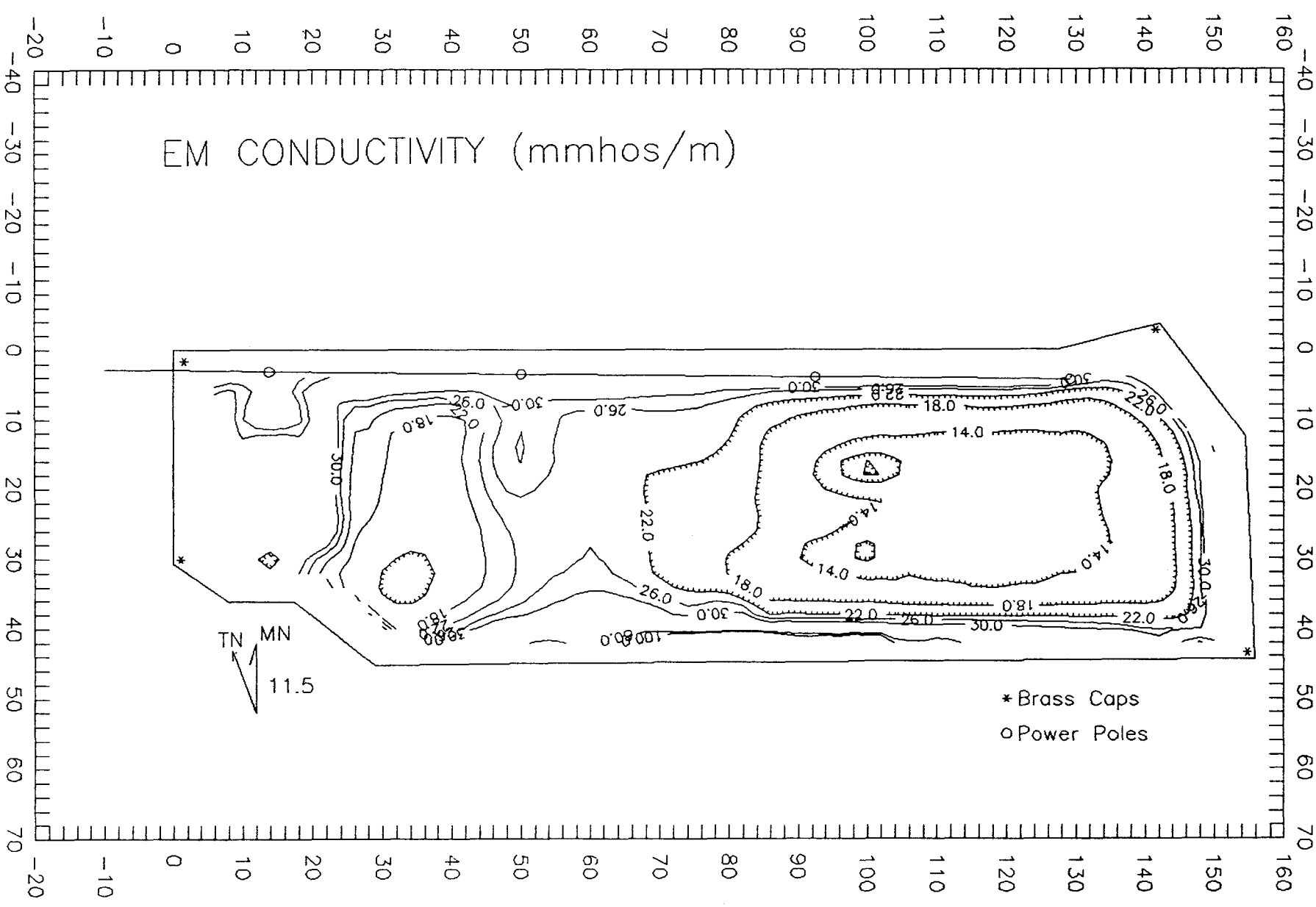

Fig. 57. Smoothed EMI quadrature component contour map. The contour interval is irregular to detail the conductivity structure of the data. Contour lines are placed at 0, 4, 8, 10, 14, 18, 22, 26, 30, 80, 100, and 400 mS/m.

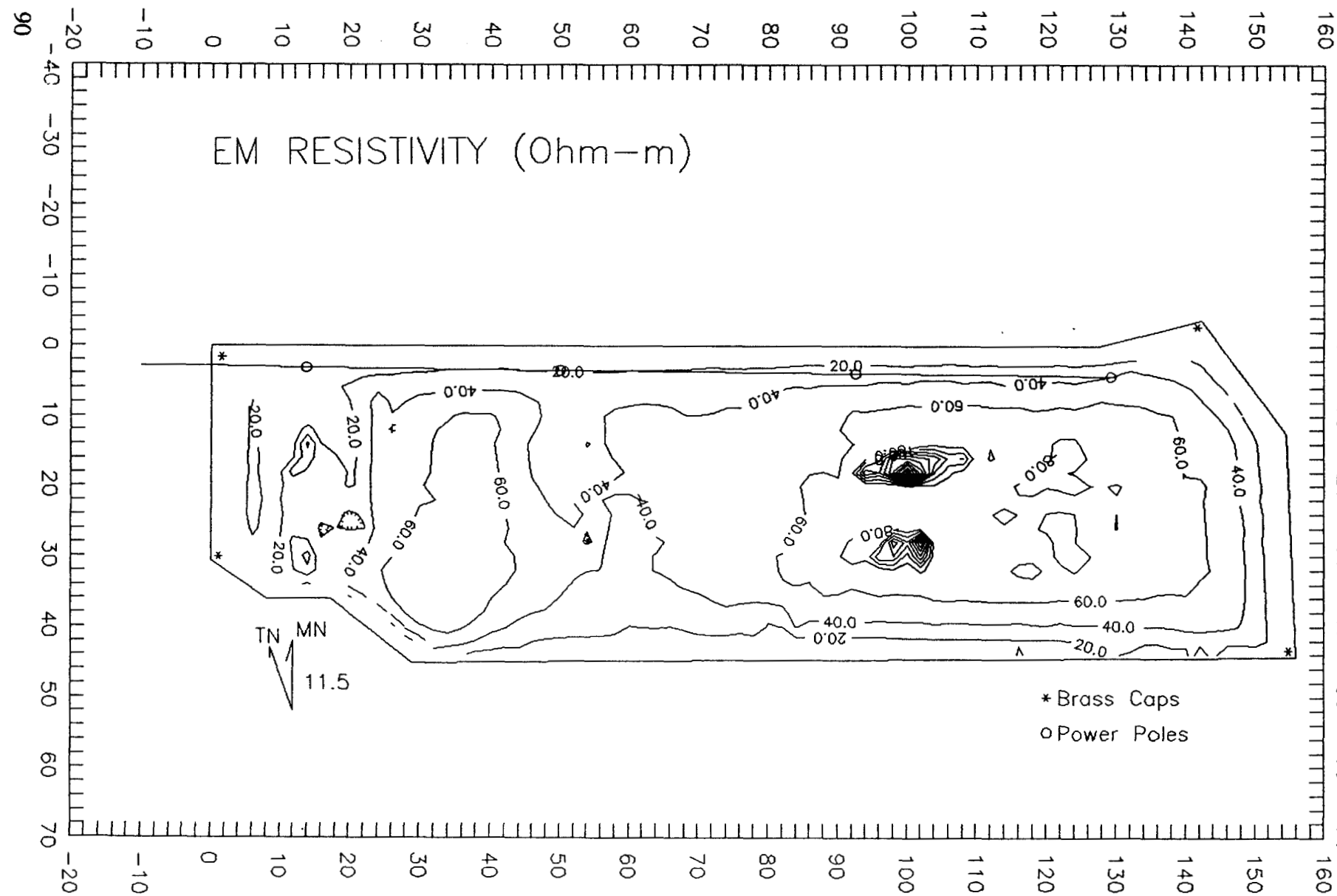

Fig. 58. Electromagnetic resistivity as calculated from the smoothed quadrature conductivity of Fig. 57. Contour interval is 20 ohm-m.

This report has been reproduced directly from
the best available copy.

Available to DOE and DOE contractors from
the Office of Scientific and Technical Information
P.O. Box 62
Oak Ridge, TN 37831
prices available from
(615) 576-8401, FTS 626-8401

Available to the public from
the National Technical Information Service
U.S. Department of Commerce
5285 Port Royal Rd.
Springfield, VA 22161

Microfiche A01

Page Range	NTIS Price Code	Page Range	NTIS Price Code	Page Range	NTIS Price Code	Page Range	NTIS Price Code
001–025	A02	151–175	A08	301–325	A14	451–475	A20
026–050	A03	176–200	A09	326–350	A15	476–500	A21
051–075	A04	201–225	A10	351–375	A16	501–525	A22
076–100	A05	226–250	A11	376–400	A17	526–550	A23
101–125	A06	251–275	A12	401–425	A18	551–575	A24
126–150	A07	276–300	A13	426–450	A19	576–600	A25
						601-up*	A99

*Contact NTIS for a price quote.

Los Alamos National Laboratory
Los Alamos,New Mexico 87545